TABLE DES MATIÈRES

Page

INTRODUCTION 1

CHAPITRE 1 REVUE DE LA LITTÉRATURE, MÉTHODOLOGIE, ET STRUCTURE DE LA THÈSE 5
1.1 Introduction 5
1.2 Modèles de tolérancement 5
1.3 Paramétrage de surfaces avec des défauts de forme 11
1.3.1. Paramétrage par des composantes harmoniques 11
1.3.2. Paramétrage par des polynômes 16
1.3.3. Paramétrage par décomposition modale discrète 20
1.4. Génération des assemblages des surfaces avec des défauts géométriques 22
1.5. Conversion d'un nuage de points vers une caractéristique 32
1.6. Objectifs de la recherche 35
1.7. Contributions scientifiques projetées du projet 36

CHAPITRE 2 CAD/TOLERANCING INTEGRATION: MECHANICAL ASSEMBLY WITH FORM DEFECTS 41
2.1 Abstract 41
2.2 Introduction 42
2.3 State of the art 43
2.4 Modeling realistic component 45
2.4.1 Modeling of component with position and orientation defects 45
2.4.2 Modeling of component with form defects 48
2.4.3 Review of thin plate spline interpolation method 50
2.5 Modeling of realistic assemblies 52
2.5.1. Algorithms for modelling realistic joints 52
2.5.2. Algorithm for modelling a planar joint in realistic model 54
2.5.3. Determination of OBB 54
2.5.4. Finding the optimal rotation and translation 56
2.6 Motion simulation with planar joint 58
2.6.1. 1rst Solution: part relative displacements without guaranteeing contact.. 59
2.6.2. 2nd Solution: relative displacements with guaranteeing contact 60
2.7 Case of cylindrical joint 62
2.7.1. Algorithm for modelling a cylindrical joint in realistic model 62
2.8 Optimized cylinder algorithm 63
2.8.1. Determination of the Minimum Circumscribed Circle (MCC) 65
2.8.2. Determination maximum inscribed circle (MIC) 67
2.9 Motion simulation with Cylindrical joint 68
2.10 The case of a revolute joint 71
2.11 Conclusion 74
2.12 Acknowledgments 74

CHAPITRE 3 EVALUATION OF THE ALGORITHMIC ERROR OF A FITTING CIRCLE USING ISO 14405 SPECIFICATIONS 75
3.1 Abstract 75
3.2 Introduction 76
3.3 New specifications of size tolerances, as defined by the ISO 14405-1 77
3.4 Stat of art 79
3.5 Proposed benchmark of The ISO 14405-1 specification modifiers (PBISM) 80
3.5.1 Proposed Methodology 81
3.5.2 Circularity Modelling 81
3.5.3 Adding measurement noise 86
3.6 Selection of specification modifiers 88
3.6.1. Minimum Circumscribed Size (GN) 88
3.6.2. Global- Least Squares Size (GG) 89
3.6.3. Maximum Inscribed Size (GX) 90
3.6.4. Minimum Size (SN) 91
3.7 Experiments and evaluation 94
3.8 Performance Measures 94
3.9 Artificial Numerical Datasets 95
3.10 Complete Data 95
3.10.1. Influence of the Number of Points 95
3.10.2. Influence of measurement noise 97
3.10.3. Influence of Noise on Form Defect 100
3.11 Incomplete Data 101
3.12 Experimental Datasets 107
3.13 Conclusion 109
3.14 Acknowledgments 110

CHAPITRE 4 REPRODUCIBILITY EXPERIMENTATION AMONG COMPUTER-AIDED INSPECTION SOFTWARE FROM A SINGLE POINT CLOUD 111
4.1 Abstract 111
4.2 Introduction 112
4.3 Background 113
4.4 Experimental protocol 117
4.5 Methodology analysis 120
4.6 Results 122
4.6.1 Analysis of circle #1 122
4.6.2 Analysis of circle #2 124
4.6.3 Analysis of the oblong hole 126
4.7 Analysis of Plan A 127
4.8 Analysis of Plan D 129
4.9 Conclusion 130
4.10 Acknowledgments 131

CHAPITRE 5 A HYBRID APPROACH FOR DEFORMED CYLINDER FEATURES EXTRACTION BY ROBUST PRINCIPAL COMPONENT ANALYSIS AND ORIENTED BOUNDING BOX USING ISO 14405- 1:2016 SPECIFICATIONS....133
5.1 Abstract....133
5.2 Introduction....134
5.3 Literature review....136
5.4 Specifications of size tolerances....137
5.4.1 GN Algorithm....138
5.4.2 GX Algorithm....139
5.4.3 GG Algorithm....140
5.4.4 SN Algorithm....140
5.4.5 Principal Component Analysis (PCA)....141
5.4.6 Oriented Bounding Box....142
5.5 Proposed approach....144
5.6 Experimental protocol....146
5.7 Artificial Datasets....149
5.7.1 Cylinder fitting for missing data....149
5.7.2 Influence of noise measurement....151
5.7.3 Influence of Deformed cylinders....153
5.8 Experimental datasets....154
5.9 Conclusion....157
5.10 Acknowledgments....158

CONCLUSION....159

RECOMMANDATIONS....163

ANNEXE I ARTICLE MOSIM 2016....165

ANNEXE II ARTICLE IDETC/CIE 2018....166

ANNEXE III ARTICLE GMAI 2019....167

LISTE DE RÉFÉRENCES BIBLIOGRAPHIQUES....171

LISTE DES TABLEAUX

Page
Tableau 1.1 Les principaux modèles de tolérancement 9
Tableau 1.2 résumé des techniques de paramétrage de surfaces 21
Tableau 1. 3 Références bibliographiques des conférences, période : 2016-2019 39
Tableau 2. 1 Tolerance impacts (without guaranteeing contact) 60
Tableau 2. 2 Tolerance impacts (with guaranteeing contact) 61
Tableau 2. 3 Result of the execution of optimized algorithm 67
Tableau 2. 4 Results of Gap computation 70
Tableau 3. 1 Four Specification modifiers and symbols Of ISO 14405-1:2016 79
Tableau 3. 2 Feature table of the circles 108
Tableau 3. 3 Results of real datasets (Max fit, Min fit best fit and Best Fit Sigma) 108
Tableau 3. 4 Results of developed algorithms (GN, GX, GG and SN) With: d DiameterOOR: Out-of-roundness 109
Tableau 4. 1 Options for three software's 120
Tableau 4. 2 Results for circle #1 123
Tableau 4. 3 Results for the inspection of the oblong hole (width =13,333 mm, length=22,666 mm) 127
Tableau 4. 4 Results for the inspection of Plane A 128
Tableau 4. 5 Results of inspection of Plane D 129
Tableau 5. 1 Feature table of the cylinder 154
Tableau 5. 2 Results of real datasets 155
Tableau 5. 3 Comparing the results of a model with experimental measurements 156

LISTE DES FIGURES

Page

Figure 1. 1 Différent type de zones de tolérances (tiré de (Samper 2007)) 6

Figure 1. 2 Représentations des relations entre les éléments géométriques 7

Figure 1. 3 Améliorations de modèle nominales (CAO) 8

Figure 1. 4 Méthodes de tolérancement [1] (Turner 1993).....10

Figure 1. 5 Paramétrages de surfaces.....11

Figure 1. 6 Transformation rigide linéaire [(Petit 2004)] 22

Figure 1. 7 Les classes d'écarts géométriques [tiré de (Schleich, Anwer et al. 2014)].....26

Figure 1. 8 Références bibliographiques des conférences, période : 2016-2019.....40

Figure 2. 1 Modeling of realistic component.....46

Figure 2. 2 The improved PCCPTP algorithm.....47

Figure 2. 3 (a) Definition of the random direction,.....50

Figure 2. 4 Thin plate spline interpolation method.....52

Figure 2. 5 Example of variational surface.....53

Figure 2. 6 Example of 2D OBB 54

Figure 2. 7 Determination of OBB 55

Figure 2. 8 Nominal configuration without mates,.....56

Figure 2. 9 Sub-algorithm to redefine planar joint 58

Figure 2. 10 The distance D and the maximum Gap 59

Figure 2. 11 Part relative displacements without guaranteeing contact.....60

Figure 2. 12 Part relative displacements with guaranteeing contact.....62

Figure 2. 13 Optimized cylinder algorithm.....62

Figure 2. 14 Algorithm of cylindrical joint.....63

Figure 2. 15 The main steps of calculating the optimized cylinder 64

Figure 2. 16 Maximum Inscribed.....64

Figure 2. 17 Determination of the Minimum.....66

Figure 2. 18 Execution time of method 1 with /without Convex Hull 67

Figure 2. 19 Determining the inscribed circle 68

Figure 2. 20 Two coaxial cylinders (a) without triangular mesh (b) with triangular mesh 69

Figure 2. 21 Algorithm for computing of gap.....69

Figure 2. 22 Nominal and realistic models 72

Figure 2. 23 Case of ψw rotation $Pmnw$=Puv 72

Figure 2. 24 Sub-algorithm used to determine.....73

Figure 3. 1 Geometrical fitting process.....77

Figure 3. 2 Example of the specification of size.....78

Figure 3. 3 Proposed methodology 80

Figure 3. 4 Asymmetry 82

Figure 3. 5 Example of three lobes: 82

Figure 3. 6 Example of egg.....83

Figure 3. 7 Part circle: lobbing with Circularity Defect c =0.1, and $n = 50$.....85

Figure 3. 8 Example of measurement data with c =0.1 mm, v=0.3 mm and n =50 87

Figure 3. 9 Minimum circumscribed size of 100 points with r=0.4 and a=0.3 88

Figure 3. 10 Least Squares Size of 100 points with r=0.4 and a=0.3 89

Figure 3. 11 Maximum Inscribed Size (GX) of 100 points with $r = 0.4$ and $a = 0.3$.....90

Figure 3. 12 Four points of two 92

Figure 3. 13 Minimum size (SN) of 100 points with r=0.4 and a=0.3 93

Figure 3. 14 Boxplot diagram 94

Figure 3. 15 The influence of the defect form on the evaluation of ISO 14405-1.....96

Figure 3. 16 Illustration of the influence of noise.....98

Figure 3. 17 The influence of Noise level on the evaluation.....99

Figure 3. 18 Influence of Noise level on the evaluation of the 14405-1 specification methods (c=2%, v = [2%, 5%, 10%, 15%, and 20%])(a) GN method, (b) GX method, (c) GG method, (d) SN method.....99

Figure 3. 19 The influence of the form defect on the evaluation of 14405-1.....100

Figure 3. 20 The influence of the form defect on the evaluation.....100

Figure 3. 21 Scale of different angles.....101

Figure 3. 22 The influence of the angle on the evaluation of 14405-1 specification methods (GN, GX, GG and SN) with c = 0.02 mm, v =0.05 mm.....103

Figure 3. 23 The influence of the angle on the evaluation of 14405-1.....105

Figure 3. 24 The influence of the Noise level on the evaluation of 14405-1.....105

Figure 3. 25 Inspection's operation of circle point clouds.....107

Figure 3. 26 Point clouds of the scan of Cylinder 1.....109

Figure 4. 1 Inspection Process.....113

Figure 4. 2 GD&T of the sample part with numbering items.....118

Figure 4. 3 Proposed benchmark.....119

Figure 4. 4 Elements measured for analysis.....122

Figure 4. 5 Results for circle #1.....124

Figure 4. 6 Results of the circle #2 analysis.....126

Figure 4. 7 Results for the oblong hole.....127

Figure 4. 8 Results of flatness analysis (Plan A).....128

Figure 4. 9 Result of flatness analysis in Plan D.....129

Figure 5. 1 ISO 14405-1: GX, SN, GG & GN methods.....138

Figure 5. 2: Minimum Circumscribed Circle.....139

Figure 5. 3 Projection of 3D cylinder on the 2D circle 142

Figure 5. 4 the different cylinders cases in the industry.....143

Figure 5. 5 results of the OBB on the created deformed cylinders 143

Figure 5. 6 projection of 3D deformed cylinder 144

Figure 5. 7 Main steps of cylinder fitting.....146

Figure 5. 8 Main steps of cylinder fitting.....147

Figure 5. 9 Synthetic data with form error simulations on cylinder surfaces, n =2000.....148

Figure 5. 10 Example of synthetic data with noise (v=0.1 mm and n =2000) 148

Figure 5. 11 Scale of different angles 149

Figure 5. 12 Results of fitting incomplete data n=750×5, v=20%, and T=2000. 150

Figure 5. 13 Empirical cumulative for diameters; the influence of incomplete data.....151

Figure 5. 14 The influence of noise level on the evaluation of 14405-1 specification.....152

Figure 5. 15 the influence of defect forms on the evaluation of ISO 14405-1 specification methods: (a) GG method, (b) GN method, (c) GX method, (d) Sn method 153

Figure 5. 16 the four cylinders made 155

Figure 5. 17 Measurement and evaluation process.....156

Figure 5. 18 Empirical cumulative of proposed.....157

LISTE DES ABRÉVIATIONS, SIGLES ET ACRONYMES

AMT	Appareil de mesures tridimensionnelles
ASME	*American Society of Mechanical Engineer*
ACP	Analyse en composantes principales
CAT	*Computer-Aided Tolerancing*
CSG	*Constructive Solid Geometry*
CAO	Conception Assistée par Ordinateur
CPD	*Coherent Point Drift Algorithm*
CMM	*Coordinate Measuring Machine*
CLR	Les radars laser cohérents
CVG	*Constructive Variational Geometry*
DMU	*Digital Mock-up*
DOF	*Degree of Freedom*
DCT	Transformation de Cosinus Discrète
DFT	Transformation de Fourier Discrète
EGRM	Élément Géométrique de Référence Minimum
FC	*Fitting Conditions*
GD&T	Geometric Dimensioning and Tolerancing
ISO	International Organization for Standardization
IEEE	*Institute of Electrical and Electronics Engineers*
GN	*Minimum circumscribed size*
GX	*Maximum inscribed size*
GG	*Least squares size*
GPS	Spécification géométrique des produits
LMC	*Least Material Condition*
LM	*Levenberg marquardt*
MMC	*Maximum Material Condition*
RNN	*Regression Neural Network*
OFA	*Objective Function of the Assembly*

OBB	*Oriented Bounding Box*
MMP	*Maximal Material Part*
PCA	*Principal Component Analysis*
SN	*Minimum size*
TPD	Torseurs de Petits Déplacements
TPS	*Thin plate spline*
VBR	*Virtual Boundary Requirement*

INTRODUCTION

Du concept au client, différentes phases du cycle de vie du produit s'écoulent séquentiellement : conception, fabrication, inspection, assemblage, utilisation et fin de vie. Afin de garantir les requis d'assemblage et les critères de performance (requis fonctionnels), il est nécessaire de gérer les défauts qui seront tolérés, ces derniers sont générés par la variation inhérente des procédés de fabrication. Il faut assurer à l'utilisateur final un bon fonctionnement conforme aux prévisions des clients. Par conséquent, il est utile de faire parler les intervenants du cycle de vie du produit.

Le tolérancement est le terme employé généralement pour l'étude, incluant l'analyse et la distribution, des étendues des erreurs dimensionnelles et géométriques permises à la fabrication afin de maintenir un niveau de qualité acceptable. Cette qualité est propre à un produit et doit se traduire par une bonne capacité de garantir les besoins établis par le concepteur dans le cahier des charges. Pratiquement, l'unité de conception exprime ses besoins à travers des dessins et devis techniques qui définissent le produit. Durant cette phase le concepteur définit les différents types et valeurs de tolérances. Il doit donc évaluer le comportement du système en fonction des variations physiques (ex. la température, les contraintes mécaniques, etc.) des pièces pendant leur fonctionnement. Le concepteur précise ces exigences à l'aide de tolérances qui définissent les marges permises pour les caractéristiques critiques. Bien sûr, ces choix vont influer sur les étapes subséquentes lors la réalisation de produit, sur la qualité et sur le coût de production. À son tour, l'unité de fabrication prépare la meilleure gamme de fabrication afin d'élaborer un produit répondant parfaitement aux exigences du client tout en minimisant le temps et le coût de fabrication.

Si la fonction principale du tolérancement est d'assurer la fonctionnalité du produit, il pèse sur les coûts de fabrication. En effet, avoir des tolérances faibles nécessite des procédés de fabrication précis, donc coûteux. Le nombre d'interventions de fabrication est le facteur qui contribue à ce coût élevé de production. La prise en compte de ces facteurs amène à spécifier, pour un besoin spécifique, des tolérances bien adaptées aux procédés de fabrication (on parle dans la littérature du domaine du *tolérancement optimal*).

À un autre niveau, l'unité d'inspection ou de contrôle intervient toujours pour contrôler le respect des contraintes prédéfinis, elle permet aussi d'identifier le niveau des variations du procédé de fabrication dans le but de les corriger. Le progrès technologique des moyens de contrôle a stimulé le développement de nouvelles approches permettant la mise en place de ces nouveaux moyens (par exemple, machine de mesure tridimensionnelle AMT/CMM, numériseurs sans contact, etc.).

L'opération de tolérancement a toujours été, et demeure, une tâche complexe qui nécessite une grande expérience du concepteur. Par conséquent, un outil d'aide au tolérancement est souhaitable. À noter que le tolérancement dimensionnel et géométrique d'un produit est aujourd'hui géré par des normes et des codes de pratiques largement reconnus par les industries (ex. ASME Y14.5 ou la série ISO-GPS). Ces standards codent le symbolisme et l'interprétation, ils ne proposent pas de méthode de calculs pour effectuer l'exercice de synthèse ou d'analyse des tolérances.

Le tolérancement comme tel est un sujet intéressant et d'actualité pour les industriels. En effet, la maîtrise des défauts pour assurer les requis fonctionnels (assemblage, performance, esthétique, etc.) lors de cycle de vie d'un produit rend aux industries des gains en termes de coût de production et de compétitivité. Depuis environ (3) décennies, un grand effort de recherche a été porté pour développer des outils de simulation, de gestion et d'application pour assister les concepteurs dans leurs exercices de synthèse de tolérances.

Pour résumer, nous pouvons citer quelques éléments qui motivent notre étude. Le premier est que la technologie et les équipements de la métrologie dimensionnelle ont progressé beaucoup ces dernières années (nombre de points mesurés, méthodes de modélisation de défauts, etc.) fournissant ainsi plus de données pour caractériser les états réels des composants fabriqués. Le deuxième constat est que les récents travaux des chercheurs ont contribué à proposer des solutions robustes pour la gestion des défauts de localisation et d'orientation. Seuls les défauts de forme (ex. profil, planéité, cylindricité, etc.) présentent encore un défi. Ces défauts de forme influent sur les requis fonctionnels (assemblage, performance, esthétique, etc.) ; il est donc important de modéliser les variations géométriques des formes (géométrie observable) pour inclure tous les effets et prédire leur effet lors de l'assemblage et après assemblage. On parle

donc d'un modèle CAO réaliste qui tiendra en compte de l'amplitude et l'allure de ces défauts de forme. Ainsi, la précision obtenue lors de la simulation des assemblages réalistes sera améliorée.

À long terme, notre étude vise le développement de modèles d'intégration des tolérances de forme dans les modeleurs CAO et de développer des approches robustes pour évaluer l'erreur géométrique de forme à partir d'un nuage de points mesurés. Plus spécifiquement, nous visons la modélisation des tolérances géométriques de forme (ex. circularité, cylindricité, planéité), la simulation d'assemblages des pièces rigides avec des défauts de forme et l'analyse de l'effet de l'erreur algorithmique sur l'estimation de la dimension des surfaces ayant des défauts de forme. Nos contributions pourront assister les concepteurs dans leurs exercices de synthèse de tolérances ou encore pour assister l'ingénierie des méthodes lors de la création des gammes de fabrication et d'inspection.

CHAPITRE 1

REVUE DE LA LITTÉRATURE, MÉTHODOLOGIE, ET STRUCTURE DE LA THÈSE

1.1 Introduction

La revue de la littérature décrit les récents travaux effectués dans les domaines de recherche associés à notre thèse. Notre bibliographie a été constituée volontairement selon les phases typiques de la gestion de défauts de forme : (*i*) modélisation des défauts de forme (*ii*) simulation de défauts de forme dans l'assemblage et (*iii*) l'estimation de défauts de forme à partir d'un nuage de points mesurés.

1.2 Modèles de tolérancement

Le tolérancement est un langage d'expression des écarts permis tel que décrit par la famille des normes ISO-GPS (ex. ISO 8785) ou leur équivalent comme la norme ASME Y14.5 (2009). Le tolérancement permet de définir les variations admissibles sur des pièces mécaniques pour les intervenants dans le cycle de vie du produit. En 1903, Taylor a proposé d'améliorer la productivité en se basant sur le facteur temps. Son idée était d'utiliser des techniques de sélection des ouvriers, d'offrir des meilleures rémunérations et de normaliser les opérations manufacturières. Une autre innovation est apparue, elle consiste à standardiser les pièces permettant ainsi leur interchangeabilité. En 1908, les tolérances dimensionnelles ne sont pas encore prises en compte dans les industries. Lors de la Deuxième Guerre, le développement de la cotation évolue considérablement avec une production de haut volume des automobiles et du matériel militaire. En plus des tolérances dimensionnelles, de nouveaux défauts sont prise en considération et un nouveau langage graphique est apparu qui définit les tolérances géométriques. Ce langage avait évolué au cours des années. Aujourd'hui, il est intégré des normes internationales en ISO, ASME, etc. (Petit, 2004) et (Germain, 2007).

D'après la norme ISO 8015, il y a deux (2) types de tolérances : 1) dimensionnelles et 2) géométriques (Figure 1. 1). Les tolérances dimensionnelles regroupent les tolérances linéaires

et angulaires. En outre, les tolérances géométriques englobent les tolérances de forme, d'orientation, de position et de battement (Abdessalem Hassani, 2010). Les tolérances dimensionnelles permettent de traiter des grandeurs (taille, Size). **Les tolérances dimensionnelles** ne suffisent pas pour définir les géométries d'un objet. Malgré la cotation des tolérances dimensionnelles, les requis de fonctionnement, nécessitent toujours un contrôle « géométrique ». **Les tolérances géométriques** limitent les écarts admissibles de l'élément réel par rapport à sa géométrie (Germain, 2007) et (Kataya, 2002).

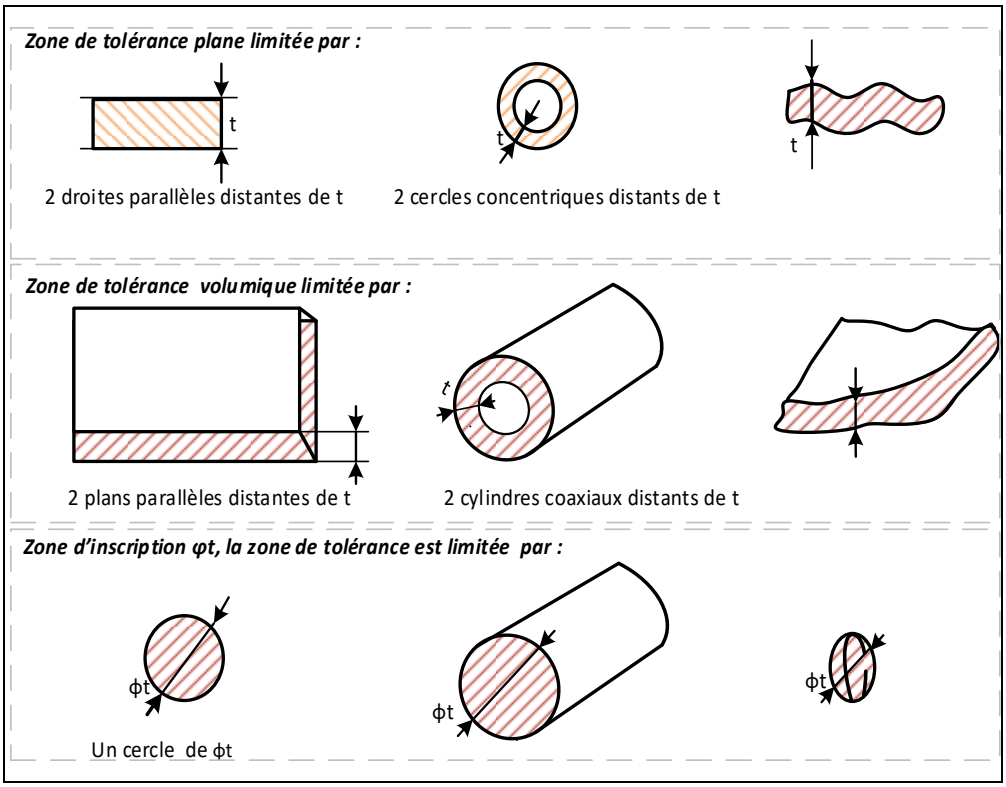

Figure 1. 1 Différent type de zones de tolérances [tiré de (Samper, 2007)]

Actuellement, Les normes de tolérancement sont les résultats de l'évolution des technologies et de différentes méthodes appliquées au sein des industries. Les organismes de normalisation ont défini des normes afin de faciliter les échanges entre ces industries grâce à la standardisation de ces valeurs. Différents travaux sont en cours afin de faire évoluer les normes des tolérances. Nous soulignons aussi l'existence de travaux pour normaliser le traitement

mathématique. Ce qui a abouti à la définition de la première norme de tolérancement: (ASME-Y14-5M, 1994).

La famille des normes ISO-GPS : Cette famille de normes internationales traite du domaine de la spécification géométrique d'un produit. Son but est de définir les limites de variations des surfaces réelles par rapport aux surfaces nominales. Lorsqu'on cite la cotation fonctionnelle, cela englobe les tolérances dimensionnelles et géométriques. Aux États-Unis, on utilise l'expression « *Geometric Dimensioning and Tolerancing* » (GD&T).

Les éléments géométriques : La norme ISO 14660 donne la définition des éléments géométriques des pièces. Les principaux termes utilisés sont: **élément d'une pièce** peut-être un point, une ligne ou une surface (Germain, 2007); **élément nominal** c'est l'élément de géométrie parfait; **élément dérivé nominal** peut-être un centre, un axe, le plan médian d'un élément nominal; **élément réel** c'est l'élément réel avec des défauts; **élément extrait** c'est la représentation de la pièce par le nuage de points de la pièce réelle mesuré; **élément associé** c'est l'élément de géométrie parfaite associé à l'élément réel
(Voir Figure 1. 2).

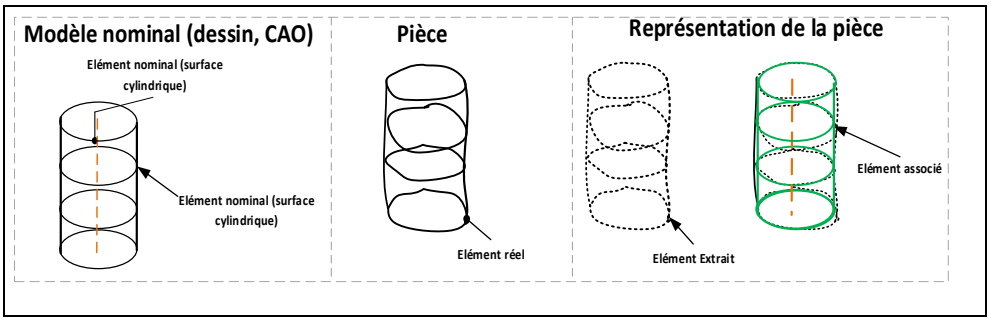

Figure 1. 2 Représentations des relations entre les éléments géométriques

Pour définir correctement une spécification dimensionnelle ou géométrique, six (6) opérations basées sur les différents groupes d'éléments ont été introduites. Les groupes d'éléments sont les éléments idéaux et les éléments non idéaux. L'ensemble de ces opérations est détaillé dans la norme ISO 22432. Le paragraphe suivant va servir à présenter les (6) opérations :

1. **Partition** : C'est la première opération, elle permet d'identifier les éléments géométriques (des éléments non idéaux à partir du modèle de peau « *Skin Model »*).
2. **Extraction** : Cette opération permet d'identifier un nombre de points.
3. **Filtrage** : L'opération de filtrage permet de distinguer l'ondulation, la rugosité, etc.
4. **Collection** : Cette opération permet d'extraire un élément à partir d'un groupe de plusieurs éléments.
5. **Association** : Son but est d'associer des éléments idéaux à partir des éléments non idéaux.
6. **Construction :** Son but permet de construire des éléments idéaux.

Pour assurer l'assemblage du produit et les exigences fonctionnelles, le tolérancement vise à spécifier des limites admissibles pour les écarts de parties géométriques. Ces derniers résultent inévitablement des imprécisions de fabrication. Dans ce contexte, l'analyse des tolérances est un outil clé pour prévoir les effets des écarts géométriques sur les caractéristiques d'assemblage sans nécessiter de maquettes physiques (Schleich and Wartzack, 2016). La recherche dans ce domaine vise essentiellement à établir des modèles mathématiques pour exprimer et représenter les écarts et les exigences géométriques et de modéliser les effets de ces écarts géométriques sur l'assemblage et le comportement du système (Figure 1.3).

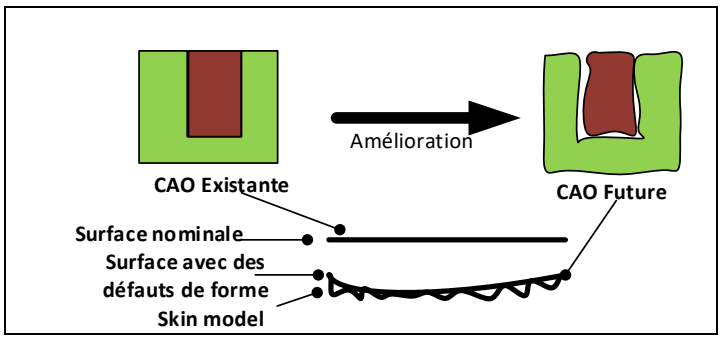

Figure 1. 3 Améliorations de modèle nominales (CAO)

Dans le but d'éviter des opérations chronophages et des carences de productivité, les industries cherchent donc à développer des méthodes et des outils de modélisation des zones de tolérance d'une pièce. Un modèle de tolérancement est l'outil pour résoudre ces problèmes. La maîtrise numérique de tolérancement est donc un gain industriel. Dans le Tableau 1.1, nous recensons une revue succincte de la littérature du domaine et qui cible particulièrement les différents modèles de tolérancement.

Tableau 1.1 Les principaux modèles de tolérancement

Modèles de tolérancement	Techniques	Auteurs	Année
Les classes variationnelles	CSG MMC LMC	Requicha (Requicha, 1984, Requicha, 1993)	1984, 1993
	VBR	Srinivasan and Jayaraman. (Srinivasan and Jayaraman, 1985)	1985
	MMP	Robinson (Robinson, 1998)	1998
Tolérancement vectoriel	Premier Modèle	Wirtz. (Wirtz, 1993)	1993
	TPD	Bourdet et Clément (Bourdet, 1987)	1987
	SATT EGRM	Clément et al. (Clément et al., 1994)	1994
Les espaces de faisabilité	Espaces de faisabilité	Turner (Turner, 1993)	1990, 1993
	CVG	Pino (Pino, 2000b)	2000
Modèle T-Map	T-Map	Gaurav (Gaurav 2007)	2007
Modèle cinématique		Rivest et al. (Rivest et al., 1994)	1994
		Bennis et Pino (Pino, 2000a)	2000

En se basant sur les modèles de représentation de la géométrie tolérance, tels que le modèle cinématique et vectoriel, plusieurs travaux de recherche ont ainsi contribué au développement de modèles d'aide au tolérancement en tenant compte de l'aspect

fonctionnel de l'assemblage et de l'empilement des tolérances; tels que le modèle T-Map (Jian et al., 2007), la méthode de linéarisation de matrice de passage, la méthode des domaines, la méthode CLIC et autres approches: (Srinivasan and Jayaraman, 1985), (Bourdet, 1987), (Rivest et al., 1994), (Robinson, 1998) (Pino, 2000b), (Anselmetti, 2007),et (Anselmetti, 2010), etc.

Ces travaux de recherche proposent des solutions par des formulations mathématiques, des représentations graphiques (ex. polytopes) ou modélisations simplifiées. L'utilisation et la compréhension de certaines solutions restent difficiles à l'échelle industrielle. De plus, ces travaux ne pris pas en considération le processus d'assemblage et l'évolution des contacts entre les pièces. Bien que d'autres travaux de recherche tiennent compte de ces deux aspects, ils ne permettent pas l'utilisation des solutions obtenues dans des étapes ultérieures de la maquette numérique, telles que l'analyse de l'impact de l'empilement des tolérances sur le fonctionnement du produit ou la détermination des effets des écarts géométriques et dimensionnels sur les déformations (Figure 1.4).

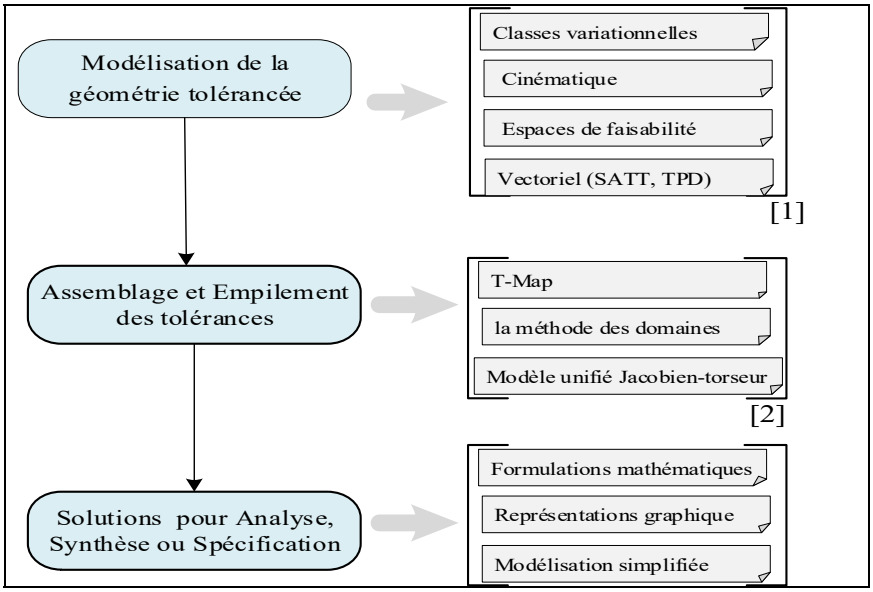

Figure 1. 4 Méthodes de tolérancement [1] (Turner, 1993) (Requicha, 1993, Rivest, 1994) ,(Rivest et al., 1994), (Wirtz, 1993); [2](Gaurav 2007) (Pino, 2000b) (Anselmetti, 2007), (Dantan et al., 2005).

1.3 Paramétrage de surfaces avec des défauts de forme

Dans les normes de spécification géométrique des produits de forme, il existe (2) types de paramétrages de forme: (1) le paramétrage local et (2) le paramétrage global. Le paramétrage local agit localement sur les éléments géométriques. Cette méthode consiste à partitionner l'élément géométrique en plusieurs sous-éléments puis d'appliquer le paramétrage descriptif, et la synthèse de ces paramètres décrit la forme géométrique globale de l'élément. Le principe du paramétrage global est basé sur l'identification des descripteurs qui caractérise la forme de l'élément géométrique. L'identification de cette méthode permet de décomposer la forme de l'espace de descripteurs (Favreliere, 2009). À noter qu'il existe deux types de descripteurs : les bases de description *a priori* et *a posteriori*. Ces différentes méthodes dépendent de la nature des surfaces (continu, discret).

(Favreliere, 2009) propose (3) paramétrages de forme des surfaces 1) les méthodes par des composantes harmoniques, 2) les méthodes par des polynômes et 3) les méthodes par décomposition modale discrète (Figure 1.5).

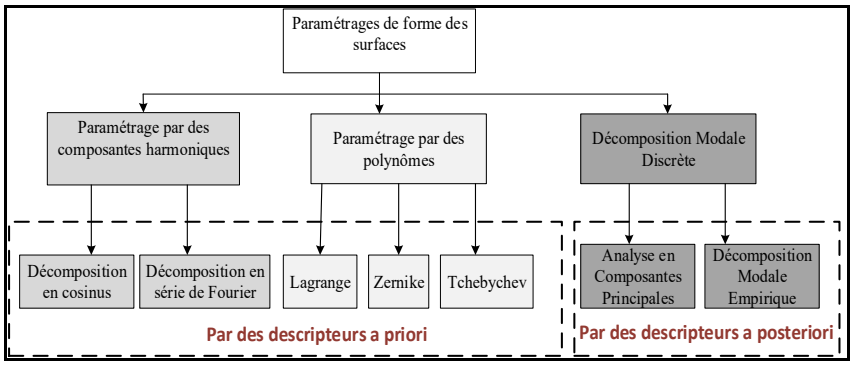

Figure 1. 5 Paramétrages de surfaces

1.3.1. Paramétrage par des composantes harmoniques

Décomposition en cosinus : (Ahmed et al., 1974) ont introduit une nouvelle décomposition de surfaces: la DCT. Elle consiste de passer d'une représentation en domaine spatial à une

représentation en domaine fréquentiel. Elle est très employée dans la compression d'images. Son principe est de décomposer l'image numérique en $N \times N$ blocs puis une DCT est appliquée sur chacune de case des blocs (Equation.1.1).

$$DCT(u,v) = \frac{1}{\sqrt{2}} c(u)c(v) \sum_{x=0}^{N-1} \sum_{y=0}^{N-1} f(x,y) \cos\left(\frac{(2x+1)u\pi}{2N}\right) \cos\left(\frac{(2x+1)v\pi}{2N}\right) \quad (1.1)$$

Pour $u, v = 0,1,2 \dots N$. La DCT inverse sur une matrice $N \times N$

$$f(u,v) = \frac{1}{\sqrt{2N}} c(u)c(v) \sum_{v=0}^{N-1} \sum_{u=0}^{N-1} c(u)c(v) \cos\left(\frac{(2x+1)u\pi}{2N}\right) \cos\left(\frac{(2x+1)v\pi}{2N}\right) \quad (1.2)$$

Avec,

$$c(x) = \frac{1}{\sqrt{2}} \text{ si } x \text{ vaut } 0 \text{ , } et \text{ } 1 \text{ si } x > 0 \quad (1.3)$$

Les coefficients $DCT(u,v)$ sont les amplitudes de la fonction cosinus où chaque fréquence correspond à la position du coefficient $DCT(u,v)$. Dans la littérature, la méthode DCT a été utilisée pour décrire les variations de formes d'une surface. En effet, nous pouvons remplacer les pixels et les couleurs des images par la hauteur de défaut de forme; (Huang and Ceglarek, 2002) ont proposée d'utiliser la DCT pour décrire des surfaces planes avec des défauts de forme. Ils ont remplacé les pixels par les dimensions x et y et les couleurs par z. (Lecompte et al., 2010) utilisent ce paramétrage pour modéliser les défauts de forme (les défauts de fabrication) d'une surface plane . L'algorithme 1.1 décrit l'aspect conceptuel de modélisation des variations géométriques de forme par DCT. (Lecompte et al., 2010) de complexité cubique $O(n^3)$

Algorithme 1.1. Pseudocode de l'algorithme de modélisation des variations géométriques de forme par DCT

Algorithme 1.1 - Pseudocode de l'algorithme de modélisation des variations géométriques de forme par DCT (Lecompte et al., 2010)

Entrées: n: Nombre de points, $P_i = [x_i, y_i, z_i]$: Nuage de points.
Sortie: $\widehat{P_i} = [\widehat{x_i}, \widehat{y_i}, \widehat{z_i}]$: Nuage de points avec déviation de forme.

Début Algorithme

1. Pour i de 1 à n
2. Pour j de 1 à n
3. Calculer la matrice de la transformée de cosinus DCT
    a. Si $x(i,j) = y(i,j)$=0 alors
    b. $c(i,j) = \frac{1}{\sqrt{n}}$
    c. Sinon
    d. $c(i,j) = \sqrt{\frac{1}{n}} cos \frac{(2x(i,j)+1)y(i,j)\pi}{2n}$
    e. Fin Si.
4. Fin Pour
5. Fin Pour
6. Pour i de 1 à n
7. Pour j de 1 à n
8. Calculer la matrice de la transformée inverse de cosinus DCT
    a. $ct(i,j) = \frac{1}{\sqrt{2}} \sum_{x=0}^{n-1} \sum_{y=0}^{n-1} c(i,j) \cos(\frac{(2x(i,j)+1)i\pi}{2n}) \cos(\frac{(2y(i,j)+1)j\pi}{2n})$
9. Fin Pour
10. Fin Pour
11. Pour i de 1 à n
12. Pour j de 1 à n
13. $\hat{z}(i,j) = ct(i,j) * c(i,j) * z(i,j)$
14. $\widehat{x_i} = x_i$
15. $\widehat{y_i} = y_i$
16. Construire un maillage $\widehat{P_i} = [\widehat{x_i}, \widehat{y_i}, \widehat{z_i}]$
17. Fin Pour
18. Fin Pour

Fin algorithme

Décomposition en série de Fourier: La transformation de Fourier discrète (DFT) est appliquée sur des objets discrets. Le DFT est plus général que DCT, elle décompose la forme géométrique en une série finie de sinus et cosinus (Favreliere, 2009). Elle est exprimée par l'équation (1.4):

$$DFT(u,v) = \sum_{x=0}^{N-1}\sum_{y=0}^{N-1} f(x,y).\exp(-2\pi j\frac{ux+vy}{N}) \quad (1.4)$$

Avec :

$$F(u,v) = \sum_{x=0}^{N-1}\sum_{y=0}^{N-1} f(x,y)\exp(-2\pi\frac{ux+vy}{N}) \quad (1.5)$$

La DFT emploie des coefficients complexes alors que la DCT applique uniquement des coefficients réels. (Raja and Radhakrishnan, 1977) appliquent la décomposition en série de Fourier pour modéliser des mesures de profils. (Chien, 1982) propose des modèles de prédiction basés sur les séries de Fourier pour paramétrer les profils circonférentiels de circularité. (Henke et al., 1999) réalisent une extension de l'approche et proposent (2) types de caractérisation pour décrire la forme géométrique des cylindres. Le premier modèle utilise les DFT pour modéliser les défauts géométriques radiaux et les polynômes de Chebyshev pour les défauts axiaux. Le deuxième modèle applique l'analyse en composantes principales (ACP).

Polynômes de Zernike **:** Les polynômes de Zernike sont composés d'une base descriptive. Ils sont très utilisés dans le domaine optique. Ils permettent de décrire les défauts d'aberrations (Favreliere, 2009). Les polynômes pairs et impairs sont :

$$Z_n^m(\rho,\theta) = U_n^m(\rho,\theta) = R_n^m(\rho)\cos(m\theta) \quad (1.6)$$

$$Z_n^m(\rho,\theta) = U_n^m(\rho,\theta) = R_n^m(\rho)\sin(m\theta) \quad (1.7)$$

$R_n^m(\rho)$ est la fonction radiale avec $n \geq m \geq 0$:

$$R_n^m(\rho) = \begin{cases} \sum_{l=0}^{\frac{n-m}{2}} \frac{(-1)^l(n-l)!}{l!\,(\frac{1}{2}(n+m)-l)!\left(\frac{1}{2}(n-m)\right)!} p^{n-2l} & pour\ n-m\ pair \\ 0 & pour\ n-m\ impair \end{cases} \quad (1.8)$$

Ce paramétrage est décrit dans la norme NF-ISO 10110-5 pour représenter les exigences fonctionnelles en optique. (Favreliere, 2009) présente une description détaillée sur les premiers polynômes de Zernike et sa présentation associée.

***Polynômes de Chebyshev*:** (Summerhays et al., 2002) proposent d'employer le caractère orthogonal des polynômes de Chebyshev T_n pour modéliser des pièces cylindriques. Cette base est exprimée par la fonction :

$$f(x) = \sum_{n=0}^{\infty} a_n T_n(x) \tag{1.9}$$

Avec $T_n = \frac{n}{2} \sum_{k=0}^{E\left(\frac{n}{2}\right)} (-1)^k \frac{(n-k-1)!}{k!(n-2k)!} (2x)^{n-2k} pour\ n \neq 0$

(Pierce and Rosen, 2007) , (Morière et al., 2010) emploient les fonctions polynomiales de degré 2 (les polynômes de Lagrange ou encore les Splines) pour modéliser les surfaces avec défauts. Ce paramétrage s'applique sur des surfaces très variées ce qui nécessite de décomposer la surface en plusieurs zones.

***Harmoniques sphérique* :** Elle permet de paramétrer des formes complexes composées d'harmoniques sphériques dans une base de description. Une surface biparamétrée est écrite comme (Équation. 1.10) :

$$f(\theta, \phi) = \sum_{l=0}^{\infty} \sum_{m=-1}^{l} c_l^m Y_l^m(\theta, \phi) \tag{1.10}$$

Où c_l^m définissent les coefficients des harmoniques sphériques et Y_l^m : les harmoniques sphériques.

***Analyse en composante principale*:** Ce modèle a été créé à l'origine par (Pearson, 1901). Cette analyse est aujourd'hui largement utilisée dans le domaine de l'imagerie numérique et de

l'apprentissage à partir des données. Cette méthode transforme un nombre de variables corrélées en des variables dé corrélées, appelées composantes principales. Ces composantes principales définissent un nouvel espace (généralement à dimensionnalité réduite) pour l'ensemble des données. Le but de l'ACP est d'identifier les structures de dépendance qui existent entre des observations multi variables afin d'obtenir une description ou une représentation compacte de ces dernières. La projection des données permet d'identifier les descripteurs les plus significatifs. Mathématiquement, l'ACP consiste à calculer les valeurs propres de la matrice de covariance. Prenant une matrice. Xp, n donnée, , l'ACP est décrite par (l'équation.1.11) :

$$Y = W^T X \tag{1.11}$$

Où Y est la matrice de la projection des vecteurs de X, et W est la matrice de l vecteurs propres de la matrice de covariance G; où $G = XX^T$. L'inconvénient de l'ACP se situe au niveau de l'invariance temporelle de la représentation obtenue alors que la plupart des processus physiques évoluent au cours du temps. Par conséquent, une mise à jour périodique de la représentation est nécessaire.

1.3.2. Paramétrage par des polynômes

Courbes et surfaces paramétrées **:** Les B-splines, les surfaces NURBS (*Non-Uniform Rational B-Splines*) et les courbes de Béziers, sont les représentations paramétriques les plus courantes.

1. Une courbe de Béziers de $n + 1$ point de contrôle $(P_0, \dots P_n)$ est décrit comme suit : $\sum_{i=0}^{n} B_i^t(t)P_i$ avec $t \in [0,1]$ et où les B_i^n sont les polynômes de Bernstien :

$$B_i^n(u) = \binom{m}{i} u^i (1-u)^{m-i} \tag{1.12}$$

2. NURBS est une courbe qui provient d'une généralisation de B-splines et se définit comme suit :

$$C(t) = \sum_{i=0}^{m-n-1} R_{i,n} P_i \tag{1.13}$$

pour $(m-n)$ points de contrôle P_i, avec $R_{i,n} = \frac{w_i b_{i.n}(t)}{\sum_{j=0}^{m-n-1} w_j b_{j,n}(t)}$ sont les fonctions rationnelles.

Modèles de contours actifs **:** Plus connus sous le nom de *Snakes,* ces modèles sont employés pour approximer des formes ou des contours dans la segmentation de l'imagerie médicale. Ces modèles sont des splines paramétrés (Kass et al., 1988). Leur principe consiste à minimiser une fonction d'énergie d'une courbe qu'on déplace d'une manière itérative. On considère une image 2D définit par les coordonnes (x,y), le vecteur de contour est:

$$v(s,t) = (x(s,t), y(s,t))^T \tag{1.14}$$

Où $s \epsilon$ [0,1] est l'abscisse curviligne, t est le temps et [0,1] sont les extrémités de courbe.
La fonction de l'énergie du contour est:

$$\varepsilon(v) = S(v) + P(v) \tag{1.15}$$

Avec $S(v)$ l'énergie interne de déformation de la courbe:

$$S(v) = \int_0^1 w_1(s) \left|\frac{\delta v}{\delta s}\right|^2 + w_2(s) \left|\frac{\delta^2 v}{\delta^2 s}\right|^2 ds \tag{1.16}$$

Le premier terme $w_1(s)$ vérifie la continuité de la courbe appelée élasticité. Le deuxième terme $w_2(s)$ qui est le terme de rigidité vérifie la rigidité du contour de déformation. $w_1(s)$ et $w_2(s)$ sont deux coefficients de régularisation et $P(v)$ est l'énergie de la fonction $P(x,y)$:

$$P(v) = \int_0^1 P(v(s))\, ds \tag{1.17}$$

Enveloppe convexe **:** Les enveloppes convexes sont bien utilisées dans le domaine de l'imagerie. Ce modèle permet de définir une région englobant tous les points. En mécanique, l'enveloppe convexe est utilisée pour évaluer les tolérances de planéité (Ceglarek, 2002). Ils permettent aussi de calculer les points de contact.

Les formes technologiques **:** Ce paramétrage consiste à reconstruire la forme géométrique par des fonctions polynomiales ou trigonométriques. Il se base sur l'utilisation d'une famille de formes technologiques, qui ont un sens physique (ex. déformation en suivant les modes propres). La base technologique est un ensemble de surfaces qui représentent différents types de défauts qui sont imaginés pour simuler les surfaces fabriquées. Les équations de surfaces sont :

$$Z_1 = \frac{xy}{150^2} \tag{1.18}$$

$$Z_2 = 2H(x) - 1 \tag{1.19}$$

$$Z_3 = 2\frac{1000 - \sqrt{1000^2 - y^2}}{1000 - \sqrt{1000^2 - 150^2}} \tag{1.20}$$

Les surfaces considérées sont une surface torsadée (Z_1), une surface avec une marche (Z_2) et une surface courbe (Z_3) (Ballu et al., 2017).L'algorithme 1.2 décrit l'aspect conceptuel de l'algorithme décrit par (Ballu et al., 2017) de complexité algorithmique cubique $O\ (n^3)$.

Algorithme 1.2. Pseudocode de l'algorithme de génération des surfaces par les formes technologiques (Ballu et al., 2017)

Algorithme 1.2- Pseudocode de l'algorithme de génération des surfaces par les formes technologiques (Ballu et al., 2017)

Entrées: n: nombre de points, a_1 =0.02, a_2 = 0.01 et a_3 = 0.015, μ=0; σ: paramètre d'écart type. m=100: nombre de surfaces.
Variables: z_{T1}=$[x, y]$: une surface tordue, z_{T2}=$[x, y]$: une surface à une étape, z_{T3}=$[x, y]$: une surface incurvée.
Sortie: $T = [x_n, y_n, z_n]$: Surface plane déformé.

Début algorithme

1. Création de grille $T = [x, y]$ de $n \times n$ points.
2. Générer des données pour l'axe z.
3. Pour i de 1 à n:
4. Pour j de 1 à n:
   a. z_{T1}(i,j)← x(i,j)*y(i,j)/ 150^2
   b. $z(i,j)$ ←heaviside($x(i,j)$)
   c. $z_{T2}(i,j)$ ←2* $H(i,j) - 1$
   d. $z_{T3}(i,j)$ ←$(1 - 2 * \left(1000 - \sqrt{1000^2 - y(i,j)^2}\right)$/(1000-$\sqrt{1000^2 - 150^2}$)
   e. $z(i,j) \leftarrow a_1 z_{T1}(i,j) + a_2 z_{T2}(i,j) + a_3 z_{T3}(i,j)$
5. Fin Pour
6. Fin Pour

7. Construire un maillage de $T_{z1} = [x, y, z_{T1}], T_{z2} = [x, y, z_{T2}], T_{z2} = [x, y, z_{T3}]$.
8. Pour i de 1 à m:
   a. Générer un nombre aléatoire à partir de la distribution normale :
   b. a_1 ←normrnd(0,sqrt(a_1),1,1); a_2 ←normrnd(0,sqrt(a_2),1,1);
   c. a_3 ←normrnd(0,sqrt(a_3),1,1);
   d. $z \leftarrow a_1 z_{T1}(i,j) + a_2 z_{T2}(i,j) + a_3 z_{T3}(i,j)$
   e. Construire un maillage $T = [x, y, z]$.
9. Fin Pour

Fin algorithme

1.3.3. Paramétrage par décomposition modale discrète

L'équipe SYMME (Pitard et al., 2017) a introduit un nouveau paramétrage basé sur la corrélation entre la vibration et les défauts géométriques d'une cloche. Ce paramétrage consiste à construire une base de défauts. Cette dernière est définie par des primitives géométriques (cercle, sphère, plan, etc.). Une analyse vibratoire de ces surfaces permet de dégager les modes propres de vibration, dont chaque mode décrit une géométrie, définissant les défauts de forme d'une surface. Les modes sont déduits à partir de l'équation différentielle:

$$\boldsymbol{M}.\frac{\partial^2 \boldsymbol{u}}{\partial t^2} + \boldsymbol{K}.\boldsymbol{u} = 0 \tag{1.21}$$

Où $\boldsymbol{K}$ est la matrice de rigidité, $\boldsymbol{M}$ est la matrice de l'inertie et $\boldsymbol{u}$ est le vecteur des déplacements. La résolution de l'équation 1.21 donne :

$$\left(\boldsymbol{M}^{-1}\boldsymbol{K} - \frac{1}{w_i}.\boldsymbol{I}\right).\boldsymbol{Q}_i = 0 \tag{1.22}$$

Où $\boldsymbol{I}$: est la matrice identité. La résolution de l'Équation (1.22) permet de calculer les modes propres $\boldsymbol{Q_i}$ correspondant à la pulsation (fréquence) w_i. Pour modéliser des surfaces avec de défauts de forme, il faut diviser la surface puis calculer les modes, et générer les coefficients modaux. Chaque surface est décrite avec l'équation (1.23) :

$$\boldsymbol{Ms} = \boldsymbol{Q}\,\boldsymbol{m} \tag{1.23}$$

Où $\boldsymbol{Q}$ est la matrice des modes et $\boldsymbol{m}$ est le vecteur des coefficients.

Tableau 1.2 résumé des techniques de paramétrage de surfaces

Type de Paramétrage	Technique	Auteurs	Année	Images
Global	Décomposition en cosinus	Ahmed et al. (Ahmed et al., 1974)	1974	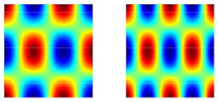
		Raja et Radhakrishnan (Raja and Radhakrishnan, 1977)	1977	
		Huang et Ceglarek (Huang and Ceglarek, 2002)	2002	
		Lecompte et al.(Lecompte et al., 2010)	2010	
	Décomposition en série de fourrier	Chien (Chien, 1982)	1982	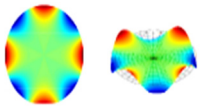
		Henke et al. (Henke et al., 1999)	1999	
	Polynômes de Zernike	Veitenhansl et al (Veitenhansl et al., 2004)	2004	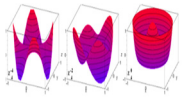
		Sicam et al. (Sicam et al., 2004)	2004	
		Novotni et Klein (Novotni and Klein, 2004)	2004	
	Polynômes de Tchebychev	Summerhays et al. (Summerhays et al., 2002)	2002	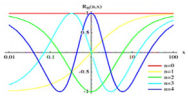
		Morière et al , (Morière et al., Morière et al., 2010)	2009	
	Harmoniques sphériques	Zhao et al. (Zhao et al., 2000)	2000	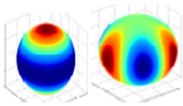
		Wang et Lai (Wang and Lai, 2008)	2008	
		Kanada (Kanada, 1995)	1995	
	Analyse en composantes principales (ACP)	Pearson (Pearson, 1901)	1901	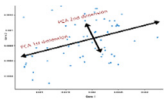
Local	Les formes technologiques	Yan et Ballu. (Yan and Ballu, 2017)	2017	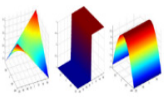
	Décomposition modale discrète	Pitard et al.(Pitard et al., 2017)	2017	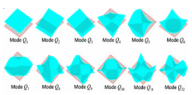
	Modèles de contours actifs	Kass et al. (Kass et al., 1988)	1988	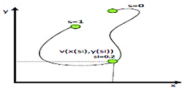

Nous constatons que dans la littérature, il y a plusieurs travaux de la modélisation de défauts de forme. Historiquement, les polynômes de Zernike sont les premiers à être utilisés pour l'écriture de défauts de forme dans le domaine d'optique, ils ont été appliqués par la suite à des surfaces complexes. Dans le domaine médical l'imagerie 3D, il existe une richesse de travaux pour paramétrer des images de forme très volumineuses (ex. les organes internes des patients). Dans le domaine mécanique, les défauts de forme ont été paramétrés par les séries de Fourier en se limitant à des surfaces biparamétrées (ex. plans, cylindres en général). Les fonctions polynomiales sont limitées par la complexité des défauts. Les surfaces de Béziers souvent sont utilisées pour paramétrer des surfaces dans une application de CAO.

1.4. Génération des assemblages des surfaces avec des défauts géométriques

Matrice de transformation: Dans l'assemblage de deux pièces (#1 et #2), la matrice de transformation (appelée aussi matrice de passage B) permet de paramétrer les déplacements de #2 par rapport à #1. L'expression du déplacement d'un point P_2 de la pièce #2 est en fonction des angles de la matrice de rotation et des composantes de la vectrice translation (Samper et al., 2009). La représentation mathématique générale de la matrice de passage est l'équation 1.23.

$$B = R_{12}A + t \tag{1.23}$$

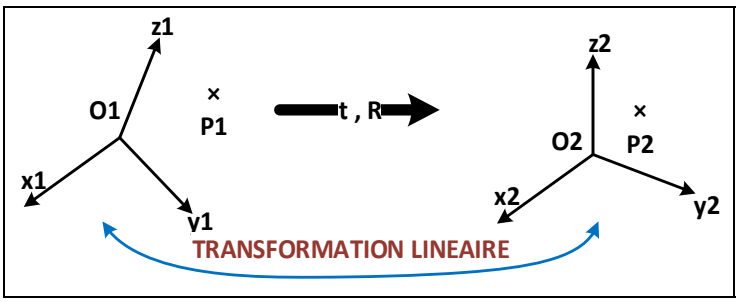

Figure 1. 6 Transformation rigide linéaire [(Petit, 2004)]

En considérant deux repères R_1 et R_2 attachés respectivement aux pièces #1 et #2, les déplacements entre les deux pièces reviennent à calculer la position des repères R_2 par rapport à R_1.

Le vecteur déplacement est :

$$t = \overrightarrow{dP} = \overrightarrow{P_1P_2} \tag{1.24}$$

Avec le point P_1 lié à la pièce #1, O_1 l'origine du repère lié à la pièce #1, O_2 l'origine du repère. Le déplacement du point P_2 est:

$$\overrightarrow{P_1P_1} = \overrightarrow{P_1O_1} + \overrightarrow{O_1O_2} + \overrightarrow{O_2P_2} \rightarrow \overrightarrow{dP} = -\overrightarrow{O_1P_1} + \overrightarrow{dO} + O_2P_2 \tag{1.25}$$

$$\overrightarrow{dP} = \overrightarrow{dO} + (R - I_3).\overrightarrow{O_1P_1} \tag{1.26}$$

Avec $\overrightarrow{dO} = \overrightarrow{O_1O_2}$ le vecteur de translation de la position d'origine O_2 de repère R_2 au repèreR_1, la matrice R représente la rotation du repère R_2 au repère R_1 est calculé par le produit des trois matrices de rotation (autour des axes x, y, z).

$$R_x(px) = \begin{pmatrix} 1 & 0 & 0 \\ 0 & \cos(px) & -\sin(px) \\ 0 & \sin(px) & \cos(px) \end{pmatrix} \tag{1.27}$$

$$R_y(py) = \begin{pmatrix} \cos(py) & 0 & \sin(py) \\ 0 & 1 & 0 \\ -\sin(py) & 0 & \cos(py) \end{pmatrix} \tag{1.28}$$

$$R_z(pz) = \begin{pmatrix} \cos(pz) & -\sin(pz) & 0 \\ \sin(pz) & \cos(pz) & 0 \\ 0 & 0 & 1 \end{pmatrix} \tag{1.29}$$

Donc[1],

[1] $\mathrm{c} = \cos(\dots)\ et\ s = \sin(\dots)$

$$R_{xyz} = \begin{pmatrix} \mathrm{c}(py)\,\mathrm{c}(pz) & -\mathrm{c}(py)\,\mathrm{s}(pz) & \mathrm{s}(py) \\ \mathrm{s}(px)\,\mathrm{s}(py) & \mathrm{c}(pz) + \mathrm{c}(px)\,\mathrm{s}(pz) & -\mathrm{s}(px)\,\mathrm{s}(py)\,\mathrm{s}(pz) + \mathrm{c}(px)\,\mathrm{c}(pz) & -\mathrm{s}(px)\,\mathrm{c}(py) \\ -\mathrm{c}(px)\,\mathrm{s}(py)\,\mathrm{c}(pz) + \mathrm{s}(px)\,\mathrm{s}(pz) & \mathrm{c}(px)\,\mathrm{s}(py)\,\mathrm{s}(pz) + \mathrm{s}(px)\,\mathrm{c}(pz) & \mathrm{c}(px)\,\mathrm{c}(py) \end{pmatrix} \quad (1.30)$$

Le développement au premier ordre de la matrice de rotation est exprimé par la matrice R:

$$R = \begin{pmatrix} 1 & -pz & py \\ pz & 1 & -px \\ -py & px & 1 \end{pmatrix} \quad (1.31)$$

Torseurs de petits déplacements (TPD) Cette méthode est employée pour modéliser les variations des éléments tolérancés. Aussi, elle permet de aussi de paramétrer les déplacements d'une surface associée d'une surface réelle par rapport à une surface nominale (Petit, 2004). Le TPD a donné lieu à plusieurs concepts :

1. Le concept SATT permet de distinguer les géométries associées aux surfaces. Sept classes ont été définies pour décrire les liaisons entre les surfaces.
2. Le concept EGRM représente l'ensemble minimum pour décrire la liaison d'une classe.

Le produit d'une matrice antisymétrique de l'équation (1.30) devient :

$$\overrightarrow{dP} = \overrightarrow{dO} + \overrightarrow{P_1O_1} \wedge \overrightarrow{d\theta} \quad (1.32)$$

Avec $\overrightarrow{dO}$ le vecteur de translation de la pièce 2 par rapport à la pièce 1 et $\overrightarrow{d\theta}$ le vecteur de rotation de la pièce 2. Les déplacements des points peuvent être exprimés par le TPD, le torseur contient six composantes :

$$\{T\} = \begin{bmatrix} p_x & \varepsilon_x \\ p_y & \varepsilon_y \\ p_z & \varepsilon_z \end{bmatrix} \quad (1.33)$$

Bien que la modélisation des défauts d'orientation et de localisation semble être aujourd'hui à la portée de plusieurs logiciels commerciaux, vu l'intérêt donné par les chercheurs par rapport ce sujet, la modélisation des tolérances de forme est loin d'être solutionnée. Récemment, une intense activité de recherche est en cours sur cette problématique.

Comme mentionné précédemment, les défauts de forme influencent les requis fonctionnels d'une pièce ainsi que les défauts dimensionnels (Samper et al., 2009). Une pièce avec défauts de forme est un modèle de surface qui comprend des écarts géométriques des pièces fabriquées. Ces imperfections géométriques des surfaces peuvent être classées en trois (3) catégories distinctes par le filtrage ; les défauts de forme, l'ondulation et la rugosité. Ils ne sont pas de mêmes grandeurs, on les quantifie généralement sur une ligne (2D) ou sur une surface (3D). Une décomposition en séries de Fourier permet de distinguer les amplitudes. Les défauts de forme ont les plus grandes longueurs d'onde. La rugosité a une très courte longueur d'onde (Samper et al., 2009).

Ces classes d'écarts géométriques diffèrent en termes de relation entre la distance et la profondeur des imperfections. Cependant, cette classification n'est pas parfaitement disjointe (Schleich et al., 2014). Les écarts géométriques décrits peuvent en outre être distingués entre les déviations systématiques et aléatoires. Cette classification est basée sur l'expérience que dans de nombreux processus de fabrication, des écarts géométriques similaires peuvent être observés sur chaque pièce, tandis que certaines déviations géométriques ne peuvent être observées que sur quelques pièces. Les écarts systématiques sont déterministes, prévisibles et reproductibles et peuvent dépendre du processus de fabrication, tels que les produits d'erreurs de serrage ou le comportement dynamique de la machine. Contrairement à cela, les écarts aléatoires proviennent des fluctuations du processus de production telles que l'usure de l'outil, les propriétés variables du matériau ou les fluctuations des paramètres environnementaux (température, humidité, etc.).

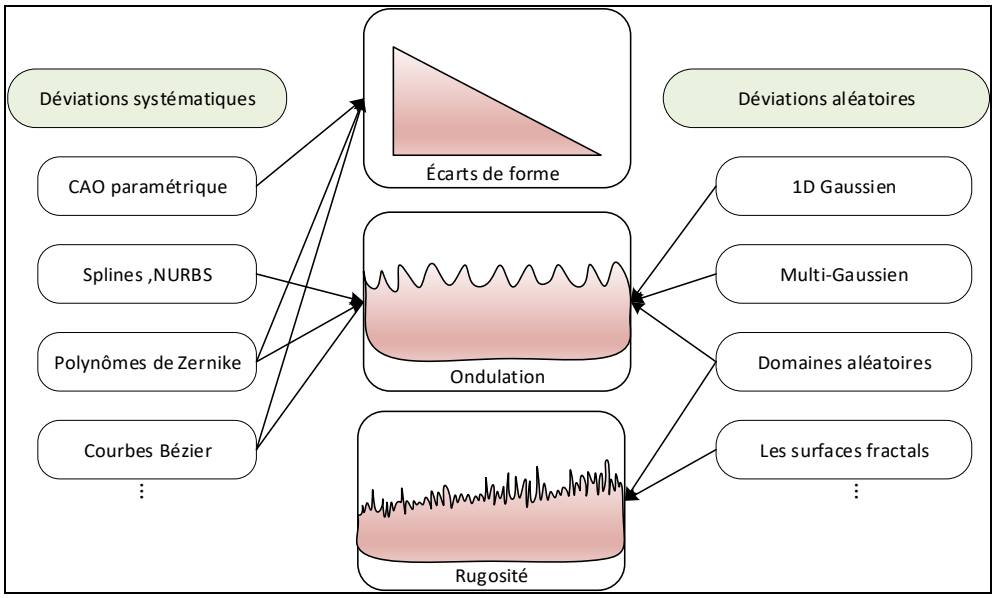

Figure 1. 7 Les classes d'écarts géométriques [tiré de (Schleich et al., 2014)]

Les normes ISO et ASME proposent la génération d'ensembles de données de référence basés sur les données nominales d'une caractéristique (Samper, 2007), à laquelle des écarts de forme sont ajoutés en déformant les données de caractéristiques nominales par des séries de Fourier. Ensuite, un bruit blanc gaussien est ajouté aux points d'échantillonnage afin de prendre en compte les erreurs de balayage. L'accumulation des écarts en assemblage aéronautique est difficile à modéliser et prédire en raison de la complexité intrinsèque tout au long du processus de propagation des incertitudes (Jin et al., 2018).

Au début, quelques approches ont été développées pour modéliser le problème des variations dimensionnelles (Chase and Parkinson, 1991). Cependant, les écarts géométriques tels les défauts de forme sont ignorés. Afin de combler cette lacune, les chercheurs ont utilisé l'analyse des déviations en trois dimensions (Salomons et al., 1996) , (Shen et al., 2005) et cette analyse a connu un développement rapide dès le début des années 1990. Les premières approches développées étaient le réseau des zones et des référentiels (Fleming, 1988), le modèle cinématique (Rivest et al., 1994) et la chaîne dimensionnelle spatiale (Portman and Weill, 1996) qui se concentre sur l'expression des déviations seulement. L'intérêt aux défauts de forme se traduit par une étude expérimentale réalisée par (Lê et al., 2014). Deux (2) concepts

sont appliqués :1) le domaine jeu et 2) la surface des différences. Le problème de contact est simplifié en considérant une surface parfaite et une autre appelée surface de différence. La surface de différence est la surface dont les défauts sont reportés. Le domaine de jeu donc est l'espace de déplacement possible.

(Favreliere, 2009) a étudié l'effet des défauts de forme dans un processus d'assemblage. L'évaluation de l'écart entre les surfaces associées montre que les défauts de forme géométriques influent sur la position relative des surfaces. Cet écart est évalué par le torseur de petit déplacement et par la méthode des domaines. Les points de contact sont définis comme étant la facette de contact calculée par l'enveloppe convexe de la surface. La méthodologie développée est efficace pour les assemblages de pièces indéformables, sans jeu et effort imposés.

Plus récemment (Adragna et al., 2010) ont réalisé des travaux similaires. Ils proposent une méthode qui permet d'identifier le domaine de contact d'une liaison de deux (2) plans avec de défauts de forme modélisée par une paramétrisation modale. La méthode proposée considère le positionnement de la paire de surfaces avec une force externe pour identifier les points de contact. L'assemblage présenté est un appui plan entre un plan parfait associé par le critère de moindre carré et un autre plan avec une déviation de forme appelé surface de distance, les formes sont en contact si deux distances d'une liaison sont mises à zéro. Les points de contact et les facettes possibles sont identifiés par le calcul de la surface convexe qui filtre les points de contact possibles. Plusieurs paramètres sont identifiés comme influents tels que la rectitude de l'écart de forme et la localisation de la forme.

Une autre étude sur l'intérêt de la considération des défauts de forme dans des liaisons est réalisée par (Grandjean et al., 2013). Les défauts géométriques y sont créés à l'aide de la méthode modale. La simulation d'assemblage consiste à définir une facette de contact de l'enveloppe convexe. Le TPD est utilisé pour analyser le respect de l'exigence fonctionnelle. Ils proposent le taux de non-conformité est comme un niveau de performance d'une spécification fonctionnelle de l'assemblage. L'assemblage étudié est un appui plan de deux

surfaces planes avec défauts de forme et position. L'interpénétration est vérifiée pour chaque positionnement relatif de la partie interne sur l'extérieur. Le positionnement relatif est trouvé par les rotations extrêmes. Une approche itérative est utilisée pour trouver les deux rotations extrêmes dans la liaison. Ces travaux montrent que les écarts de forme des pièces influent non seulement sur leur positionnement relatif, mais ont également un impact sur le domaine de jeu d'assemblage de la liaison mécanique.

(Lê et al., 2014) proposent une étude expérimentale et théorique dans des liaisons avec des défauts de forme. Deux (2) concepts théoriques sont appliqués: 1) le domaine jeu et 2) la surface des différences. Le problème de contact est simplifié en considérant une surface parfaite et une autre appelée surface de différence. La surface de différence est la surface dont les défauts sont reportés. Le domaine de jeu donc est l'espace de déplacement possible. Le domaine jeu est calculé par les contraintes et les inégalités décrites par les points de la surface des différences, ces contraintes correspondent à un demi-espace dans l'espace des petits déplacements. Un nouveau changement de paradigme pour la modélisation des variations géométriques en génie mécanique : *les formes de modèles de peau*, qui sont des représentants géométriques discrets, telles que les nuages de points et les maillages de surface. La forme de modèle de peau est un modèle abstrait de l'interface physique entre une pièce et son environnement. Le modèle de la peau (*Skin Model*) est un modèle infini et ne permet pas l'identification ou la simulation puisque la surface de la pièce théorique comprend un nombre infini de points (Schleich et al., 2014). Cependant, une opérationnalisation pour obtenir un modèle fini prêt pour la simulation est nécessaire. Ceci conduit à l'idée de formes de modèle de peau. En synthèse, la forme de modèle de peau est un outil conceptuel utile pour toutes les personnes impliquées dans la conception, la fabrication et l'inspection d'ingénierie. Le processus de génération de forme de modèle de peau est divisé en deux (2) phases une 1) phase de prédiction et une 2) phase d'observation par rapport aux informations disponibles et aux connaissances sur les déviations géométriques attendues. Ces formes de modèle de peau générées peuvent ensuite être utilisées dans diverses simulations d'ingénierie, telles que des analyses d'assemblage ou des simulations de tolérance pour prédire le comportement ultérieur du produit.

(Schleich and Wartzack, 2016) appliquent les formes de modèle de peau à l'analyse de tolérance assistée par ordinateur pour simuler le positionnement relatif et l'assemblage en tenant compte de différents types d'écarts. Dans ce contexte, le terme « Positionnement relatif » décrit le positionnement d'une pièce numérique représentative par rapport à d'autres représentants de pièces dans un assemblage. Ils introduisent deux (2) classes d'approches pour le positionnement relatif des formes de modèles de peau discrètes pour l'application dans l'analyse de tolérance assistée par ordinateur, à savoir 1) les techniques d'alignement et 2) un algorithme basé sur la différence de surface. Les deux (2) classes sont discutées et comparées dans (Schleich and Wartzack, 2016), (Schleich and Wartzack, 2015) proposent une nouvelle approche pour l'analyse de tolérance assistée par ordinateur, à savoir l'analyse de tolérance basée sur le modèle de la peau une étude comparative aussi de trois (3) approches d'analyse de la tolérance est faite, à savoir 1) les empilements de tolérance, 2) les boucles vectorielles, et 3) l'analyse de tolérance basée sur le torseur de petit déplacement. , l'algorithme 1.3 décrit l'aspect conceptuel de la nouvelle approche de (Schleich and Wartzack, 2016).

Ces trois (3) méthodes sont comparées quantitativement à l'analyse de tolérance basée sur des modèles de peau en considérant une étude de cas typique. La nouveauté de la contribution réside dans l'évaluation approfondie de ces approches et de leurs résultats. Ils montrent que l'analyse de tolérance basée sur les modèles de peau conduit à des résultats comparables à ceux des trois approches d'analyse de tolérance établies dans le cas où les écarts de forme sont considérés comme étant nuls. Ainsi, l'analyse de tolérance basée sur *Skin Model Shapes* permet une prédiction plus réaliste des caractéristiques d'assemblage dans le développement de produits virtuels et prend donc en charge la gestion holistique des variations géométriques. Les travaux de l'étude expérimentale sur le comportement de l'assemblage des défauts de forme sont limités et amènent parfois des écarts importants par rapport à la simulation. Toutes les recherches effectuées montrent que les défauts de forme ont une influence sur l'assemblage final. L'algorithme 1.3 présente l'aspect conceptuel de l'approche de la modélisation des variations géométriques proposée par (Schleich and Wartzack 2016).

Dans le même contexte, notre première contribution (Jbira et al., 2017) a permis de développer une approche de modélisation et de simulation pour prendre en compte l'effet des tolérances

de forme et de profil des pièces rigides. Notre approche permet de générer automatiquement des assemblages réalistes en redéfinissant les contraintes d'assemblage. Cette modélisation réaliste permet ainsi une analyse de tolérance en prenant en compte de l'évolution des contacts entre les composants au cours du fonctionnement du produit. Les impacts de tolérance sur le mouvement d'assemblage réaliste sont quantifiés. Cette approche fournit un résultat d'assemblage plus proche de l'assemblage réel du système mécanique. Le modèle d'analyse des tolérances développé ne pris pas en considération les conditions de déplacements et les forces subies par les pièces assemblées.

Tout récemment, dans les travaux de (Yan and Ballu, 2017), (Yan and Ballu, 2018) ont présenté les modèles de simulations et les conditions d'assemblage en tenant compte des défauts de forme. Pour fournir une prédiction de résultat de l'assemblage, un assemblage virtuel des pièces avec défauts de fabrication a été simulé. Pour simuler l'assemblage avec des conditions réelles, différents facteurs sont considérés comme la modélisation de forme de surface avec des déviations de fabrication, les conditions de déplacement (ex. forces de réactions internes, conditions aux limites).

Algorithme 1.3. Pseudocode de l'algorithme de la modélisation des variations géométriques de (Schleich and Wartzack 2016)

Algorithme 1.3- Pseudocode de l'algorithme de la modélisation des variations géométriques de (Schleich and Wartzack 2016)

Entrées: n: nombre de points, $P_i = [x_i, y_i, z_i]$: nuage de points (modèle nominal)
Variables: h_{P_i}: la déviation systématique**.**
v : Matrice des vecteurs propres.
D: Matrice diagonale des valeurs propres.
A: Matrice de transformation
μ: Vecteur moyen du champ aléatoire
$n_i = [a_i\, b_i c_i]^{\,T}$: direction de déviation choisie pour le point i.
σ: Matrice des écarts-types
ε: Vecteur de variables aléatoires de moyenne nulle et variance d'unité
χ: Vecteur de valeurs aléatoires
Sorties:
$\widehat{P_i} = [\widehat{x_i}, \widehat{y_i}, \widehat{z_i}]$: Nuage de points avec déviation systématique.
$\widetilde{P_i} = [\widetilde{x_i}, \widetilde{y_i}, \widetilde{z_i}]$: Nuage de points avec déviation systématique et aléatoire.

Début Algorithme:

1. Extraire les données d'une entité d'un nuage de points $P_i[x_i, y_i, z_i]$
2. **Fonction de Modélisation des déviations systématiques**
    a. Appliquer les formes quadriques
    b. $0 = ax^2 + by^2 + cz^2 + 2fyz + 2gyzx + 2hxy + 2px + 2qy$
    c. Choisissez une forme de second ordre
    d. $\widehat{P_i}$=$P_i + h_{P_i} n_i$
3. **Fonction de Modélisation des déviations aléatoires**
    a. Appliquer la méthode champ aléatoire
    b. Appliquer le PCA
    c. Calculer la matrice de corrélation ρ
    d. Calculer la matrice de transformation:
    e. $A = VD^{1/2}$
    f. Calcule le vecteur sommet normal n_i
    g. Calculer le vecteur de valeurs aléatoires χ :
    h. $X = \mu + \sigma A \varepsilon$
    i. Ajouter la déviation aléatoire au modèle avec systématique déviations
    j. $\widehat{P_i}$=$\widehat{P_i} + X_i n_i$

Fin algorithme

Pour conclure cette partie, nous pouvons retenir que les travaux expérimentaux sur le comportement de l'assemblage avec des défauts de forme sont relativement limités et amènent quelquefois des écarts importants. Toutes les recherches effectuées montrent que les défauts de forme ont une influence sur l'assemblage. Toutes les études de cas réalisées sont de type appui plan ou cylindre. La non-prise en compte de défauts de forme conduit à calculer des spécifications sur chacune des pièces qui engendrent des assemblages non conformes. Finalement, la prise en considération des écarts de pièces dans la modélisation virtuelle de mécanisme assemblée demeure un défi d'actualité dans la recherche sur le tolérancement assisté par ordinateur.

1.5. Conversion d'un nuage de points vers une caractéristique

La taille est un descripteur fondamental des objets. Elle nous permet de quantifier les objets et de comparer et classifier les objets en fonction de cette notion. Dans le monde de la spécification des produits géométriques de l'Organisation Internationale de Normalisation (ISO), la taille est définie beaucoup plus étroitement : elle est limitée aux caractéristiques de taille et les méthodes d'induction des valeurs de taille d'une pièce réelle sont strictement contrôlées. La publication de l'ISO 14405-1: 2010 a introduit un nouvel ensemble de modificateurs de taille, incluant les tailles locales à deux points et sphériques, les moindres carrés, les associations maximales et minimales circonscrites, ainsi que les diamètres calculés (déduits de la circonférence, zone ou volume de la caractéristique d'intérêt). D'autres modificateurs permettent la spécification de statistiques de mesures de taille locale, telles que le maximum, le minimum, la moyenne et autres (Morse and Srinivasan, 2013). La taille (*Size*) y est présentée comme une notion d'ingénierie à partir de plusieurs points de vue et retracer son évolution dans les dessins d'ingénierie. On y discute dans l'étude des implications de l'utilisation des modificateurs de taille récemment normalisée dans la conception technique et dans l'interprétation de ces extensions à la taille. Dans notre deuxième contribution, nous avons développé quatre algorithmes des modificateurs GG, GN, SN, et GX définit par la norme ISO14405-1 :2010. Une étude comparative de ces algorithmes (Complexité algorithmique,

temps de réponse et hyperparamètre etc.) a été réalisé, et elle a fait l'objet d'une publication IEEE (Voir Annexe III).

Dans ces dernières années, certaines approches ont été développées pour convertir un nuage de points en une caractéristique (taille, erreur de circularité etc.); (Nurunnabi et al., 2018) ont proposé un nouvel algorithme robuste d'ajustement de cylindre 3D. Ils ont démontré des performances sur des nuages de données artificiels et réels, en présence de valeurs aberrantes et de bruit, et dans le cas d'un nombre petit et grand de points et pour différentes tailles de rayon. Ils ont proposé d'utiliser une approche hybride qui compose deux algorithmes robustes PCA et a régression linéaire, l'algorithme 1.4 décrit l'aspect conceptuel de l'approche proposée par (Nurunnabi et al., 2018). (Zhao et al., 2018) ont proposé de calculer les tailles réelles par réseau de neurones (RNN). Les modèles formés pour l'évaluation des tailles calculées ont été vérifiés. Les résultats pourraient satisfaire à l'exigence de précision de mesure de la taille calculée. Cela peut être un moyen de résoudre le problème de la taille calculée des cylindres pour la mise en œuvre du ISO 14405-1. Récemment (Guo and Yang, 2019) ont proposé une nouvelle procédure pour l'ajustement de cercle. Ils ont utilisé l'approche de Taubin pour calculer la centre et rayon, puis ils ont identifié et enlevé les valeurs aberrantes en calculant les distances géométriques des points de données au cercle. Leurs expériences ont démontré que la procédure itérative peut résister à l'effet des valeurs aberrantes.

Dans l'assemblage de pièces circulaires, les tolérances dimensionnelles sur le diamètre ne suffisent pas, elles doivent être accompagnées par un contrôle géométrique (forme : circularité ou cylindricité). Ceci a alimenté nos réflexions et nous a poussés à investiguer l'influence algorithmique sur l'évaluation du diamètre et du défaut de circularité à partir d'un ensemble fini de points de mesure.

Algorithme 1.4. Pseudocode de l'algorithme de conversion d'un nuage de points en cylindre de (Nurunnabi, Sadahiro, and Laefer 2018)

Algorithme 1.4 - Pseudocode de l'algorithme de conversion d'un nuage de points en cylindre

Entrées: n: Nombre de points, $P(x, y, z)$: Nuage de points, ⌀: Diamètre nominal, t: La taille de simulation de Monte Carlo, v: Bruit de mesure, μ=0, σ: Paramètre d'écart type.
Sortie: d:Diamètre de cylindre; C: Centre de cylindre; R: Rayon de cylindre, Longueur de cylindre L, O : Orientation de cylindre.

Début Algorithme:

4. Extraire les données cylindriques d'un nuage de points $P(x, y, z)$
5. Ajouter un bruit de mesure par une simulation de Monte-Carlo
6. Pour chaque cylindre C:
7. Pour i=1 à t:
8. Pour j=1 à n:
9. Générer des nombres aléatoires gaussiens a
10. $x_n(i,j) \leftarrow x(j,1) + a\, cos(theta(j,1))$;
11. $y_n(i,j) \leftarrow y(j,1) + a\, sin(theta(j,1))$;
12. $z_n(i,j) \leftarrow z\,(j,1)$;
13. Appliquer la fonction RPCA (Robust Principal Component Analysis) sur $[\, p_i(x_n(i,j), y_n(i,j), z_n(i,j))$ pour $i = [1 \dots n]]$.
14. Trouvez les PCs vecteurs propres (v_1 , v_2 et v_3) et valeurs propres (γ_1, γ_2,et γ_3).
15. Projetez le nuage de points 3D $[p_i = (x_i, y_i, x_z)\ pour\ i = [1 \dots n]$ pour obtenir des points 2D.
16. q_i =$(v_2, v_3)^t$ (p_i-p)
17. [(a,b),r] ← Ajustement du cercle q_i avec la fonction LSR (Least Square Regression)
18. Construire des paramètres de cylindre (C, R, L, O):
19. $C = c$.
20. $R = r$.
21. $L = \max(p_i^t v_2) - \min(p_i^t v_2)$
22. $O = v_2$.
23. Fin Pour
24. Fin Pour

Fin algorithme

Dans cette étape de notre étude, nous étudions l'influence de défaut de forme sur les requis dimensionnels et géométriques dans le cas spécifique des éléments cylindriques. Nous nous concentrerons sur l'influence de défauts de forme sur l'identification des requis dimensionnels et géométriques, plus précisément sur les nouveaux modificateurs de spécifications des

tolérances de taille, telles que définies dans ISO 14405-1. Nous étudions comment les stratégies de mesure des systèmes influents sur différents algorithmes pour l'évaluation de ces nouvelles spécifications. Un logiciel d'analyse a été développé pour comparer la sensibilité de différents paramètres (nombre de points, amplitude de bruit et nature du défaut de circularité) sur les modificateurs ISO 14405-1.

1.6. Objectifs de la recherche

L'objectif principal de ce projet de recherche est de **développer une méthodologie robuste et précise pour estimer ou simuler lors de l'assemblage les spécifications géométriques de forme.**

À titre complémentaire, les sous-objectifs de la recherche proposée seront :

- **Objectif 1 :** Développer des approches de modélisation et de simulation pour prendre en compte de l'effet des défauts de forme lors de l'assemblage de pièces rigides. *Comment peut-on simuler le comportement à l'assemblage des composants rigides ayant un défaut de forme ?*
- **Objectif 2 :** Proposer des algorithmes qui permettent de générer automatiquement des assemblages réalistes en redéfinissant les contraintes d'assemblage, tout en considérant les défauts de forme (toujours pour des pièces rigides). Cette modélisation réaliste permet une analyse (ou une synthèse) de tolérances en prenant en compte de l'évolution des contacts entre les composants au cours du fonctionnement du produit.
- **Objectif 3 :** Étudier l'effet de l'erreur (ou le choix) algorithmique sur l'estimation de la taille et la localisation des éléments géométriques affectées par une erreur de forme selon les modificateurs proposés par la norme ISO 14405-1 :2016.
- **Objectif 4 :** Investiguer la reproductibilité des logiciels d'inspection assistée par ordinateur dans le cas de l'évaluation des défauts de forme.
- **Objectif 5 :** Proposer de nouvelles approches robustes pour l'estimation de la taille des éléments géométriques affectée par une erreur selon la norme ISO 14405-1 : 2016.

1.7. Contributions scientifiques projetées du projet

La recherche proposée contribue à évoluer la capacité de prédiction des modèles de synthèse de tolérances en incluant les défauts de forme. Comme mentionné précédemment, aujourd'hui des modèles de simulation existent dans des outils commerciaux et qui permettent d'inclure lors de l'exercice de tolérancement les défauts de localisation et d'orientation (Mehdi et al., 2013) (Tlija et al., 2019). Si plusieurs recherches se sont déjà penchées sur la génération et la modélisation des défauts de forme (ex. planéité, circularité, etc.), à notre connaissance, seulement des solutions limitées (Yan and Ballu, 2018) ont proposé d'inclure les effets des défauts de forme et profil (sans référentiels/Datum) dans le cas d'un assemblage.

Une méthodologie qui inclura ces effets contribuera à améliorer la précision des simulations et procura ainsi un outil additionnel pour les concepteurs lors des opérations de tolérancement. Par conséquent, le modèle de synthèse de tolérances permet ultérieurement des gains à l'industrie.

Nous conjecturons que nos travaux de recherche proposent plusieurs retombés techniques et par conséquent, économiques. Dans le cycle de vie du produit, un gain de productivité engendre un gain économique. L'enjeu à long terme de ces travaux de thèse est d'explorer le domaine de l'analyse de tolérances intégrées à la CAO. Il s'agit de faire la simulation des tolérances des mécanismes qui permettront d'aider le concepteur à mieux spécifier les tolérances et les dimensions des pièces. D'une manière plus spécifique, on peut citer des retombés aux étapes de :

- La conception : on établit une méthode numérique de tolérancement et une modélisation réaliste des assemblages mécaniques afin de déterminer les configurations les plus réalistes. Aussi, on offre un outil de simulation permettant des analyses du type *What-If* permettant un choix judicieux des tolérances de forme tout en analysant leurs effets sur l'assemblage.
- La production : l'optimisation de l'intervalle des tolérances permet de maîtriser le coût de production, un intervalle plus large entraîne un coût moins élevé.

- La relation client-fournisseur : proposer différents outils, complémentaires de l'analyse des tolérances qui aident à empêcher les conflits, par suite de gagner du temps à la prise de décision dans un contexte industriel.
- La satisfaction du client : la simulation de tolérance géométrique et dimensionnelle qui améliore la maîtrise des écarts, donc de bien satisfaire le client.

1.8. Méthodologie proposée et Structure de la thèse

Dans notre thèse certaines hypothèses de travail communes à tous les jalons de notre recherche sont émises et d'autres hypothèses sont spécifiques pour chaque chapitre-article :

- Nous utilisons un formalisme reconnu : ISO-14405-1 (accessoirement la norme ASME Y14.5-2009) pour la définition du tolérancement dimensionnel et géométrique. Aussi, nos travaux seront basés sur l'utilisation de la maquette numérique pour modéliser, générer des défauts et simuler l'assemblage.
- Dans nos travaux nous avons exploiter les schémas de représentation de la géométrie discrète tels que les nuages de points et les maillages de surface afin de créer une base de donnes virtuelles. Ils sont simples et semblent adéquats pour la représentation des pièces déviées.
- Pour valider nos approches, nous avons réalisé une validation par simulation numérique et par expérimentation ; la validation numérique consiste à créer de formes géométrique avec de défauts synthétiques par modélisation modale et par une modélisation aléatoire. La validation expérimentale a été réalisée aussi dans le laboratoire LIPPS.
- Caractéristiques dimensionnelles et géométriques : cercle, cylindre, trou oblong et plan en considérant une rigidité infinie.
- Toutes les mesures sont effectuées dans un environnement contrôlé (laboratoire de métrologie ou installations). Par conséquent, l'incertitude induite par les conditions environnementales peut être considérée comme négligeable dans cette étude par rapport aux défauts d'amplitude.

- La reproductibilité décrite dans cette étude (u_{AV}) représente les variations dues à l'erreur algorithmique et principalement à l'erreur de programmation l'opérateur utilise toutes les options logicielles, il s'agit donc d'une variation observée;
- Nous avons utilisé le niveau de confiance pour représenter l'intervalle 95% (type d'erreur I = 0,05) ; le cas échéant, les valeurs aberrantes et les données manquantes ont été incluses dans les calculs.

Cette thèse comporte (5) chapitres, une conclusion qui résume les principales contributions et finalement, des recommandations pour des futurs travaux de recherche. Les contributions de cette thèse sont réalisées par de la publication de trois (3) articles de revues (avec comité de lecture), et la participation à quatre (4) conférences. Le Tableau 1.3 et la Figure 1.8 récapitulent les références des articles des revues et des conférences.

Tableau 1. 3 Références bibliographiques des conférences, période : 2016-2019

MOSIM **Montréal, Canada** **Août, 2016**	Ibtissem JBIRA, Mehdi TLIJA, Borhen LOUHICHI, Antoine TAHAN, «CAD/tolerancing integration: mechanical system with geometric defects», *11th International Conference on Modeling, Optimization and Simulation MOSIM'16*, article publié en 24 Août 2016
ADES **Août, 2017**	Ibtissem JBIRA, Mehdi TLIJA, Borhen LOUHICHI, Antoine TAHAN, «CAD/tolerancing integration: mechanical system with geometric defects»*, Advanced Engineering Software (ADES)*, article publié en 12 Août 2017
IDETC/CIE **Québec, Canada** **Août, 2018**	Ibtissem JBIRA, Antoine TAHAN, Mohamed Ali MAHJOUB, Borhen LOUHICHI, «Evaluation of the Algorithmic Error of Circle Size and Roundness Using ISO 14405 Specifications*» International Design Engineering Technical Conference ET Computers and Information in Engineering Conference (IDETC/CIE) de l'American Society of Mechanical Engineers (ASME)*, article publié en 29 Août 2018.
ACFAS **Gatineau, Canada** **Mai, 2019**	Ibtissem JBIRA, Antoine TAHAN, Serge BONSAINT, Mohamed Ali MAHJOUB, Borhen LOUHICHI, « Une étude de la reproductibilité entre les logiciels d'inspection assistée par ordinateur à partir d'un nuage de points *», (ACFAS),* 27 Mai 2019
GMAI **Paris, France** **Juillet, 2019**	Ibtissem JBIRA, Aicha Ben MAKHOULF, Borhen LOUHICHI, Antoine TAHAN, Mohamed Ali MAHJOUB, Dominique Dominique DENEUX «A comparative study of extraction cylinder features in industrial point clouds» *15th International Conference Geometric Modelling and Imaging, (GMAI),* article publié en 5 Juillet 2019
IJSAEM **2019**	Ibtissem JBIRA, Antoine TAHAN, Mohamed Ali MAHJOUB, Borhen LOUHICHI, «Evaluation of the Algorithmic Error of a Fitting Circle Using ISO 14405 Specifications» *International Journal of System Assurance Engineering and Management,* article accepté en Juillet 2019
JCSE **2019**	Ibtissem JBIRA, Antoine TAHAN, Mohamed Ali MAHJOUB, Borhen LOUHICHI, «Reproducibility Experimentation Among Computer-Aided Inspection Software from a Single Point Cloud» *Journal of Control Science and Engineering*, article publié en Octobre 2019
EAAI **2019**	Ibtissem JBIRA, Antoine TAHAN, Mohamed Ali MAHJOUB, Borhen LOUHICHI, «A new approach for deformed cylinder features extraction by robust principal component analysis and oriented Bounding Box» article soumis en 2019 dans le journal *Engineering Applications of Artificial Intelligence.*

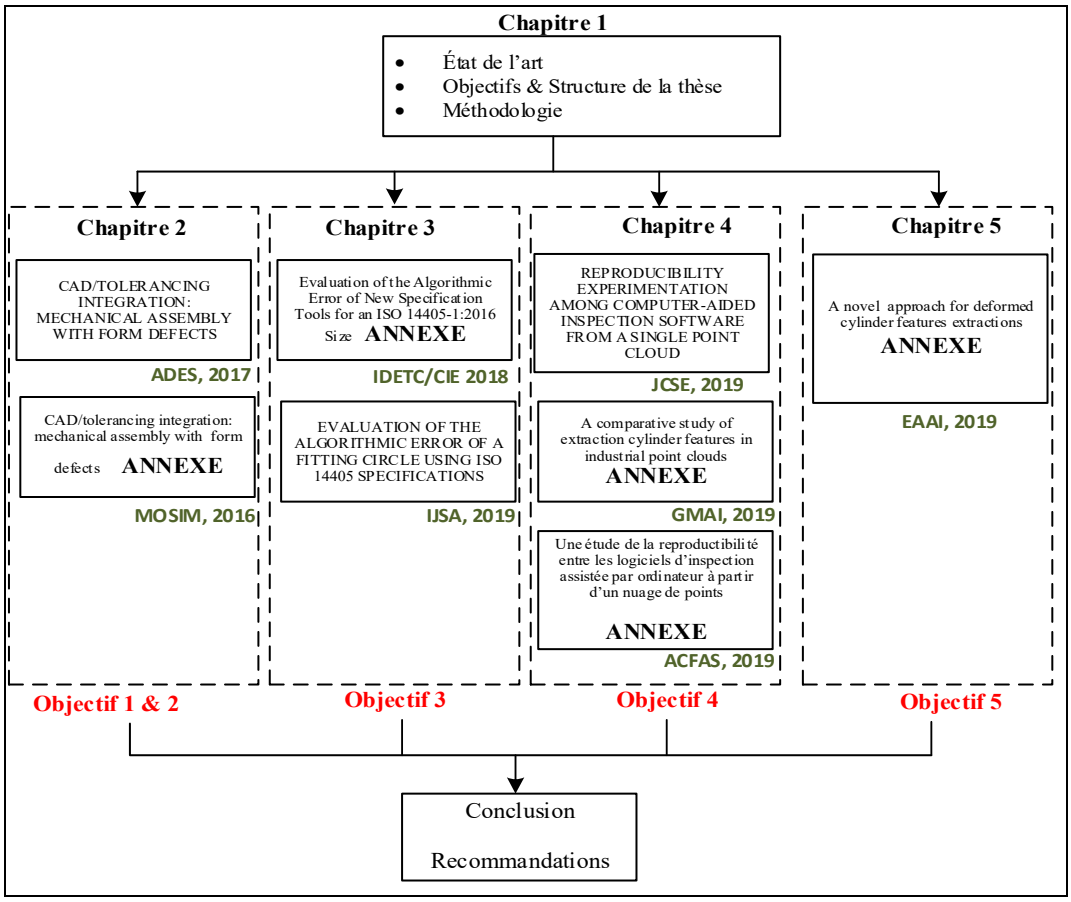

Figure 1. 8 Références bibliographiques des conférences, période : 2016-2019

CHAPITRE 2

CAD/TOLERANCING INTEGRATION: MECHANICAL ASSEMBLY WITH FORM DEFECTS

Ibtissem Jbira[a,b,c] , Mehdi Tlija[d], Borhen Louhichi[d] ,Antoine Tahan[a]

[a] École de Technologie Supérieure (ÉTS), 1100 Notre-Dame ouest, Montréal, Québec, H3C 1K3, Canada
[b] Institut Supérieur d'Informatique et des Technologies de Communication, G.P.1 Hammam Sousse-4011, Tunisie
[c] Université de Sousse, École Nationale d'Ingénieurs de Sousse, LATIS- Laboratory of Advanced Technology and Intelligent Systems, Tunisie
[d] Université de Sousse, Institut Supérieur des Sciences Appliquées et de Technologie de Sousse, LMS, Cité Taffala 4003, Sousse, Tunisie

Article publié dans le journal « Advanced in Engineering Software », Août 2017

2.1 Abstract

The geometric deviations affect the assemblability and functional compliance of products, since small part variations accumulate through large-scale assemblies and lead to malfunction. The Digital Mock up (DMU) upgrades requires the tolerance consideration in CAD model. The improvement of tolerancing leads to an industrial success. Therefore, improving the CAD model to be closer to the realistic model is a necessity to verify and validate the mechanical system assemblability. In our previous works, an approach to consider the dimensional, positional and orientation tolerances in CAD model was developed. In this paper, the above approach is improved to take into account the form defects in CAD model. To model the component with form defects, the tolerance face is modeled by gird vertices. According to the form tolerance value white Gaussian Noise (WGN) to gird vertices is computed. The realistic face is obtained by an interpolation based on the tessellation using Thin Plate Surface (TPS) modelling. The realistic assembly configurations were performed by updating the mating constraints. In fact, in realistic modelling, a new method to redefine constraints, while respecting an Objective Function of the Assembly (OFA), is established. In the case of a planar joint, a sub-algorithm based on

Oriented Bounding Box (OBB) and the matrix transformation is developed. Relative part displacements are simulated with or without guaranteeing contact. Tolerance impacts on the realistic assembly motion are quantified. The realistic cylindrical joint is performed using an optimization method :the minimum cylinder inside a realistic hole and the maximum cylinder outside a realistic pin .Finally, in the case of a revolute joint a sub-algorithm to redefine the mating constraints between two realistic parts is performed .This paper proposes a new approach to incorporate the tolerances on CAD models in the case of planar and cylindrical faces by determining configurations with positional, orientation and form defects. This approach provides an assembly result closer to the real assembly of the mechanical system. Integrating tolerances in CAD allows the simulation and visualization of the mechanical assemblies' behavior in their real configurations.

2.2 Introduction

Manufacturing processes are incapable of producing mechanical components with exact sizes and shapes. Thus, designers use Geometric Dimensioning and Tolerancing (GD&T) to specify allowable limits for geometry variations based on ISO standards. However, the realistic modelling of mechanical assemblies still to be an important challenge in Computer-Aided Tolerancing (CAT) research.In our previous researches (Louhichi et al., 2015) a new approach to integrate the tolerances in CAD models by determining configurations with defects is established. The realistic parts are computed according to the dimensional, positional and orientation tolerances. However, the non-consideration of form defects generates non-compliant assemblies of compliant parts especially in the case of small clearance (Adragna et al., 2010) (Anselmetti, 2010) and form defects have impacts on the functional specifications of a mechanism (Beaucaire et al., 2013). Thus, form deviations should be considered in assembly simulations. In this paper, a new method for tolerance analysis is proposed while considering the following requirements: dimensional, positional, orientation and form tolerances, assembly process planning, contact types and assembly motion. This paper is organized as follows. First, a review of literature is presented. Then, the realistic component modelling approach is proposed: The algorithms used to model

components with position and orientation defects, as well as components with form defects are detailed. Subsequently, the realistic assemblies modelling approach is proposed: the redefinition of the mating constraints is introduced and followed by the tolerance analysis that enables to verify and validate the mechanical system assemblability: The algorithms used to simulate relative part displacements with or without guaranteeing contact are detailed. Tolerance impacts on the realistic assembly motion are quantified. After that a sub algorithm to simulate the cylindrical joint between parts with defects is proposed using an optimized cylinder algorithm: the minimum cylinder inside a realistic hole and the maximum cylinder outside a realistic pin. Finally, an algorithm of revolution joint between two parts is proposed. The conclusions and perspectives for this work are presented at the end.

2.3 State of the art

Many CATsystems used the parametric/variational approach to model the geometry (Shen, 2005) as Siemens VSA® and eM-TolMate® from Tecnomatix. The geometric solver of CAD system is used to determine values of dependent geometric parameters from other parameters. The geometry is defined by 3D features (simplified models) derived from the CAD model. Thus, the assembly mating constraints and the tolerance specifications are loosed.

In Siemens VSA software (named VisVSA from EDS/Unigraphics a decade ago), the redefinition of the assembly constraints is performed by constraint solver “Conjoin”. The user intervention is often required to adequately redefine constraints (Shen, 2003) (Shen et al., 2005). The CAT software can apply default tolerances to features or the user specifies manually the tolerances. Thus, the software takes into account the actual assembling sequence. VSA does not support all tolerance types despite it is consistent with ISO/ASME tolerance standards. The variational geometry is obtained by transformations of nominal features (derived CAD model) within the zones. Those zones are computed according to the specified limits on rotation and translation parts of the transformation matrix. The software uses point-based analysis method and does statistical tolerance analysis. eM-TolMate software use its

own derived features. However, the user needs to mathematically derive some feature from existing features in many cases and to specify dimensional and geometrical tolerances. In the software interface, a tree structure represents the assembly sequence which is defines by the user using the source components. The definition of the mating constraints is performed manually or automatically. The user intervention is required for complex assemblies when using the automatically method. The real mating conditions based on contact between components are determined using a “High Point Method”. eM-TolMate allows an assembly component to float relative to the other mated parts as it is really happened. However, this eM-TolMate method presents a limitation: problem of optimal floating direction. eM-TolMate allows statistical tolerance analysis on the basis of Monte Carlo simulations. To detect the interferences between parts the only method consists on defining proper features and control measurements. Therefore, before simulation, the user should predict the parts, which will generate eventual interferences.

Zou and Morse propose the GapSpace model to capture the Fitting Conditions (FC) existing in 2D mechanical assemblies (Zou and Morse, 2004). The model uses gaps to describe the possible mating or clearance condition between features inside assemblies. The value of each gap is the shortest distance between the two related features. A GapSpace sine law is computed to describe the characteristic inside each constraining simplex. Using an assembly graph, an algorithm is developed to search the FC inside the assembly. Each FC is represented by a weighted linear sum of gaps sizes and geometric (length, angle) parameters. After the identification of all FCs, tolerance analyses can be easily performed. The model can be integrated with commercial CAD products (such as Pro/E, CATIA) for tolerance analysis. (Adragna et al., 2010) generate form deviations basing on modal analysis to evaluate a measured form deviations. A combination of elementary form deviation is used to characterize any type of geometry and form deviation this model allows establishing a method to identify the clearance domain of a mechanical assembly with form defects The virtual assembly of planar surfaces is established by computing the convex difference surface. The contact points or facets are determined by applying external forces to link a surface pair. The surface with form deviations is generated using the modal parametrization and geometrical parameters.

(Grandjean et al., 2013) use the above modal tool to model surface and then to analyse and quantify the assembly of parts with positional and form defects which is subjected to local deformations and external loads (Grandjean et al., 2013). (Lê et al., 2014) present two experimental methods, surface and displacement measurements, to analysis mechanical joint behaviour with position and form defects. The surface defects are defined using the gap hull or difference surface concepts. Basing on the bijection relation between the gap hull and the convex difference surface computations, a comparison study between the results of the two above experimental methods is established. The validation is limited to the case of planar joint.

(Schleich et al., 2014) present a new paradigm shift for geometric variations modelling in mechanical engineering: Skin Model Shapes, which are particular Skin-Model representatives from a simulation perspective. Skin Model Shape is an abstract model of the physical interface between a workpiece and its environment. The model comprises deviations from manufacturing and assembly. The process for generating Skin Model Shapes (SMS) is split into a prediction and an observation stage with respect to the available information and knowledge about expected geometric deviations.

2.4 Modeling realistic component

The realistic component modelling approach is based on two algorithms (Figure.2. 1): The first algorithm is used to model components with position and orientation defects. The second models components with form defects.

2.4.1 Modeling of component with position and orientation defects

In previous work, (Louhichi et al., 2015) (Thlija, 2014)developed an algorithm to determine all components with orientation and positional defects. The method of computing realistic component configurations depends on tolerance zone geometry and tolerance type. Indeed, according to the degree of freedom defined by the Small Displacement Torsor (SDT), the tolerance zone is discretized to determine the realistic configurations of the tolerance element.

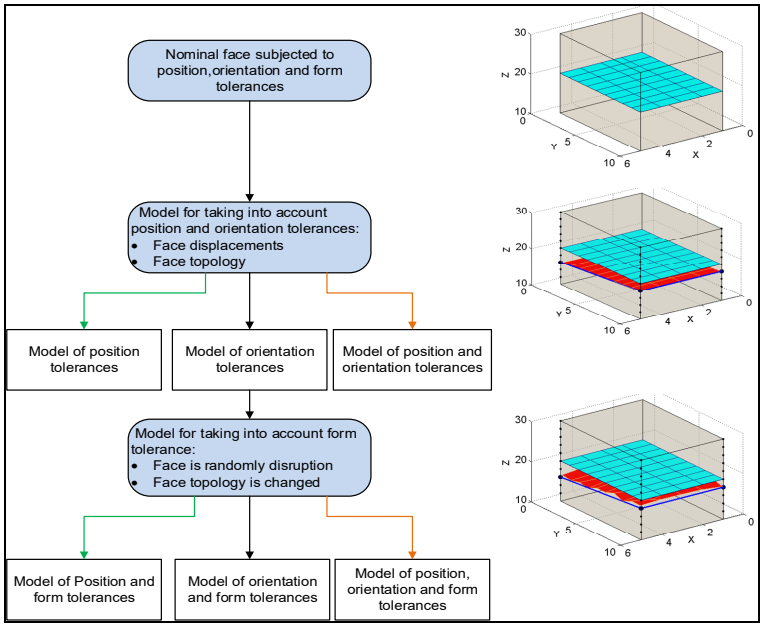

Figure 2. 1 Modeling of realistic component

In a CAD model, the realistic part configurations were obtained with face displacements (2 rotations and/or translation) using the parameters deduced from the discretization. The approach considers the perfect planar and perfect cylindrical faces subjected to orientation and\or positional tolerances. In this paper, the description is limited on the case of planar face with positional tolerance. The conformity domain of a planar surface P, which is subjected to a positional tolerance zone $\left[-\frac{T_p}{2};\frac{T_p}{2}\right]$, is define between two parallel planes spaced by a distance T_P.

A sub-algorithm to determine all the Possible Component Configurations according to Positional Tolerance allocated to Planar face (PCCPTP) was improved. Epp is the deviation torso of P on point O (the centre of P) by the equation (2.1):

$$\{Epp\}_o = \begin{Bmatrix} \alpha & 0 \\ \beta & 0 \\ 0 & TZ \end{Bmatrix}_{(O,X,Y,Z)} \tag{2.1}$$

The sub-algorithm of based on the flowing steps. Initially, three lateral edges (E_1, E_2 and E_3) of Tz are discretized by an increment i. The integer i is defined by the designer according to the desired precision of the results. Then, the nominal face P is defined by three points N_1, N_2 and N_3.Therefore, a target position of the realistic face P_{uvw} is defined by three new points ($N_{1\mathrm{u}}$, $N_{2\mathrm{v}}$ and $N_{3\mathrm{w}}$; with u, v and w range from 1 to i).

(Louhichi et al., 2015) proposed to determinate the geometric deviation between the two faces (nominal face P and target face P_{uvw}) three parameters, two angles: α_{vw} and β_{vu}, and a linear distance d_v. Thus, the obtaining of realistic parts requires the face displacements to the target positions. Those displacements are performed by two rotations and one translation. In this paper PCCPTP algorithm was improved; the geometric deviation is determinate by computing transformation matrix which is based on the correspondence between the three points (N_1, N_2, N_3) and $(N_{1\mathrm{u}}, N_{2\mathrm{v}}, N_{3\mathrm{w}})$. The main steps of the improved algorithm are as shown in Figure 2.2.

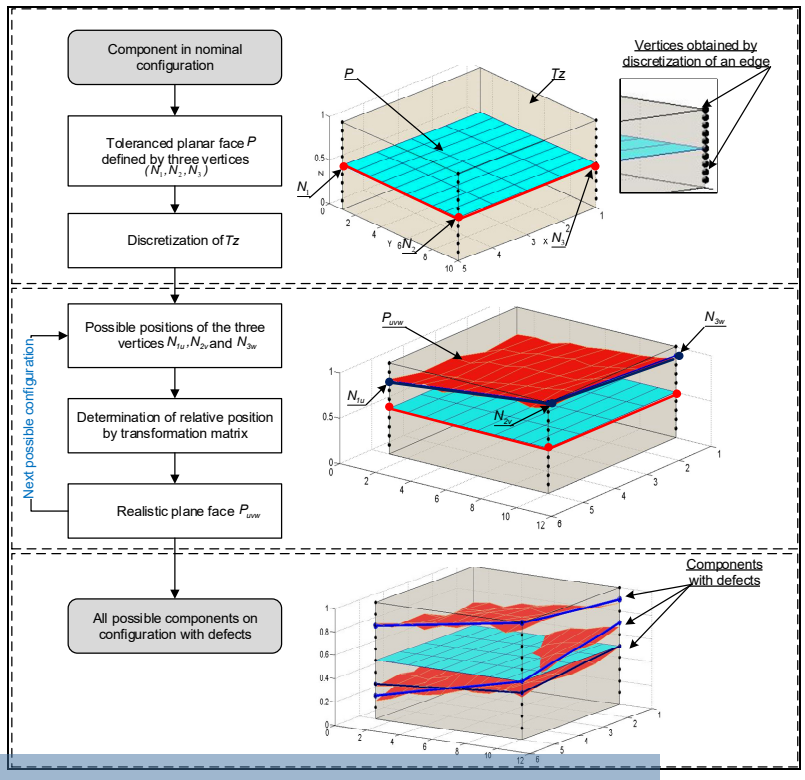

Figure 2. 2 The improved PCCPTP algorithm

2.4.2 Modeling of component with form defects

A grid interpolation is used for modelling the variational surface of the parts. An example of variational surface of the parts is shown in Figure 2.3. Different interpolated surface is constructed with the Toolbox Grid-based interpolation of Matlab®. Experiments were performed using Matlab R2015 on a PC with an Intel Core i3 2.4 GHz processor and a 4.0 GB physical memory. The main steps for modelling the variational surface are presented in the pseudo code:

1. Define a Cartesian system $\left(\vec{X}_S, \vec{Y}_S, \vec{Z}_S\right)$ of the surface. In the case of planar and cylindrical surface, where $\vec{Z}_S$ is the surface normal vector.
2. Generate N random points $P_i(x_i, y_i, z_i)$ on the surface .
3. Define a regular grid to smooth the random points. A grid is not just a set of points that meet certain geometric. Grid is a common and useful way to organize data. This data format represents values or intensities at discrete grid point locations. Thus, gird vertices V_i are deduced. The grid is useful just in the case planar.
4. Generate a uniform random values for angles φ, θ and ψ (Euler angles), where $\varphi \in [0,2\pi]$, $\theta \in [0,2\pi]$ and $\psi \in [0,2\pi]$. In a 3D Euclidean space, the following rotations of matrices correspond to rotations around the axes x, y and z by angles φ, θ and ψ respectively: With the notation $c_\alpha = \cos(\alpha)$ and $s_\alpha = \sin(\alpha)$, a rotation of ψ radians about the x-axis is defined as (Equation. 2.2):

$$R_x(\psi) = \begin{bmatrix} 1 & 0 & 0 \\ 0 & c_\psi & -s_\psi \\ 0 & s_\psi & c_\psi \end{bmatrix} \tag{2.2}$$

Similarly, a rotation of θ radians about y-axis is defined as (Equation 2.3):

$$R_y(\theta) = \begin{bmatrix} c_\theta & 0 & s_\theta \\ 0 & 1 & 0 \\ -s_\theta & 0 & c_\theta \end{bmatrix} \tag{2.3}$$

Finally, a rotation of φ radians about z-axis is defined as (Equation. 2.4):

$$R_z(\varphi) = \begin{bmatrix} c_\varphi & -s_\varphi & 0 \\ s_\varphi & c_\varphi & 0 \\ 0 & 0 & 1 \end{bmatrix} \tag{2.4}$$

A general rotation matrix will have the form (Equation 2.5):

$$R_{3\times3} = \begin{bmatrix} R_{11} & R_{12} & R_{13} \\ R_{21} & R_{22} & R_{23} \\ R_{31} & R_{32} & R_{33} \end{bmatrix} \tag{2.5}$$

The complete expression of the matrix product $R_{3\times3} = R_z(\varphi)R_y(\theta)R_x(\psi)$ is:

$$R_{3\times3} = \begin{bmatrix} c_\theta c_\varphi & s_\psi s_\theta c_\varphi - c_\psi s_\varphi & c_\psi s_\theta c_\varphi + s_\psi s_\varphi \\ c_\theta s_\varphi & s_\psi s_\theta s_\varphi + c_\psi c_\varphi & c_\psi s_\theta s_\varphi - s_\psi c_\varphi \\ -s_\theta & s_\psi c_\theta & c_\psi c_\theta \end{bmatrix} \tag{2.6}$$

Thus, a random vector $\vec{R}$ is deduced from R (Figure 2. 3(a)) with i = [1,2,3].

$$\vec{R} = \begin{pmatrix} R_{1i} \\ R_{2i} \\ R_{3i} \end{pmatrix} \tag{2.7}$$

5. Random points V_{r_i} are computed using Gaussian perturbations of the gird vertices V_i according to the specified form tolerance T_f. These points are generated with a normal (Gaussian) distribution with a specified mean and variance using the function "*randn*" of Matlab. For each vertex V_i, a perturbation value $r_i \in \left[-\frac{1}{2}T_f, +\frac{1}{2}T_f\right]$ is performed along $\vec{R}$ (Figure. 2.4(b)).

6. Apply an interpolation based on the tessellation using TPS modelling. TPS interpolation method is detailed in the next section. The modelling respects the ISO standards: without losing the generality, in the case of planar surface subjected to flatness tolerance T_f, the

random form defect T_{rf} generated is defined by the relation (Equation. 2.8); with an error ($\xi = \xi_1 + \xi_2$). Where ξ depends on the interpolation fitness. r_i^{max} and r_i^{min} are the maximum and the minimum values of r_i respectively. The form tolerance is automatically respected, since $T_{rf} \leq T_f$. The TPS method is used in the case of planar surface.

$$\begin{cases} \text{before interpolation} & T_{\text{rf}} = r_i^{max} - r_i^{max} \\ \text{after interpolation} & T_{\text{rf}} = r_i^{max} - r_i^{max} \ \textit{with } \xi \textit{ error} \end{cases} \quad (2.8)$$

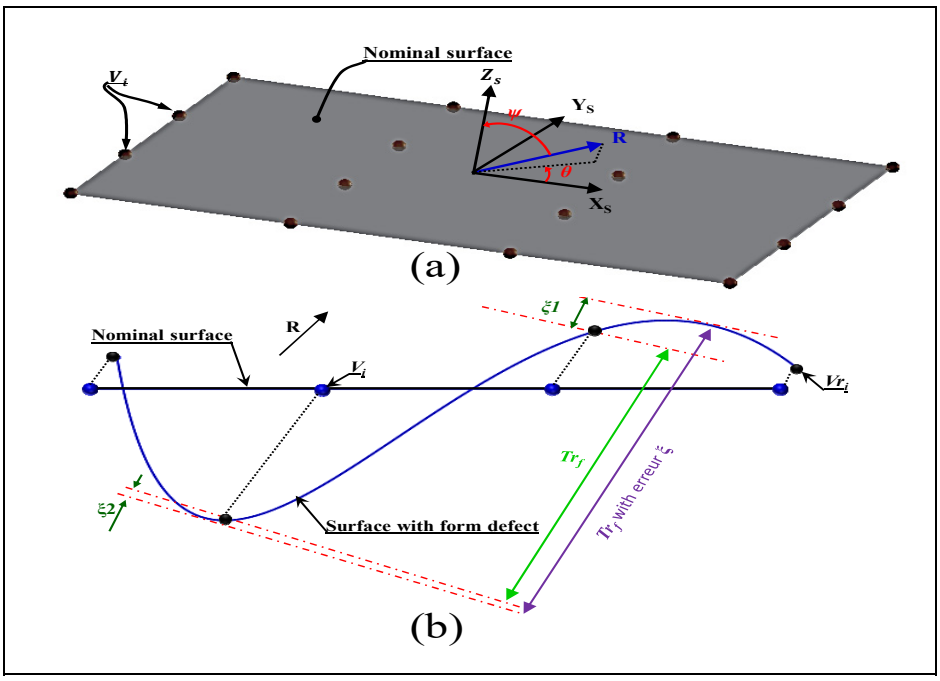

Figure 2. 3 (a) Definition of the random direction,
(b) 2D representation of the generation of the surface with form defect

2.4.3 Review of thin plate spline interpolation method

Thin Plate Spline (TPS) is an interpolation method to determine a continuous smooth surface that passes through all given n points $Q_i(x_i, y_i, z_i)$ with $i = 0, \ldots, (n-1)$(See Figure. 2.4).

Consider $Q(x, y, z)$ a point on the surface, the relation between x, y and z is defined by the equation (Equation. 2.9):

$$z(x, y) = a_1 + a_2 x + a_3 y + \sum_{i=0}^{n-1} w_i \, f((x_i, y_i) - (x, y)) \tag{2.9}$$

Where $(x_i, y_i) - (x, y)$ is the distance between the control point (x_i, y_i) and a position (x, y), f is a continus function and w_i is a coefficient for each control point.

To estimate the $(3 + n)$ parameters a_1,a_2, a_3 and w_i, we must solve the following system:

$$\begin{bmatrix} K_{n\times n} & Q \\ Q^T & 0_{3\times 3} \end{bmatrix} \begin{bmatrix} \vec{w} \\ \vec{a} \end{bmatrix} = \begin{bmatrix} \vec{v} \\ \vec{0} \end{bmatrix} \tag{2.10}$$

Where $\vec{w}_{n\times 1}$and $\vec{a}_{3\times 1}$are unknowns of the equation Equation 2. 10 and must be calculated and used for the computation of the regular lattice points; $\vec{v}$ is the vector of interpolation point coordinates (z_i);

$$\vec{v}_{n\times 1} = \begin{Bmatrix} z_0 \\ \vdots \\ z_{n-1} \end{Bmatrix}, \vec{0} = \begin{Bmatrix} 0 \\ 0 \\ 0 \end{Bmatrix} \; and \; Q = \begin{pmatrix} 1 & x_1 & y_1 & z_1 \\ \vdots & \vdots & \vdots & \vdots \\ 1 & x_n & y_n & z_n \end{pmatrix} \tag{2.11}$$

$$K_{n\times n} = \begin{bmatrix} K_{0,0} & \cdots & K_{0,n-1} \\ \vdots & \ddots & \vdots \\ K_{n-1,0} & \cdots & K_{n-1,n-1} \end{bmatrix} \tag{2.12}$$

Where:

$K_{i,j} = f\big((x_i, y_i) - (x, y)\big) - \delta_{ij}\alpha^2\lambda$

$\alpha = \dfrac{1}{(n-1)^2} \displaystyle\sum_{i=0}^{n-1}\sum_{j=0}^{n-1} f((x_i, y_i) - (x_j, y_j))$

With $i, j \in [0, \ldots, n-1]$ and $\lambda = 0.1$ is a regularization parameter. The regularization parameter λ weights the relevance of the data term with respect to the smoothness condition, where the latter one is nearly a pure affine transformation.

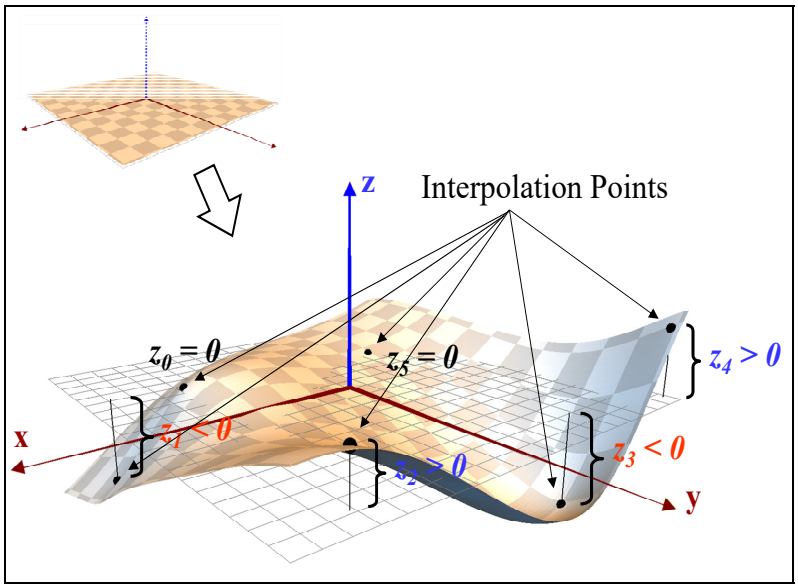

Figure 2. 4 Thin plate spline interpolation method

2.5 Modeling of realistic assemblies

2.5.1. Algorithms for modelling realistic joints

In this paper, a sequential assembly technique is used. The rebuilding of the assembly with realistic components may lead to an over-constrained assembly. Thus, the mating constraints, used in a nominal assembly, must be redefined to link realistic components.

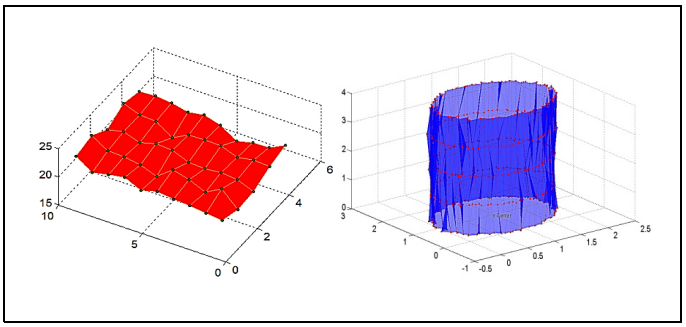

Figure 2. 5 Example of variational surface

In nominal CAD model, the primitive mates, which link the assembly components, are collinearity, perpendicularity, tangency, symmetry, coincidence and parallelism. In the context of this article, the study is limited to the cases of a coincident between two planar faces (Co: $F1\&F2$) and a co-axial constraint between two cylinder axes (Co: $A1\&A2$):

- Co: $F1\&F2$: The two unit normal vectors of planar faces are anti-aligned (the angle between the two directions is Π) or aligned (the angle between the two directions is zero). The two planar faces are located in the same plane and are in, or without, contact.
- Co: $A1\&A2$: In this case, the two axes are aligned or anti-aligned and a point from the first axis belongs to the second one.

The realistic mating constraints are obtained by modifications of the relations between MGREs (Minimum Geometrical Reference Elements) (Rivest et al., 1994). This method depends on the Objective Function of the Assembly (OFA) specified by the designer.

In CAD software, the OFA is automatically deduced from the nominal model:

- The mating constraint order, specified in the feature manager design tree of the software, defines the mounting order of the assembly and the joint order priority. Thus, the planning of the assembly process is identified.
- The cinematic state of the nominal assembly defines the DoFs which are to be conserved in the realistic model.
- The contact between the features is conserved.

- The joint type between each couple of components is respected.

2.5.2. Algorithm for modelling a planar joint in realistic model

In nominal assembly, a planar joint between two parts $P1$ and $P2$ is defined by a coincidence constraint between $F1$ and $F2$; Co($F1$& $F2$). $F1$ and $F2$ are two nominal faces of $P1$ and $P2$ respectively. In realistic model, $F'1$ and $F'2$ are two faces with defects obtained from $F1$ and $F2$ respectively. According to the OFA, the joint is modeled by a coincidence constraint between two planes $P1$ and $P2$, between plane $P1$ and edge E or between plane $P1$ and vertex V. $P1$ and $P2$ are the tangent planes to $F'1$ and $F'2$ respectively. The determination of above realistic mating constraints is obtained by modifications of the relations between MGREs. The MGRE (plane, edge and vertex) are identified using the OBB tool.

2.5.3. Determination of OBB

The OBB of a surface with defects is calculated using a very popular class of heuristic methods. The above method is based on Principal Component Analysis (PCA). The idea behind consists on the execution of a PCA to compute the eigenvectors of corresponding covariance matrix. Those eigenvectors are the axes of the orthonormal frame associate to the box (Figure. 2.6).

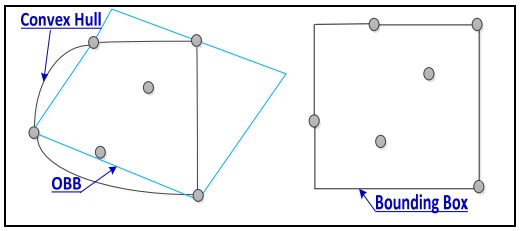

Figure 2. 6 Example of 2D OBB

The main steps for the determination the OBB are illustrated in Figure.2.7 and presented in the pseudocode:

1. Compute the convex hull of the input points to reduce the problem dramatically. The convex hull approximates the shape of the input.

2. Compute the mean position and covariance matrix of the convex hull of the input.
3. Extract the eigenvectors of the covariance matrix.
4. Build a transformation matrix using the mean position and eigenvectors.

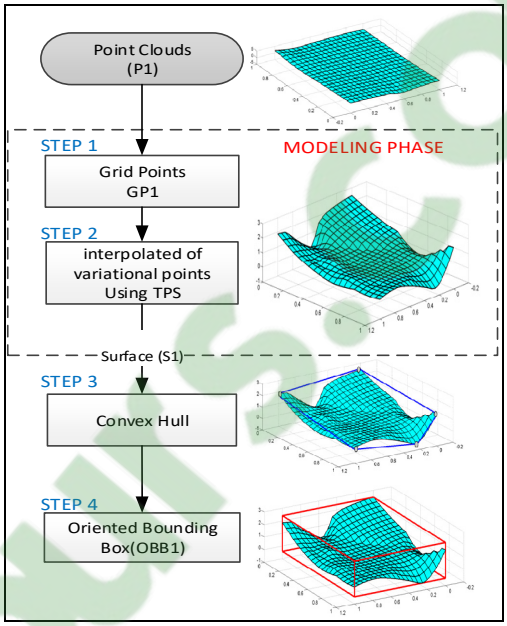

Figure 2. 7 Determination of OBB

Determinate the size of the box to fit the input Redefinition of planar joint by coincidence constraint between two tangent planes Without losing generality, the method to update a planar joint defined in nominal assembly by a coincidence constraint between two tangent planes is shown through the assembly of two parts: A and B (Figure.2.8 (a)).

In nominal configuration, a coincidence constraint is defined between the faces $Fa1$ and $Fb1$. A distance constraint is applied between the faces $Fa2$ and $Fb2$ ($Dist$: ($Fa2$ & $Fb2$)) only to simplify the illustration. The faces $F'a1$ and $F'b1$ are the realistic configurations of $Fa1$ and $Fb1$ respectively (Figure.2.8 (b)).

Those configurations are obtained using the pseudocode. OBBa and OBBb are the oriented bounding boxes of $F'a1$ and $F'b1$ respectively (Figure.2.8 (c)). Thus, the two tangent planes TPa and TPb are deduced.

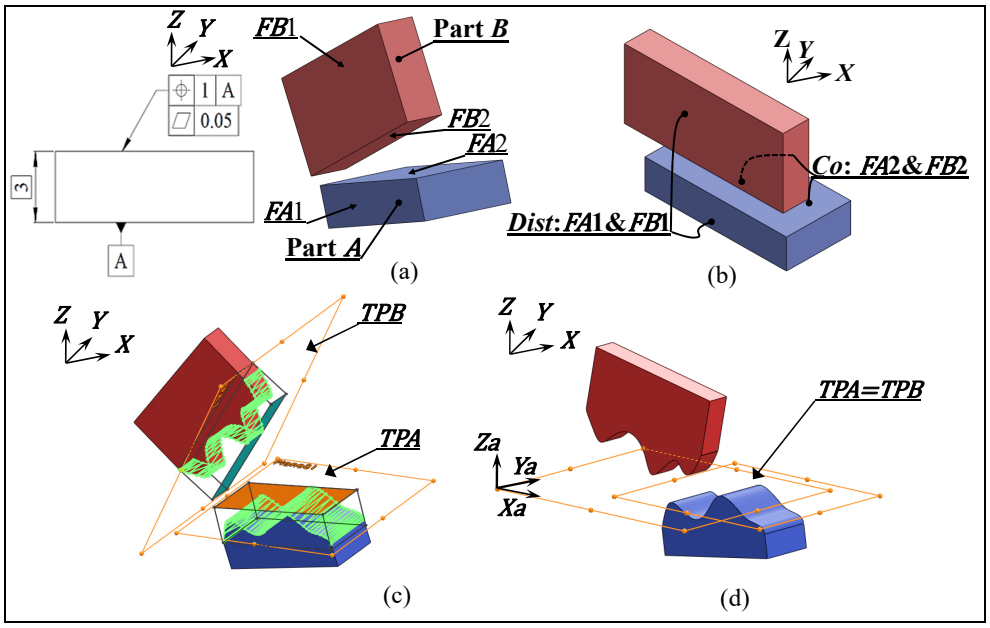

Figure 2. 8 (a) Nominal configuration without mates,
(b) Nominal configuration with mates,
(c) Realistic configuration without mates,
(d) Realistic configuration with mates.

A coincidence constraint are applied between TPa and TPb ($Co: TPa\&TBb$) (Figure.2.8 (d)). The above constrain is obtained using a transformation matrix. This matrix is computed by finding the optimal rotation and translation (Figure. 2.9).

2.5.4. Finding the optimal rotation and translation

Finding the optimal/best rotation and translation refers to compute the transformation matrix $M_{3\times3}$; that combine the rotation matrix $R_{3\times3}$ and the displacement vector $t_{3\times1}$. Indeed, the optimal transformation matrix is obtained by computing R and t using the equation (Equation. 2.13).

$$M = R\,P + t \tag{2.13}$$

Where P is a set of points $P_i(x_i, y_i, z_i)$.

The main steps for computing the transformation matrix are shown in Figure.2.9:

1. Find centroids $C(A)$ and $C(B)$ of both dataset $P(A)$and $P(B)$ of the faces $F'a1$ and $F'b1$ respectively. The points of each dataset are defined in local coordinate system. In other words, $P(A)$ and $P(B)$ are defined in $(C(A), X_a, Y_a, Z_a)$ and $(C(B), X_b, Y_b, Z_b)$ respectively. The axis of the two above coordinate system are chosen according the eigenvectors of corresponding OBB.
2. Bring both dataset $P(A)$ and $P(B)$ to the origin of global coordinate system (the assembly coordinate system); then find the optimal rotation, (matrix R).
3. Find the translation vector t.

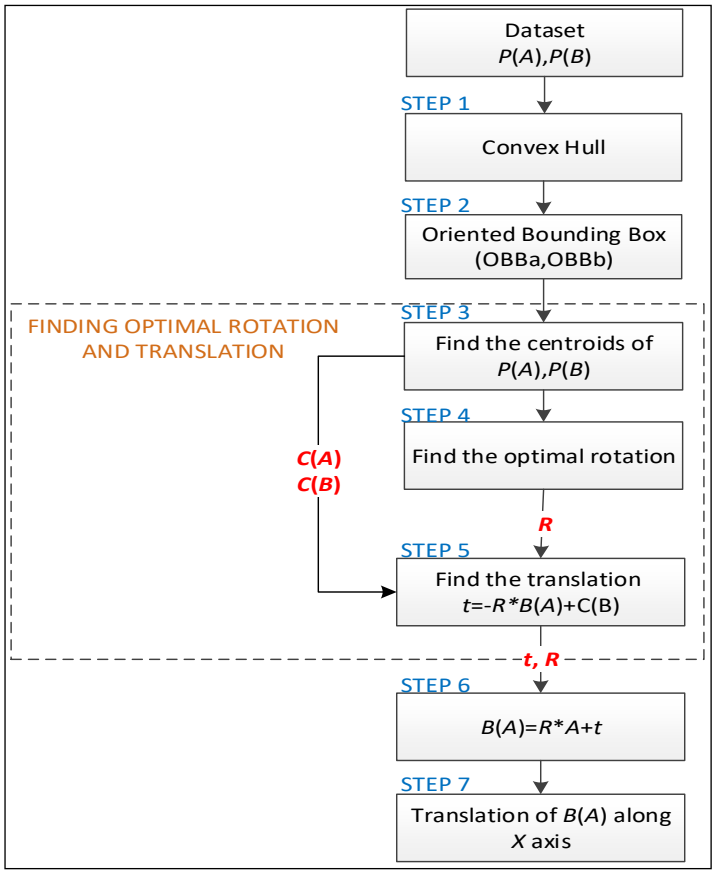

Figure 2. 9 Sub-algorithm to redefine planar joint by coincidence constraint between two tangent planes.

2.6 Motion simulation with planar joint

The objective is to determine the realistic assembly behavior in motion simulation with planar joint. An elementary assembly is chosen (Figure.2.8. (a)). In nominal configuration, the component B is fixed and $(X, Y, Z)$is the assembly coordinate system. Faces $Fa1$ and $Fa2$ are subjected to:

- Position tolerances:Tpa and Tpb respectively ($Tpa = Tpb = 1mm$).
- Flatness tolerances: Tfa and Tfb respectively ($Tfa = Tfb = 0.05\ mm$).

In Figure 2.8(c), $F'a1$ and $F'b1$ are one of possible configurations with positional and form defects deduced from $Fa1$ and $Fb1$ respectively. The coordinate system and (X_b, Y_b, Z_b) is defined according to eigenvectors of OBB of the fixed component B. The functional key

characteristics of the assembly are the distance ($D = 2mm \pm 1$) and the maximum Gap ($G_{max} = 0.1mm$) (Figure 2.10). Finally, D is defined along the Z-axis.

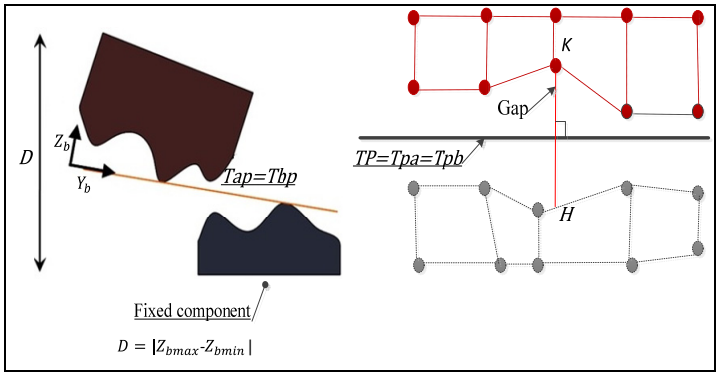

Figure 2. 10 The distance D and the maximum Gap

The gap is the maximum distance between $K(X_k, Y_k, Z_k)$ and $H(X_h, Y_h, Z_h)$. K is a point from the dataset of $F'a1$. H is the projection orthogonal of Kaccording to the normal vector $Z_b$of the plane TP :

1. Determine the equation of *TP:* $ax + by + cz + d = 0$;
2. Projection along the Z_b axis;
3. Using the relation (Equation. 2.14), Gap (G) is identified.

$$G = max(d_{kh}) ; d_{kh} = \frac{|ax_k + by_k + cz_k + d| + |ax_h + by_h + cz_h + d|}{\sqrt{a^2 + b^2 + c^2}} \qquad (2.14)$$

2.6.1. 1rst Solution: part relative displacements without guaranteeing contact

The assembly of the two parts *A* and *B* presents one DoF: During relative part displacements, a translation of the part *A* along Y_b axis relative to part *B*, the two components are not always in contact: only for a translation with ΔX_b^2 value the contact is established.

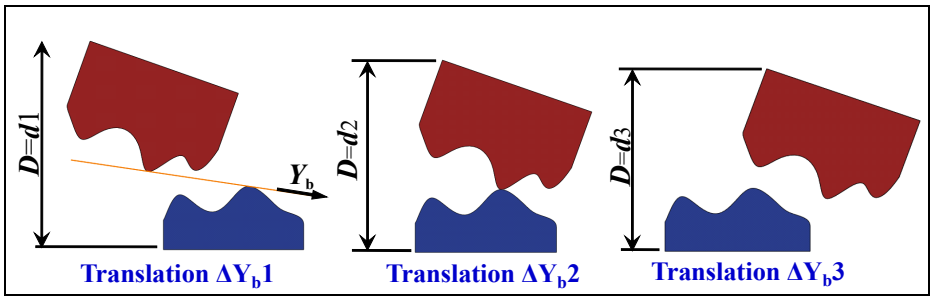

Figure 2. 11 Part relative displacements without guaranteeing contact

The Gap measuring is not adequate without ensuring the face contact. Thus, the contact must be guaranteed to more closely resemble a realistic model. The Tableau 2.1 shown tolerance impacts on the functional requirements during the assembly motion.

Tableau 2. 1 Tolerance impacts (without guaranteeing contact)

	$Xp(mm)$		
Results			
	1	*2*	*4*
Figures	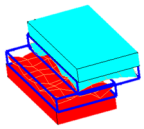	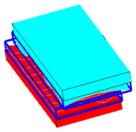	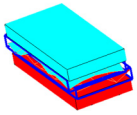
D (mm)	2,5216	2,5216	2,5216
G (mm)	0,0150	0,1459	0,0424

2.6.2. 2nd Solution: relative displacements with guaranteeing contact

A direction of an external load, which simulates an assembly operation, is definedas an assembly predominant direction $\vec{L}$. Where $\vec{L}$ is an unity vector. In fact, load velocity and value are both not considered. The sub-algorithm to simulate part relative displacements with guaranteeing contact is illustrated in Figure. 2.12. In fact, after the application of the

coincidence constraint between the planes Tpa and Tpb, the contact between the faces $F'a1$ and $F'b2$ is established. A coincidence constraint between the vertices Pa_n and V_n is applied. Pa_n and V_n are computed by the equation (Equation. 2.15). Pa_i are the vertices of the dataset $P(A)$ and V_i are the projection of Pa_i along $\vec{L}$. D and G are computed.

$$dist(Pa_n, V_n) = min\, dist(Pa_i, V_i) \tag{2.15}$$

Then, the alignment of the planes Tpa and Tpb is redefined and a displacement is established. The two functional key characteristics are calculated after making face contact using the method described previously.

Tableau 2. 2 Tolerance impacts (with guaranteeing contact)

	Xp(mm)		
Results			
	1	***2***	***4***
Figures	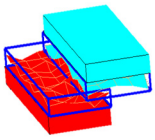	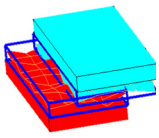	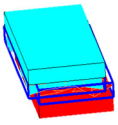
D (mm)	2,2216	2,1356	2,1764
G (mm)	0,0063	0,0120	0,0159

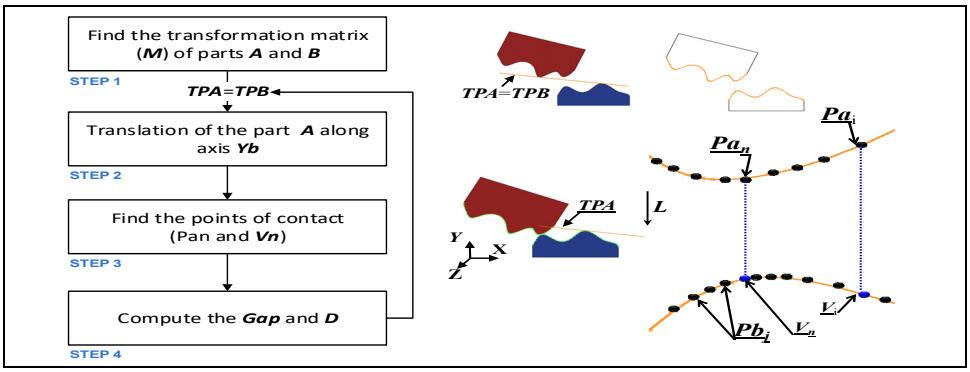

Figure 2. 12 Part relative displacements with guaranteeing contact

2.7 Case of cylindrical joint

2.7.1. Algorithm for modelling a cylindrical joint in realistic model

In nominal configuration, the cylindrical joint between two parts, as a hole Sh and a pin Sp, is performed by coaxiality constraint between two axes (Co: (Ah & Ap)); Ah and Ap are the axes of the two cylindrical surfaces Sh and Sp respectively. In configuration with defects, Sh' and Sp' are the configurations with defects of Sh and Sp. Ah' and Ap' are the axes of Sh' and Sp' respectively. According to OFA, the coaxiality constraint (Co: (Ah&Ap)) can be replaced by a coincidence relation between the two realistic axes Ah' and Ap' (Co: (Ah'&Ap')) or between a realistic axis and vertex(Co: (Ah'&V)). The method to determine the realistic axe of cylindrical surface with defects is obtained by an optimized cylinder algorithm.

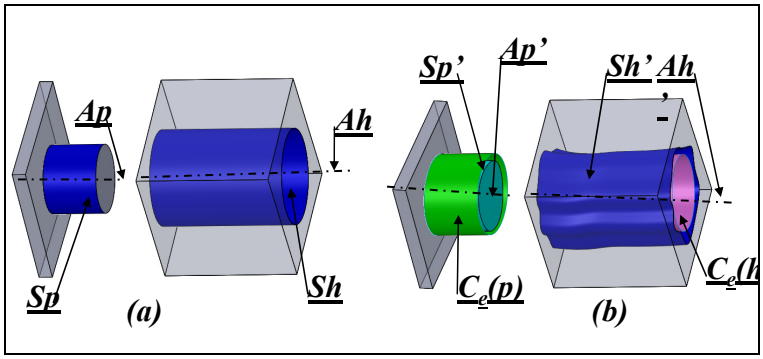

Figure 2. 13 Optimized cylinder algorithm

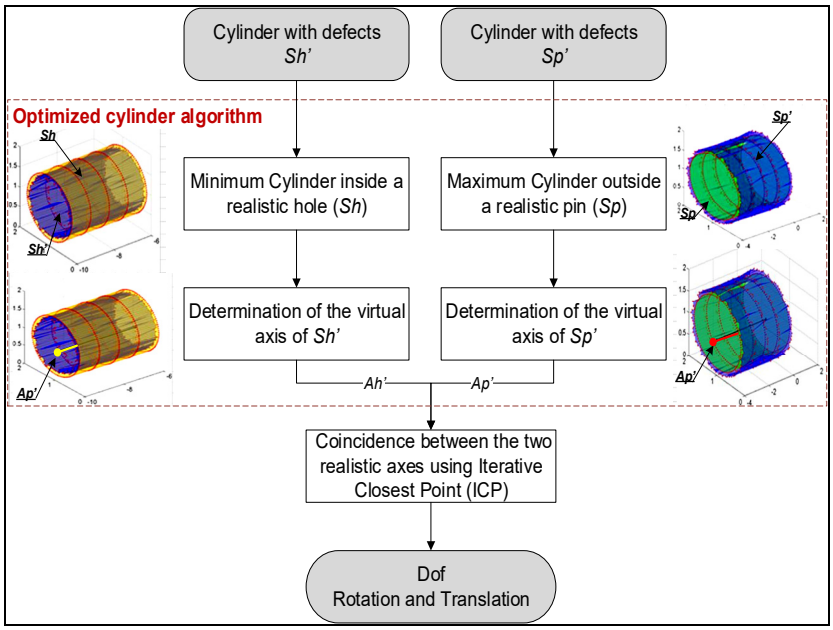

Figure 2. 14 Algorithm of cylindrical joint

2.8 Optimized cylinder algorithm

The proposed approach is based on the concept of feature operations (association, construction, etc.) of GPS standard. To calculate the optimized cylinder, the following steps are realized:

1. The first step is the cutting of the non-ideal cylindrical surface by plans, a non-ideal line on each plane is created.
2. To every line is accorded an ideal circle using Minimum Circumscribed Circle (MCC) or Maximum inscribed circle (MIC), characterized by diameter, and its centre's coordinates.
3. The cylinder's axis is obtained by the union of centre-points, resulting the non-ideal element.

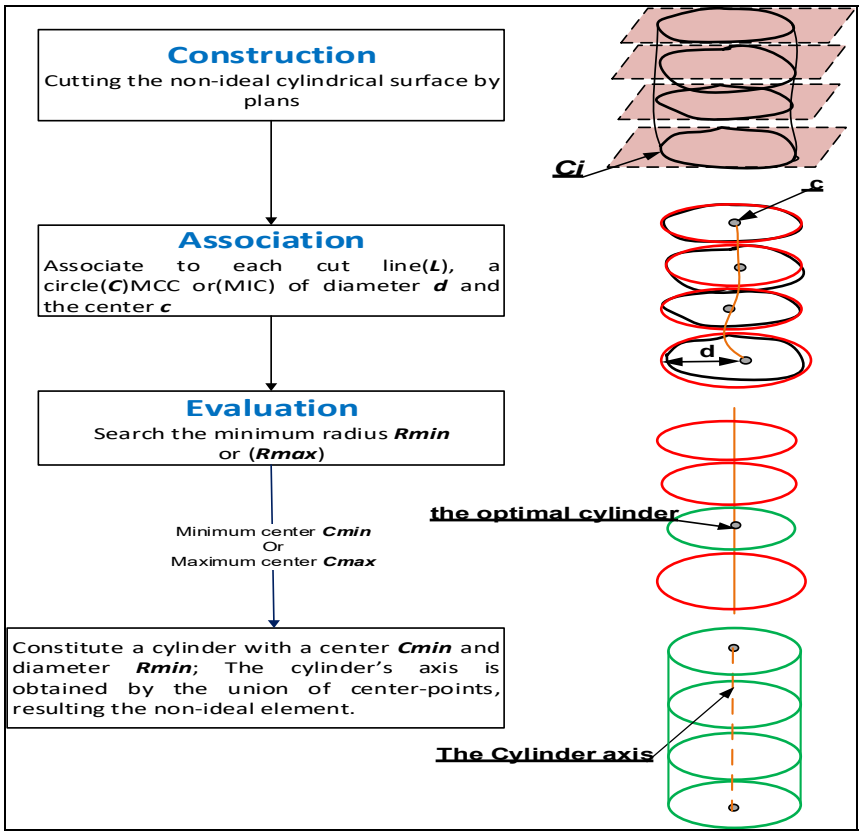

Figure 2. 15 The main steps of calculating the optimized cylinder

After cutting the non-ideal cylindrical surface by plans. The association operation is used to fit ideal features respecting specific criteria; the associated circle (C) is computed by roundness measurements (MCC) and (MIC).

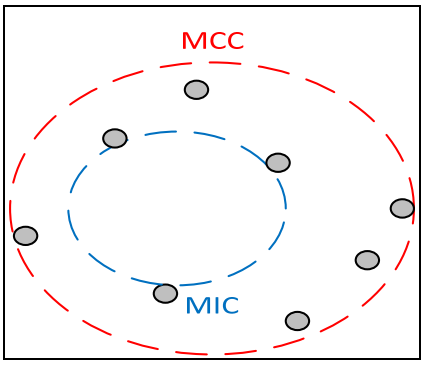

Figure 2. 16 Maximum Inscribed Circle, Minimal Circumscribed Circle

2.8.1. Determination of the Minimum Circumscribed Circle (MCC)

Thus smallest enclosing circle algorithm consists on computing the circle with minimum radius (MCC)) that encloses all circles *Ci*.

Given a set of *n* points P_i $(x_i, y_i)$to find the center $c(u_x, u_y)$ and the radius *R* of the circle that pass closest to all the points. The basic algorithm is a simple iterative given any three points in the (x, y) plane, (x_1, y_1), (x_2, y_2) and (x_3, y_3), there are two distinct possibilities:

- Two of the three points lie on a diameter of a circle that also contains the third point.
- All three of the points must lie exactly on the circumference of a circle.

In the latter event, that circle with unknown radius *R* and center (u_x, u_y) must satisfy (Equation 2. 16), (Equation 2.17), and (Equation 2.18) (the functioning of this algorithm is well detailed).

$$(x_1 - u_x)^2 + (y_1 - u_y)^2 = R^2 \quad (2.16)$$

$$(x_2 - u_x)^2 + (y_2 - u_y)^2 = R^2 \quad (2.17)$$

$$(x_3 - u_x)^2 + (y_3 - u_y)^2 = R^2 \quad (2.18)$$

The quadratic terms is eliminate in the unknowns simply by subtracting pairs of those expressions to yield (2.19) and (2.20), linear in the unknowns (u_x, u_y).

$$2(x_1 - x_2)u_x + 2(y_1 - y_2)u_y = x_1^2 - x_2^2 + y_1^2 - y_2^2 \quad (2.19)$$

$$2(x_1 - x_3)u_x + 2(y_1 - y_3)u_y = x_1^2 - x_3^2 + y_1^2 - x_3^2 \quad (2.20)$$

Solve that linear system of equations for (u_x, u_y).then use (2.18) to obtain R.

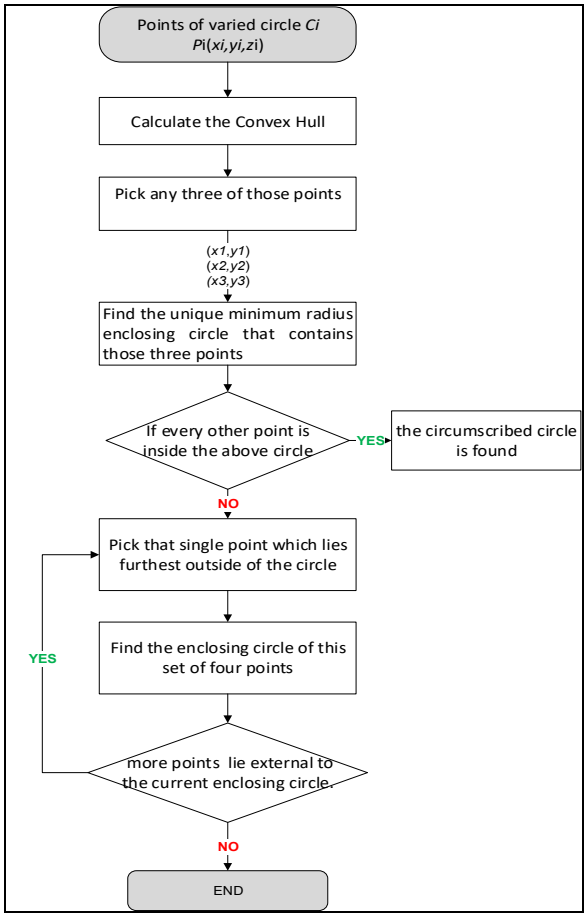

Figure 2. 17 Determination of the Minimum Circumscribed Circle (MCC)

The results of five different cases of execution (200, 500, 1000, 1500 and 200 points) are presented in Table 3. For each case the error *E* of radius is computed as shown in the Equation. 2.21.

$$E = R_{WC} - R_C \tag{2.21}$$

Where R_{WC} is the radius without convex hull and R_c the radius with convex hull of optimized cylinder.

Tableau 2. 3 Result of the execution of optimized algorithm

	Without Convex Hull		With Convex Hull		*E*
N	Time[sec]	Radius	Time[sec]	Radius	
200	1.953	1,0730	0.839	1,0778	0,0048
500	2.230	1,0882	1.174	1,0840	0,0042
1000	2.357	1,0898	1.255	1,0810	0,0016
1500	3.494	1,0883	1.290	1,0833	0,005
2000	3.605	1,0946	1.389	1,1103	0,0157

Using convex hull, the optimized algorithm terminates after a few iterations. This choice reduces the execution time (See Figure 2.18).

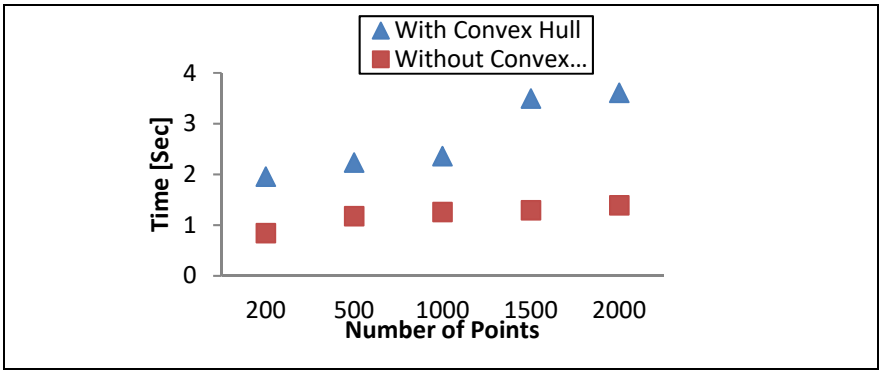

Figure 2. 18 Execution time of method 1 with /without Convex Hull

2.8.2. Determination maximum inscribed circle (MIC)

To calculate MIC Voronoi diagrams are used; Voronoi diagrams are named after Russian mathematician Georgy Fedoseevich Voronoi in 1908 (Petrík, 2009) are fundamental data structures that have been extensively studied in Computational Geometry. The associated Voronoi diagram subdivides the embedding space into regions. Each region consisting of the points that are closer to a given object than to the other (Figure 2.19). The Voronoi diagram we can use for determining the MIC. The inscribed circle has the center on Voronoi vertex or on Voronoi edge, which intersect convex hull. The radius is a distance of circle center and

convex vertex. For a calculating the convex and Voronoi diagram the Delaunay triangulation is used was invented by Boris Delaunay in 1934 (Petrík, 2009).

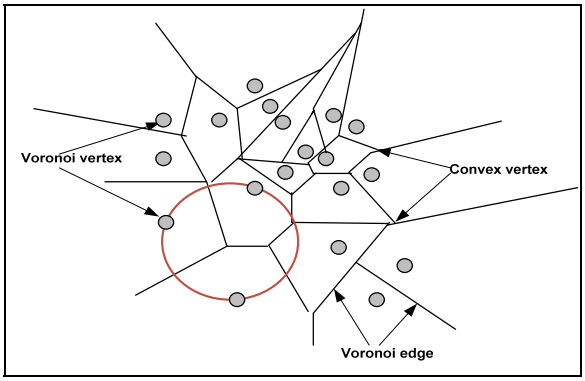

Figure 2. 19 Determining the inscribed circle

2.9 Motion simulation with Cylindrical joint

The objective is to determine the realistic assembly behavior in motion simulation with cylindrical joint. The two cylindrical surfaces Cp and Ch (of a pin and a hole respectively) are subjected to cylindricity tolerances Tfp and Tfh respectively (Tfp = 0.035mm and Tfh = 0.025mm). The functional requirement of this assembly is a minimum Gap. In proposed modelling, the above requirement is defined as the minimum distance between a point from a first surface and the triangle of the second one (See Figure 2.20).

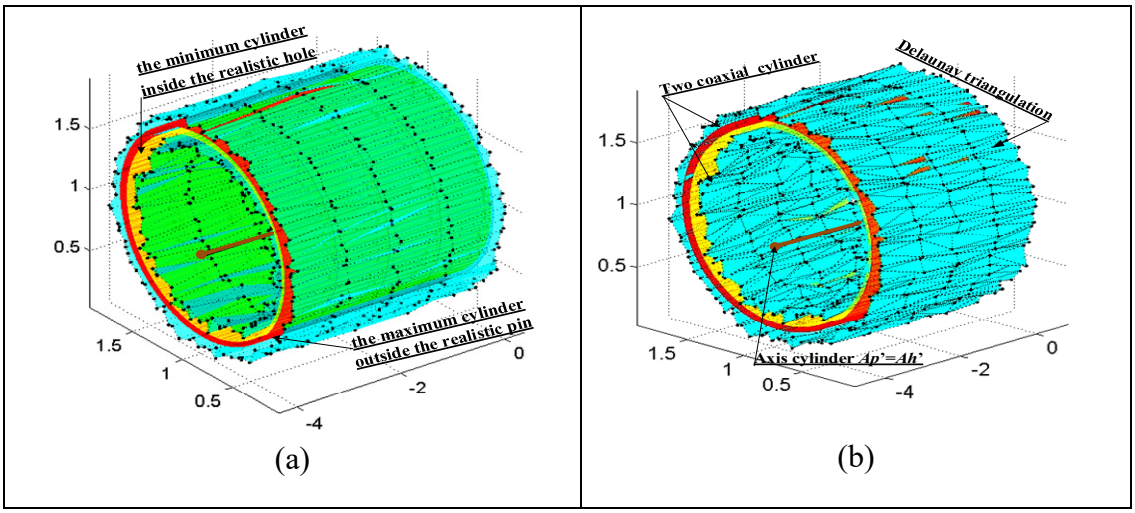

Figure 2. 20 Two coaxial cylinders (a) without triangular mesh (b) with triangular mesh

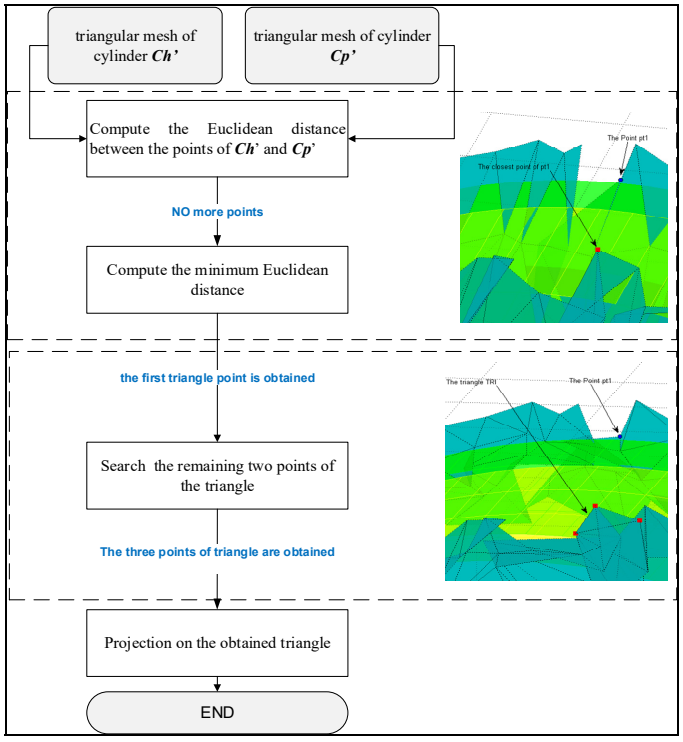

Figure 2. 21 Algorithm for computing of gap

According to tolerance requirements, surfaces with form defects are modeled: Cp' and Ch' are two realistic configurations of Cp and Ch respectively. Two datasets are obtained. The

minimum Euclidean distance between each point couple of the two datasets is determined. Thus, the first vertex $pt1$ in (Figure.2. 21) of the nearest triangle TRI is identified. The desired triangle TRI can be one of the triangles that admit $Pt1$ as vertex. The two other vertices of TRI are determined according their corresponding Euclidean distance to $Pt1$.The Tableau 2.4 shown tolerance impacts on the functional requirements during the assembly motion.

Tableau 2. 4 Results of Gap computation

Translation	Rotation	Gap	Figures
0	0	0,1075	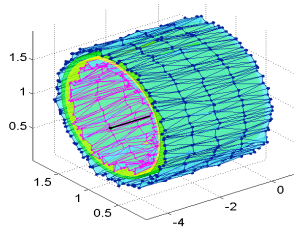
	120	0,0965	
	90	0,0993	
	150	0,1001	
	210	0,1117	
	240	0,1130	
	300	0,1327	
0.2	0	0,1282	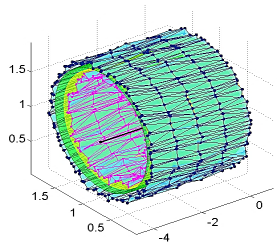
	120	0,1225	
	90	0,1238	
	150	0,1213	
	210	0,1592	
	240	0,1194	
	300	0,1218	
0.5	0	0,0666	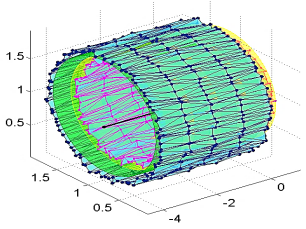
	120	0,0590	
	90	0,0736	
	150	0,0599	
	210	0,0622	
	240	0,0635	
	300	0,0666	
0.7	0	0,0468	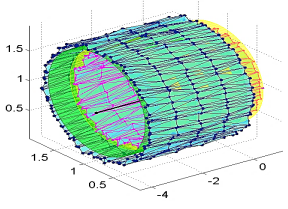
	120	0,0458	
	90	0,0446	
	150	0,0471	
	210	0,0501	
	240	0,0518	

Tableau 2.4 (continued)

Translation	Rotation	Gap	Figures
1.2	0	0,0279	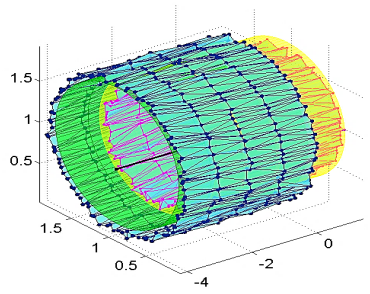
	120	0,0311	
	90	0.0294	
	150	0.0329	
	210	0.0366	
	240	0.0386	
	300	0.0427	

2.10 The case of a revolute joint

The method to redefine the mating constraints of a revolute joint is shown through the case of a revolute joint between two parts A and B obtained by a coincident constraint between two planar faces and a coaxiality condition between two axes; This joint is defined by:

- A coaxiality condition between two axes $L1$ (Co: $Ah\&Ap$).
- A coincident constraint between two planar faces $L2$ (Co: $Fa1\&Fb1$).

The parts A' and B' are the realistic configurations of parts A and B respectively: The faces $F'a1$, $F'a2$, $F'b1$ and $F'b2$ are deduced from the faces $Fa1$, $Fa2$, $Fb1$ and $Fb2$ respectively the tolerance face is modeled by V_i gird vertices then a White Gaussian Noise (WGN) is assigned . The realistic face is obtained by TPS interpolation.

According to the OFA composed by the two nominal parts A and B, the revolute joint isperformed by $L'1$ (Co: $A'h\&A'p$) and $L'2$ (Co: Q_{uv} & V_{uv}):

- $A'h$ is the axis of the cylinder Ceh. Ceh is the minimum cylinder inside the realistic hole $F'a1$.
- $A'p$ is the axis of the cylinder Cep. Cep is the maximum cylinder outside the realistic pin $F'b1$.

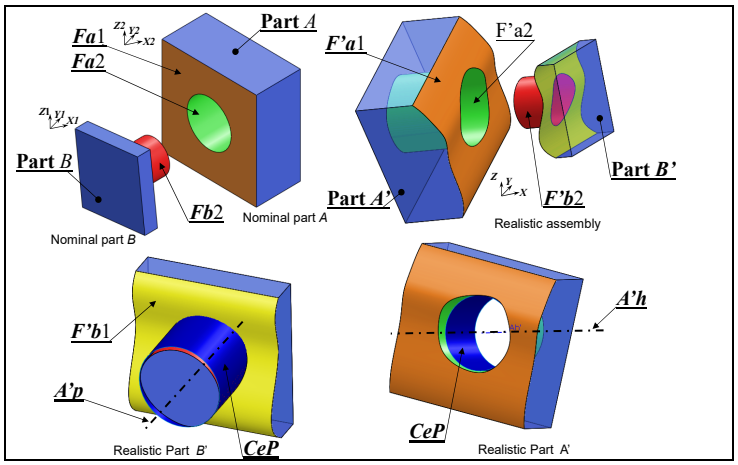

Figure 2. 22 Nominal and realistic models

After the application of the constraint $L'1$, the vertex V_{uv} and the plane Q_{uv} are determined by using the method in Figure.2. 22:

- A rotational angle ψ_e about the axis A ($A = A'h = A'p$; the rotation axis) is defined: $\psi_e = 2e\pi/N$ (e=1 to H). The choice of the integer H depends on the result accuracy intended by the designer and on the complexity of the face loop.

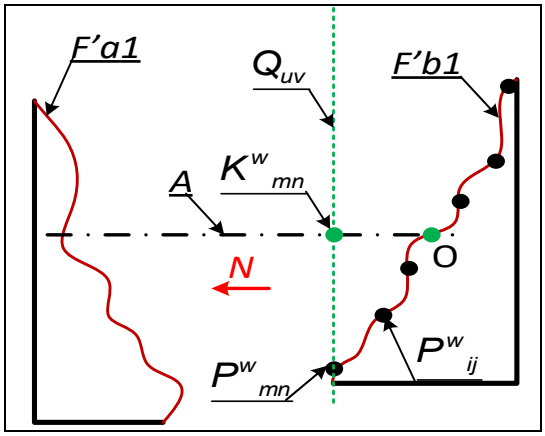

Figure 2. 23 Case of ψ_w rotation P^w_{mn}=P_{uv}

- The face $F'b1$ is modeled by a grid of vertices P_{ij} by the two parameters m and n. After each rotation of the part B' by an angle ψ_e around the A axis, P_{ij} is projected on axis A to obtain the K^e_{ij} vertices (Figure. 2.23). The vertex O is the intersection between the

axis A and the face $F'b1$. $\overrightarrow{N}$ is the driving vector of the A axis. For each ψ_e rotation, the distance D_{pq}^{e} is determined by the relation (Equation. 2.22). Then, the vertex P_{uv} corresponds to the distance D_{uv}^{w}.

$$\begin{cases} D_{pq}^{e} = max\left(D_{ij}^{e}\right); D_{ij}^{e} = OK_{ij}.Sign(\overrightarrow{OK_{ij}}.\ \overrightarrow{N}) \\ P_{uv}\ such\ as\ D_{uv}^{w} = max(D_{mn}^{e}); (e = 1\ to\ H\ and\ w\ \in [1, H]) \end{cases} \quad (2.22)$$

The plane Q_{uv} is perpendicular to A through P_{uv} .The vertex Q_{uv} is the projection of P_{uv} on $F'a1$ along the A axis. Then, a coincident constraint is applied between the plane Q_{uv} and the vertex V_{uv}

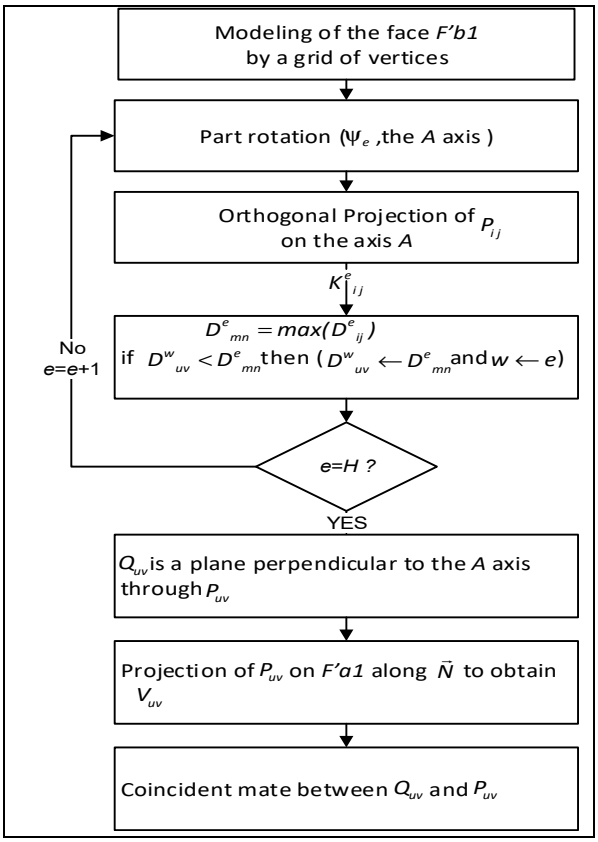

Figure 2. 24 Sub-algorithm used to determine Q_{uv} and V_{uv}

2.11 Conclusion

In this paper, a new approach to integrate tolerances in CAD models was proposed. Position, orientation and form tolerances are considered. The components with geometrical tolerances are modelled in CAD model by using two algorithms:

- The first one leads to obtain a component with positional defect; the tolerance zone is discretized to determine the realistic configurations of the tolerance element: Sub-algorithms are developed to obtain realistic configurations of a planar face. In CAD model, the realistic configurations of the part are obtained by the face displacements (rotation and/or translation) using transformation matrix.
- The second algorithm allows the determination of components with form defects: tolerance face is modeled by gird vertices a Gaussian Noise of gird vertices is computed. The realistic face is obtained by a TPS interpolation.

The realistic configurations of the assembly are performed by the updating of the mating constraints. The mating constraints considered, in this paper, are the coincident and the distance relations between two planar faces as well as the coaxiality between two cylinder axes. The developed model is a tool of the tolerance analysis while considering the assembly process planning and the contact types between parts. The developed tolerance analysis tool considers not only part deviations but also assembly process planning and contact types between components. The impact of the tolerance stack-up on the functional requirement in a dynamic environment can be quantified. The performance of the proposed tolerance analysis tool has been demonstrated by computing functional key characteristics. Future projects are underway to simulate other joint type.

2.12 Acknowledgments

The authors would like to thank the Institut Supérieur des Sciences Appliquées et de Technologie de Sousse (Tunisia), and École de Technologie Supérieure (ÉTS, Montréal, Canada) for support.

CHAPITRE 3

EVALUATION OF THE ALGORITHMIC ERROR OF A FITTING CIRCLE USING ISO 14405 SPECIFICATIONS

Ibtissem Jbira[a,b,c] , Antoine Tahan[b], Mohamed Ali Mahjoub[c], Borhen Louhichi[d]

[a]Institut Supérieur d'Informatique et des Technologies de Communication, G.P.1 Hammam Sousse-4011, Tunisie
[b]École de technologie supérieure (ÉTS), 1100 Notre-Dame West Street, Montreal, Quebec, H3C 1K3, Canada
[c]LATIS, ENISo, University of Sousse, Sousse 4023, Tunisia
[d]LMS, ENISo, University of Sousse, Sousse 4023, Tunisia

Article accepté pour publication dans la revue : International Journal of System Assurance Engineering and Management 03 Juillet 2019.

3.1 Abstract

A manufacturing process must produce components according to the technical requirements such as dimensional and geometrical specifications, Inspectors must then transmit a value and status on conformity (accepted/reject tag). Typically, a quality control operation estimates the actual object/feature size and deviations from the nominal model. While inspectors should take measurements correctly, their results may differ because they use different measurement systems and different interpretations and assumptions to convert data collected to 'size' or 'geometric deviation'. This remains a problem in industrial performance, Therefore the need for a reliable strategy to analyze errors in the inspection of part. The recent publication of ISO 14405-1:2016 defined size as a fundamental geometric descriptor. It also described a new set of specification/modifier tools for size. In this paper, we will consider the specific case of a circle. Because of the inherent variations in the manufacturing and measurement process, the actual shape of a circular element is not perfect (e.g. two or three lobes, etc.). To convert the control measurement points as captured by a device such as a CMM or scan, it is necessary to select the appropriate algorithm (e.g. least squares (GG), maximum inscribed size (GX); minimum circumscribed size (GN), minimum zone (SN)) including working hypotheses (e.g. the treatment of outliers, noise filtering, missing data, etc.). Thus, measuring the size of a circle

can be a complex subject when size includes form defects and measurement noise. This means that the person performing the analysis must also make a suitable choice of which algorithm to use, hence the importance of ISO 14405 modifiers. A Digital Benchmark was developed to compare the sensitivity of form defects on size evaluation according to the specification/modifier tools of ISO 14405-1:2016. As such, the four modifiers of the ISO 14405 standard were analyzed and detailed interpretations on the algorithm to be used for each of them have been presented. The developed Digital Benchmark demonstrates the influence of the modifier (algorithm) on the determination of the size and form defect. The study of the ISO 14405-1 specifications method presented is awaited to be an effective help in making the select of the algorithm to be used for realization of reference circle.

Keywords

Metrology, Least Squares size; Maximum inscribed size; Minimum circumscribed size; Minimum size; Form defect; Algorithmic error; Surface fitting.

3.2 Introduction

A common problem in the quality control of circular parts is the measure of the actual size and their circularity/roundness (form defect) (Chang and Lin, 1993). This is one of the basic geometric shapes common to most engineered parts. It also happens to be the most relevant geometry of industrial products since 70% of all engineering components are circular. What's more, it is also important geometry that can be found in a pin-hole assembly constraint to build the final product (Pt et al., 2018) (Jbira et al., 2017) . During the assembly phase, the out-of-roundness presents recurrent problems and produces a discrepancy between the mating components. Thus, precise roundness error is important for the functioning of assemblies. Roundness is therefore a necessary quality control parameter in the industry. Adding to the difficulties in roundness measurement operations (quick fitting operations are in high demand), the measurement tools are able to steadily acquire as many as millions of data in a few seconds. As such, the roundness measurement time can increase for these reasons, a rapid inspection operation is required to decrease inspection cost and minimize product cost. Exact and rapid

fitting operations are strict requirements (Morse and Srinivasan, 2013). The designer assigns the appropriate geometric requirements for each element in such a way that the designed elements work well during the assembly phase, these requirements are expressed by symbols described in the international standards in a drawing part, and Figure 3.1 illustrates the geometrical process. This paper introduces validation methodology for of circle fitting methods applicable to complete and incomplete points with a form defects in the presence of noise.

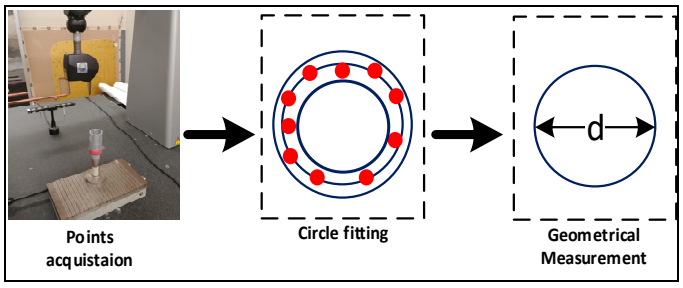

Figure 3. 1 Geometrical fitting process

3.3 New specifications of size tolerances, as defined by the ISO 14405-1

The publication of the ISO 14405-1: 2016 initiated a new set of size specification modifiers using these new tools (ISO14405 Part 1. 2016.). the designer specifies the geometry of the entities with more details than before. The ISO 14405-1 defines 14 symbols (Tableau 3.1) for the specification of linear size (Jbira et al., 2018a). Figure 3.2 illustrates an example of the 14 shapes of a cylindrical feature.

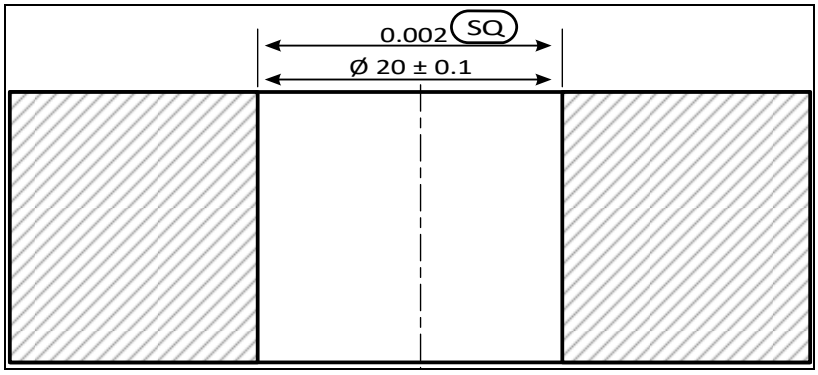

Figure 3. 2 Example of the specification of size features using the Deviation Size (SQ): lower indication; the lower and upper limits (20±0, 1) [Ref. ISO14405-1:2016].

In this paper, four new specifications of size tolerances, as defined in ISO 14405-1 are presented. This paper also limited its scope to only 2D geometric features: the "circle". In this specific case, there are only four (4) types of circularity (and diameter) evaluation methods proposed by the ISO 14405-1:2016: the center of least squares circle (GG); the center of the minimum area circle(SN); the center of the circumscribed circle(GN); the center of the maximum registered circle(GX). Future research will focus on the study of other modifiers with different geometric objects (e.g. line, plane or cylinder). A benchmark has been developed to compare the sensitivity of different parameters: (i) measurement noise; (ii) different circularity (form) defects; (iii) small and large number of points; (iv) incomplete data. The results presented can satisfy the measuring accuracy requirement of the calculated sizes, which may be one way to solve the measurement problem of a circle's calculated size to implement the ISO 14405-1 in the manufacturing industry as soon as possible. The main steps of this approach are illustrated in Figure 3.3. Four ISO 14405-1 modifiers (GN, GX, GG and SN) were studied. In addition, the paper examines the consequences of using standardized size modifiers in engineering design and investigates the influences of different parameters (measurement noise, form defects, number of points and incomplete data) in diameter evaluation and the identification of circularity defects.

Tableau 3. 1 Four Specification modifiers and symbols Of ISO 14405-1:2016

Symbol	Type of specification	Name
GG	Direct global	Least Squares size
GX		Maximum inscribed size
GN		Minimum circumscribed size
SN	Statistical	Minimum size

3.4 Stat of art

In the quality analysis of circular components, the circularity error is one of the important parameters in industry. The estimation of this parameter is mainly gotten by using a coordinate measuring machine. Many researchers have proposed different algorithms to calculate the reference circles that are used to quantify the roundness errors applied in many fields (Wang et al., 1999) (Srinivasan, 2013). Thus, with the absence of recommendations by the ISO about the method adopted to terminate roundness (Pt et al., 2018), the estimation of circularity errors remains a challenge in permitting the improvement of algorithms to calculate the best center. Many computational geometrics are used. Frequently, inspectors use laser scanning as a technology that can quickly obtain dense and accurate three dimensions (3D) called Point Cloud Data (PCD). In laser scanning the circle fitting is still an important problem in the presence of noise, outliers, etc. (Xiuming et al., 2013). (Nurunnabi et al., 2018) proposed a new 3D robust cylinder-fitting algorithm. They demonstrated performance on artificial and real datasets, in the presence of outliers and noise, and in the case of a small and large number of points and for different sizes of radius. The developed approach can be used for fitting cylindrical poles. (Nurunnabi et al., 2018) , (Nurunnabi et al., 2019) described the problem of circle fitting for complete and incomplete datasets with outliers. They proposed a robust approach for circle fitting which had to merge two algorithms: Principal Component Analysis (PCA) and robust regression. The experimental results confirmed the robustness of the proposed approach with a different percentage of tolerance of clustered outliers. They compared the proposed approach with another exciting method. (Zhao et al., 2018), proposed

to calculate the actual calculated sizes by the trained Neural Network Regression (NNR). The trained models for the evaluation of the calculated sizes were verified. The verified results could satisfy the measuring accuracy requirement of the calculated sizes. This may be one way to solve the measurement problem of the calculated sizes of cylinders for implementing the ISO 14405-1. The evaluation method of calculated sizes based on the NNR models is feasible and has higher measuring accuracy. (Guo and Yang, 2019) proposed a new procedure for circle fitting. They used Taubin's approch to compute the center and radius, then they identified and removed the outliers by computing the geometric distances from the data points to the circle. Their experiments demonstrated that the iterative procedure can resist against the effect of outliers. Finally,(Pt et al., 2018), presented a comparative study of roundness evaluation algorithms (MIC, MCC, LSC) for coordinate measurements. They proposed a selected benchmark of algorithms in the literature in order to provide the optimal choice of execution. It was concluded that no single algorithm provided the best solution.

3.5 Proposed BENCHMARK of THE ISO 14405-1 specification modifiers (PBISM)

In this work, we will study the influence of the form defects of a unitary circle (⌀ = 1) on the evolution of ISO 14405-1 modifiers. (See Figure 3.3).

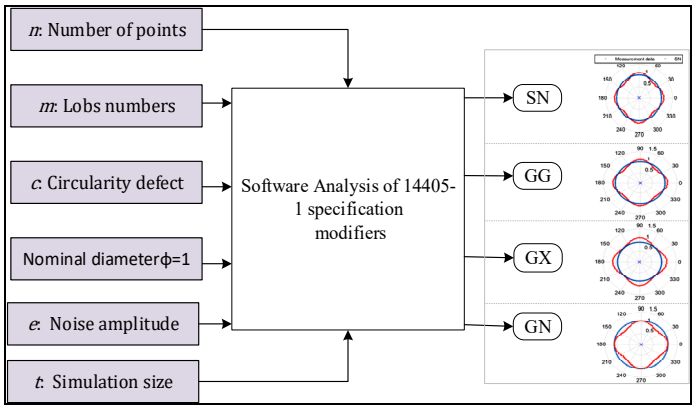

Figure 3. 3 Proposed methodology

3.5.1 Proposed Methodology

- Four types of form defects (2 lobs, 3 lobs, 4 lobs and egg asymmetry form). Lob numbers are represented by the variable (m= [2, 3, 4]).
- Four values of circularity form errors (relative to the diameter value) are represented by the variable $c = [1\%, 2\%, 5\%, 10\%]$
- Measurement noise is assumed Gaussian. The amplitude of the standard deviation is chosen in this interval $[1\%, 2\%; 5\%, 10\%, 15\%, 25\%]$ of the circularity error c.
- The number of simulations for Monte Carlo ($\geq 2 \times 10^3$) are chosen to guarantee convergence.

3.5.2 Circularity Modelling

The relative form error e is defined as the ratio between circularity defects c [mm] and nominal diameter ⌀ (defined by 14405-1 ISO). Two values of circularity defects are proposed (Jbira et al. 2018).

$$e = \frac{c}{\varnothing} \tag{3.1}$$

Where c is the circularity defect; $e \in [\,1\%, 2\%; 5\%, \ldots, 25\%]$ and $\varnothing = 1$.

(i) Lobbing: in the case of a lob number, the distances at two opposite points are constant;

(ii) Asymmetry: there is a difference between the major and minor axes (See Figure 3.4);

(iii) Irregularities without specific form.

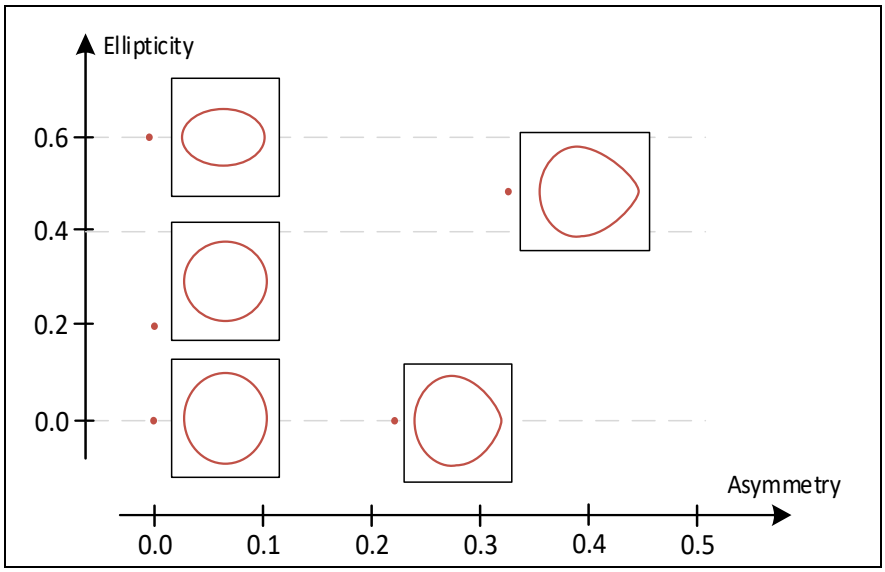

Figure 3. 4 Asymmetry

In this paper, only four types of circularity defects are considered (2, 3 4 lobes and egg (asymmetry) form). The developed algorithm for the creation of these parts are presented in Algorithm 3.1. This was implemented in Matlab R2018a. **Out-of-circularity** is either symmetrical or asymmetrical. The symmetrical lobbying has regular lobes, but in the asymmetrical ones, the lobbying is irregular.

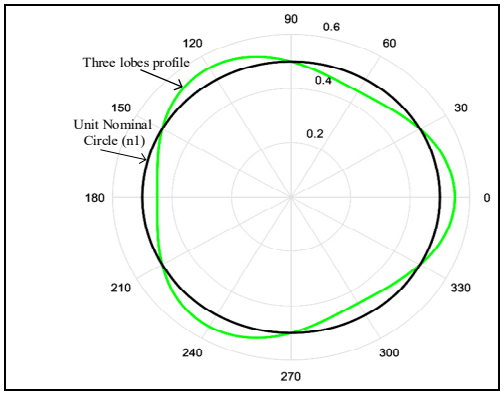

Figure 3. 5 Example of three lobes: diameters at equal places but still not circular form c=0.1 ,m=3

For cartesian coordinates, (x_i, y_i) are the i^{th} data points' coordinates in the X and Y axis (see example in Figures 3.5 and 3.6). The form error is generally a function of the deviations from the reference shape. A perfect circle is defined by the equation: $(x - x_c)^2 + (y - y_c)^2 = r^2$, r denotes the radius of the circle and the coordinates of the circle's center are (x_c, y_c). The defining parameters of the equation of a circle are thus m and c.

$$x = rc\left(\left(\frac{1}{c}\right) + cos(m\theta)\right)cos(\theta) \tag{3.2}$$

$$x = rc\left(\left(\frac{1}{c}\right) + cos(m\theta)\right)cos(\theta) \tag{3.3}$$

Where $r = 0.5$, $\theta = [0 \ldots (2\pi) - (2\pi)/n]$ and $m = [2,3,4]$.

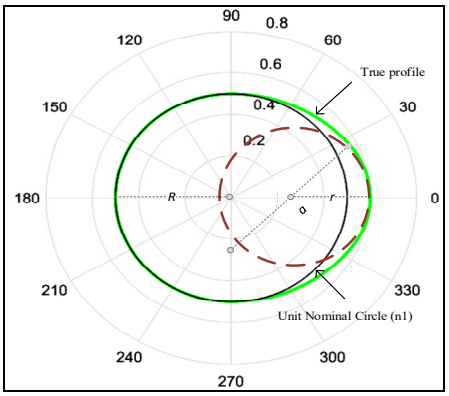

Figure 3. 6 Example of egg asymmetry: c=0.1, r=0.4 a=0.2

If the separation between left and right caps is a and the radii are R and r, respectively, with $r < R$ and $R - r < a$, then the center $(0, y)$ and radius P of the joining circle are:

$$p = \frac{a^2 + R^2 - r^2}{2(R-r)} \tag{3.4}$$

$$y = \frac{(R-r)^2 - a^2}{2(R-r)} \tag{3.5}$$

Call the three circles C_R,C_r and C_p. Let the upper point of intersection of C_r and C_p be (x_0, y_0), let the angle between the vertical dashed line and the line through (x_0, y_0) be θ, and let the angle between the horizontal radius of C_r and dashed line through (x_0, y_0) be $\emptyset$.

$$x_0 = \frac{a(a^2+R^2-r^2)}{a^2+(R-r)^2} \tag{3.6}$$

$$y_0 = \frac{2a^2r}{a^2 + (R-r)^2} - r \tag{3.7}$$

$$\theta = tan^{-1}(\frac{a}{y}) \tag{3.8}$$

Then and half the area enclosed by the oval is the sum of the areas of the leftmost quarter circle, the sector of C_p, and the sector of C_r minus the area of the triangular portion of the sector of C_p lying below the x-axis.

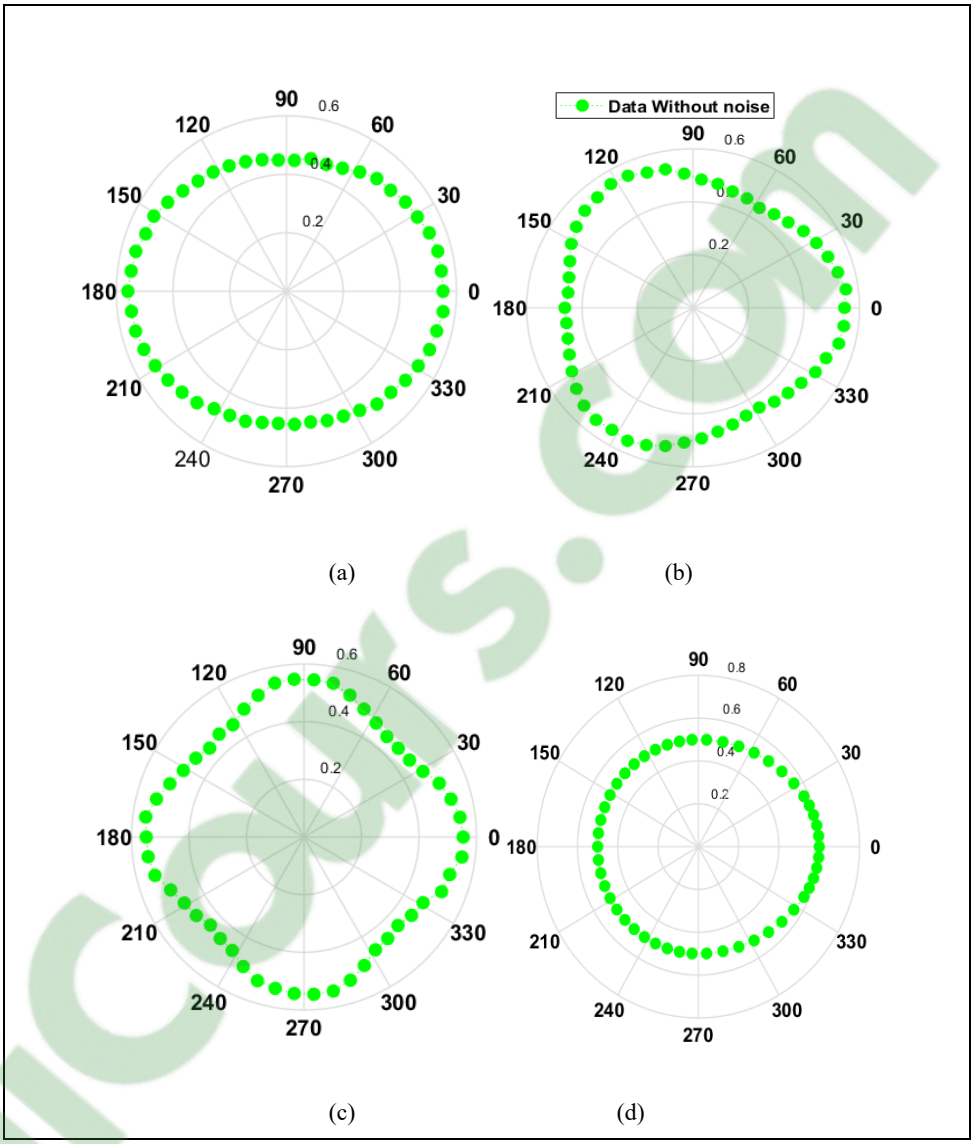

Figure 3. 7 Part circle: lobbing with Circularity Defect c =0.1, and $n = 50$

Algorithm 3.1. Pseudo-code of the proposed digital benchmark

Pseudo-code of the proposed digital benchmark

Input: m: Lobs number; n: Number of points; c: Circularity form error; $\varnothing$: Diameter nominal ; t: Number of simulation for Monte Carlo; v : Measurement noise; μ=0; σ: Standard deviation parameter;
Output: The best results(OOR , Diameter, Center)
1 Create the defects of lobbing type;
2 Calculate the noise standard deviation σ;
3 **Add the noise**

Algorithm 3.1. (Continued)

Pseudo-code of the proposed digital benchmark

For i=1: t
For j=1: n
Generates Gaussian random number a from the distribution with mean parameter $N(\mu, \sigma)$:
$x_n(i,j) = x(j,1) + a\ cos(theta(j,1))$;
$y_n(i,j) = y(j,1) + a\ sin(theta(j,1))$;
end -For
end-For
Browse all the generated circular parts;
Switch m
Case 1:
Calculate the radius r_{GN} , the center c_{GN} and the out of roundness OOR_{GN} of GN method;
Case 2:
Calculate the radius r_{GX} , the center c_{GX} and the out of roundness OOR_{GX} of GX method;
Case 3:
Calculate the radius r_{GN} , the center c_{GG} and the out of roundness OOR_{GG} of GG method;
Case 4:
Calculate the radius r_{SN} , the center c_{SN} and the out of roundness OOR_{SN} of GN method;
Otherwise the value of m is invalid;
End - Switch
End –Algorithm

The different modeled defects are illustrated in Figure 3.7.

3.5.3 Adding measurement noise

To analyze the sensitivity of the algorithm to measurement noise in the dataset, 2×10^3 simulations are generated. Thus, the data point's coordinates (x_i, y_i) are transformed in the case of the following lobbing (See Figure 3.8):

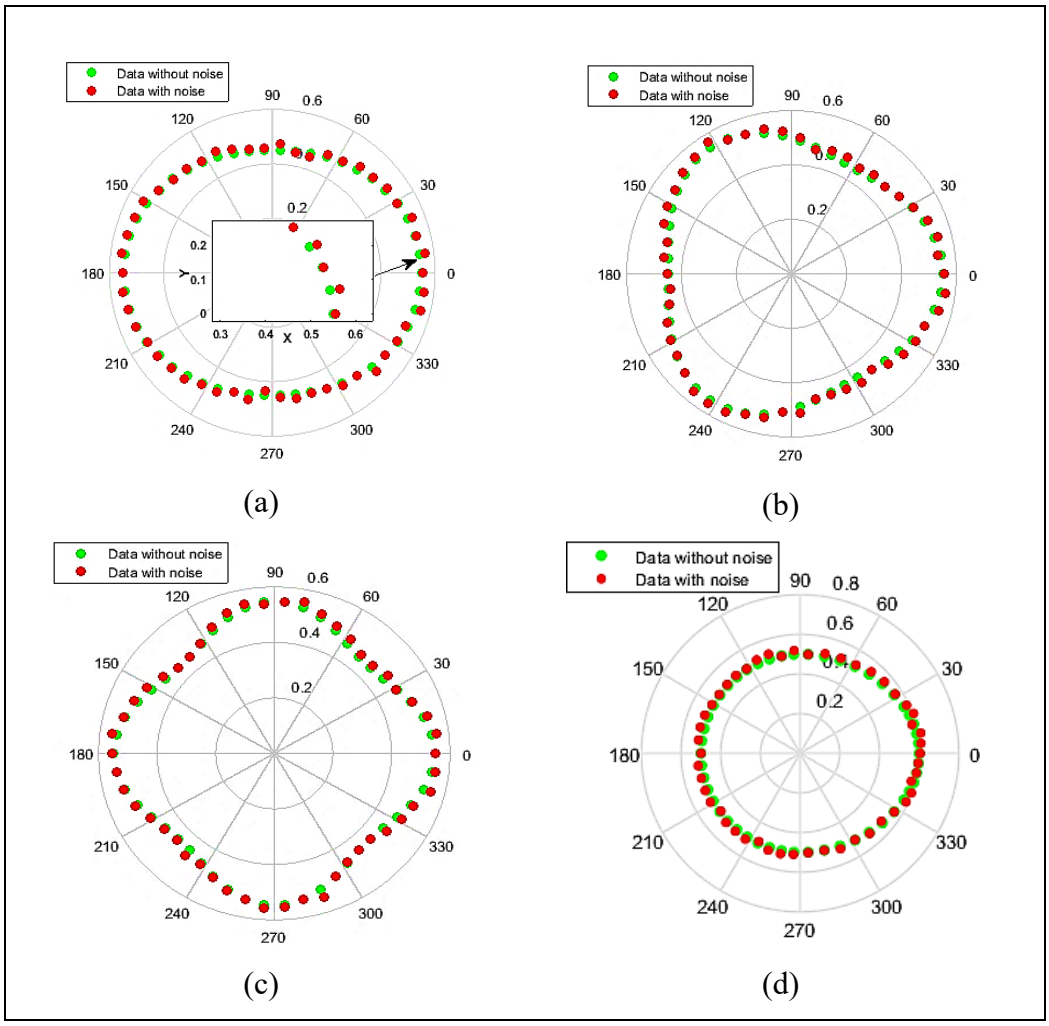

Figure 3. 8 Example of measurement data with c =0.1 mm, v=0.3 mm and n =50

$$x_{ni} = x_i + a_i\, cos(\theta_i) \tag{3.10}$$

$$y_{ni} = y_i + a_i\, sin(\theta_i) \tag{3.11}$$

Where a_i is a Gaussian random variable $N(0, \sigma)$. The standard deviation parameter σ is described as follows:

$$\sigma = \frac{1}{4} vc \tag{3.12}$$

v is the percentage of measurement noise. Figure 3.8 shows an example of measurement data.

3.6 Selection of specification modifiers

3.6.1. Minimum Circumscribed Size (GN)

The GN is defined as the circle where all data points P_i are on or inside and its radius is minimal (Jbira et al. 2017) (Gopinath et al 2014).The roundness error (OOR_{GN}) value is the difference between the largest radius and the measured modifier radius r_{GN} (Sui et al. 2012) , (Jbira et al. 2018). The roundness error (OOR_{GN}) can be calculated as follows:

$$OOR_{GN} = r_{GN} - r_{min} \tag{3.13}$$

Where r_{min} the distance between the center (c_x, c_y) of the GN and each point $P_i(x_i, y_i)$.

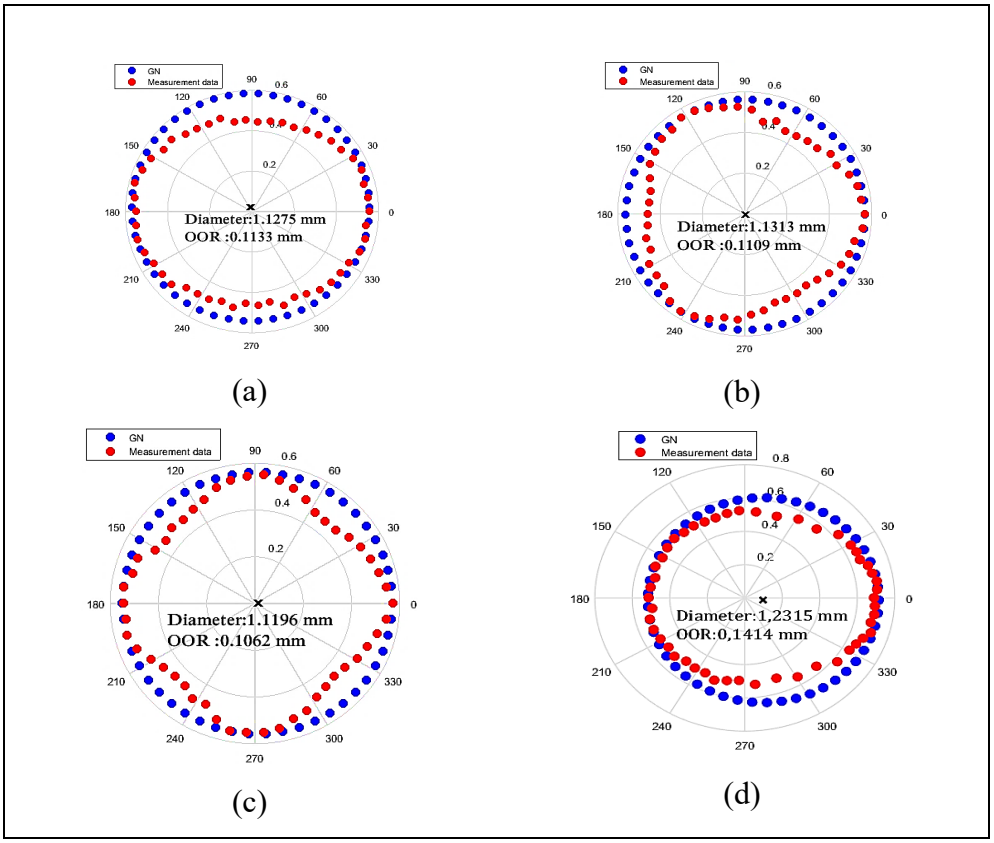

Figure 3. 9 Minimum circumscribed size of 100 points with r=0.4 and a=0.3

3.6.2. Global- Least Squares Size (GG)

This method is often called the least squares or regression method used to minimize the Euclidean norm of the deviation vector (See Figure 3.10) the objective function can be written as minimizing the sum of squared differences.

$$F = \sum_{i=1}^{n} (d_i - r_{GG})^2 \tag{3.14}$$

Where $d_i = \sqrt{(x_i - x_c)^2 + (y_i - y_c)^2}$ is the Euclidean distance between $P_i(x_i, y_i)$ and $c(x_c, y_c)$ and r_{GG} is the circle radius. The OOR_{LSZ} is calculated as follows:

$$OOR_{LSZ} = (r_{max} - r_{GG}) + (r_{GG} - r_{min}) \tag{3.15}$$

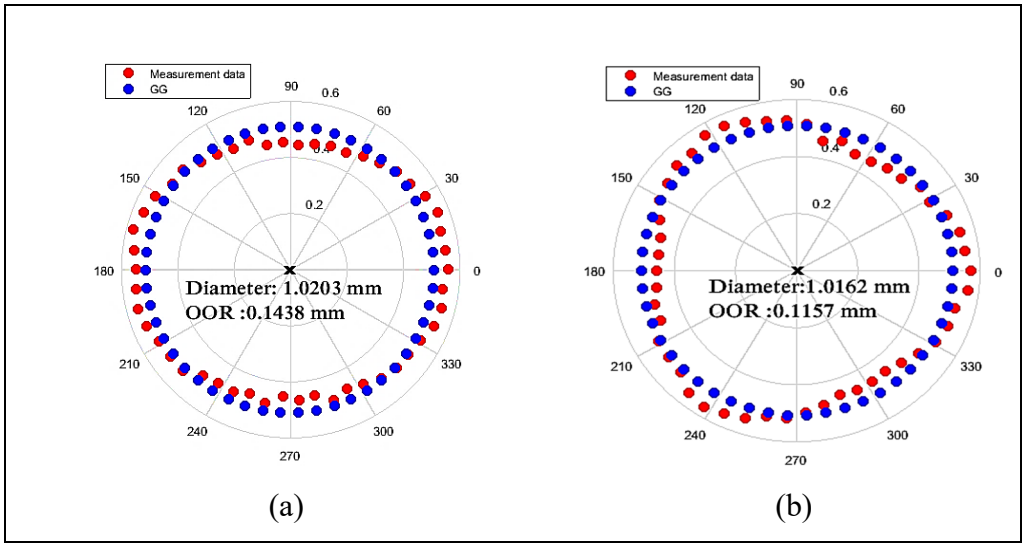

Figure 3. 10 Least Squares Size of 100 points with r=0.4 and a=0.3

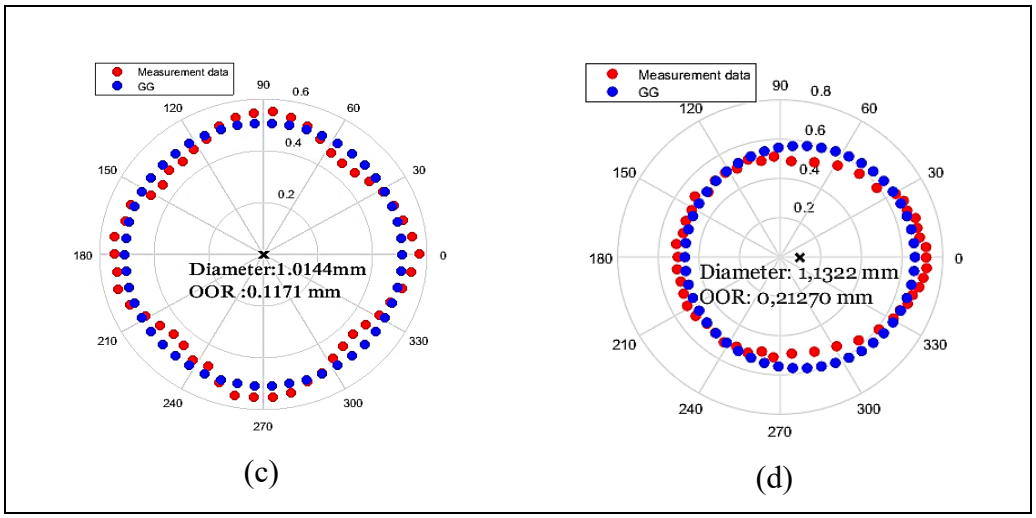

Figure 3.10 (continued)

3.6.3. Maximum Inscribed Size (GX)

The GX circle is the largest circle that can be inside the circularity profile. Voronoi diagrams are used to calculate the GX modifier, The Figure 3.11 presents some results on GX algorithm (See Algorithm 3.2) implemented in Matlab 2018.

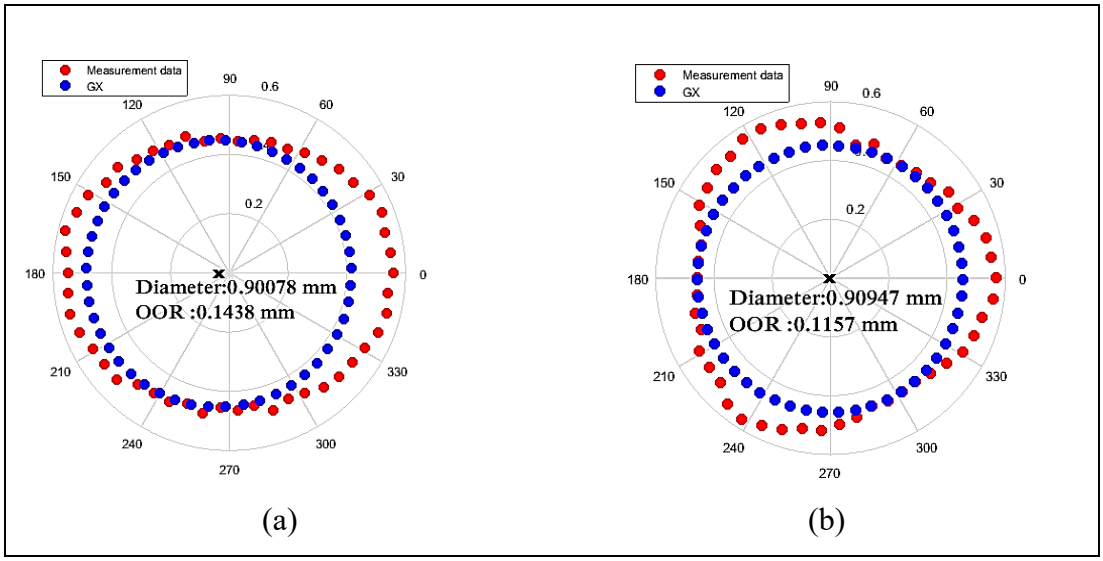

Figure 3. 11 Maximum Inscribed Size (GX) of 100 points with $r = 0.4$ and $a = 0.3$

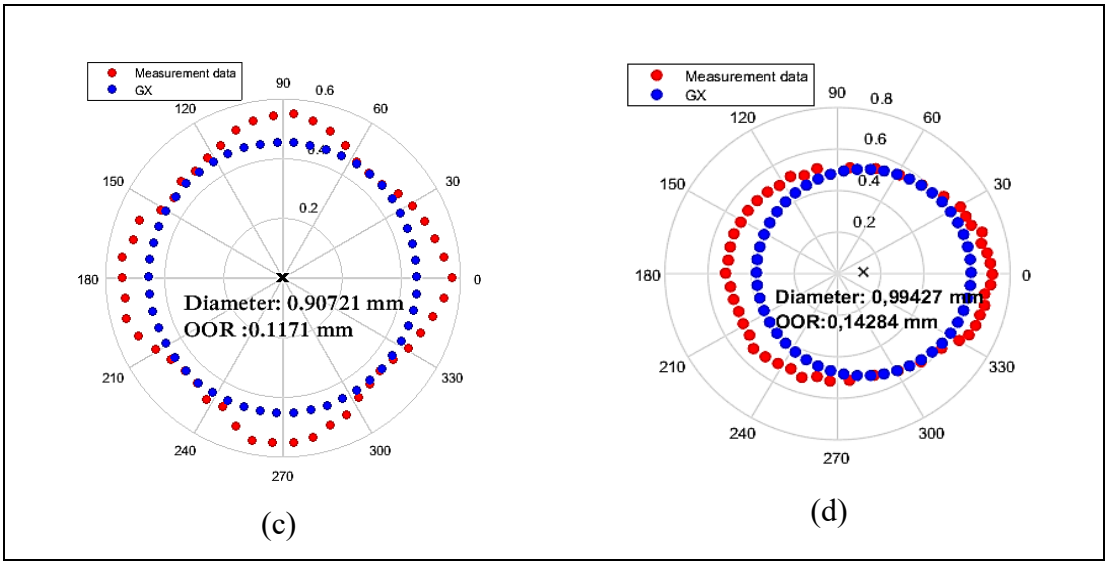

(c) (d)

Figure 3.11 (continued)

The OOR_{GX} is calculated as follows:

$$OOR_{GX} = r_{max} - r_{GX} \tag{3.15}$$

Where $r_{max}$the distance between the calculated center of the GX circle and each point.

3.6.4. Minimum Size (SN)

The SN algorithm is included in most CMM software. The SN is defined as the two concentric circles where all data points P_i lie on, or inside, them. (See Algorithm 3.2) (Kethara Pasupathy et al., 2003).

Algorithm 3.2 - Pseudo-code of SN algorithm

Pseudo-code of SN algorithm

Input: $P_i(x_i, y_i)$ i= [1… n];
Output: the center $c(c_x, c_y)$; and radius r_{GN};
1 **Begin**

Algorithm 3.2. (continued)

2 Select the coordinates of two points P_1, P_2 on the maximum circle (x_{p1}, y_{p1}), (x_{p2}, y_{p2}) using a SPF algorithm
4 Select the coordinates of two points P_3, P_4 on the minimum circle (x_{p3}, y_{p3}), (x_{p4}, y_{p4}) using a SPF algorithm
5 Construct two lines L_1 and L_2 connecting P_1, P_2 and P_3, P_4
6 Construct L_3 and L_4 are the two perpendicular lines to L_1 and L_2 at their middle points as shown in Fig. 14
7 Calculate the center of the two circles; the intersection point of L_3 and L_4 using Equation.3 16 and Equation. 3.17
8 **End-algorithm**

$$c_x = \frac{(y_{mid1} - y_{mid1}) - (m_1 x_{mid1} - m_2 x_{mid2})}{m_2 - m_1} \tag{3.16}$$

$$c_y = y_{mid1} + m_1(c_x - x_{mid1}) \tag{3.17}$$

Where m_1, m_2 are the slopes of L_3 and L_4. x_{mid1},y_{mid1} are the x and y coordinates of the middle point of L_1, $x_{mid1} = x_{p1} + (x_{p2} - x_{p1})/2$, . $y_{mid1} = y_{p1} + (y_{p2} - y_{p1_1})/2$. x_{mid2}, y_{mid2} are the x and y coordinates of the middle point of L_2, and finally, $x_{mid2} = x_{p3} + (x_{p4} - x_{p3})/2$, $y_{mid2} = y_{p3} + (y_{p4} - y_{p3})/2$.

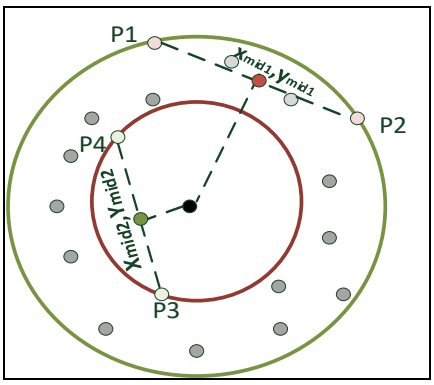

Figure 3. 12 Four points of two concentric circles

The OOR_{SN} is the minimum radial separation (r_{max} -r_{min}). Figure 3.13 shows an example of the execution of the SN algorithm in three types of defects (2, 3 and 4 lobs).

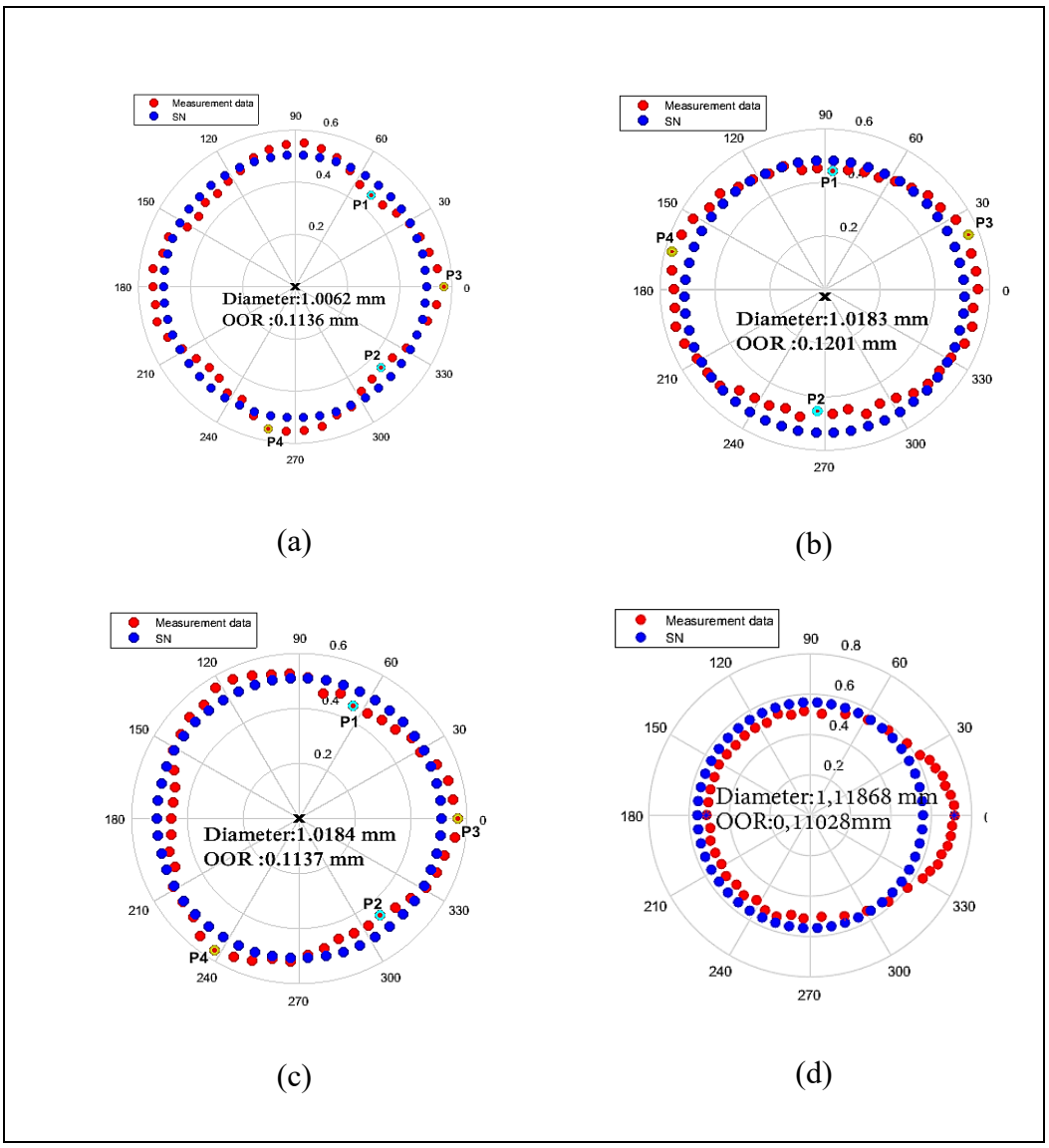

Figure 3. 13 Minimum size (SN) of 100 points with r=0.4 and a=0.3

3.7 Experiments and evaluation

In order to increase the effectiveness of the ISO 14405-1 specification methods, a suitable measurement strategy must be elaborated. In other words, the number of points must be chosen according to the purpose and parameters specified (Measurement Noise and Circularity defect). The main contribution of this paper is in the study the influence of new specifications of ISO 14405-1 on form defects. This paper introduces four algorithms of circle fitting algorithms applicable to incomplete point cloud data in the presence of noise, to compare the sensitivity of different parameters: (i) the measurement noise; (ii) different circularity (form) defects; (iii) small and large number of points; (iv) incomplete data. The results displayed can satisfy the measuring accuracy requirement of the calculated sizes. This may be one way to solve the measurement problem of the calculated sizes of the circle for implementing the ISO 14405-1 in the manufacturing industry as soon as possible.

3.8 Performance Measures

To analyze the performance of each ISO 14405-1 modifiers, estimates were made for the circle parameters: center c, diameters d. Based on those estimates, the average and the median diameters, as well as the roundness error were calculated as defined in Figure 3.14. Several experiments were undertaken on real and artificial datasets. In this paper, boxplot diagrams are used to present the results of the ISO modifiers (Figure 3.14):

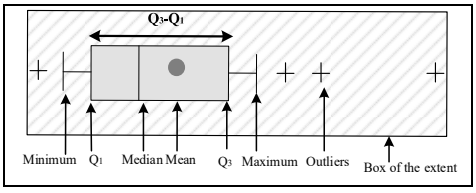

Figure 3. 14 Boxplot diagram

3.9 Artificial Numerical Datasets

in this paper an artificial dataset was created to simulates data to form defects (2 lobs, 3 lobs, 4 lobs and asymmetry), a Monte Carlo simulation was used to generate 2000 circles to obtain statistically representative results. A random noise is generated among the points with a mean of 0 and StD (Equation 3.12) in all (x and y) directions. As said, the focus of this paper is circle fitting for complete and incomplete data in the presence of a high and small percentage of noise for different number points.

3.10 Complete Data

3.10.1. Influence of the Number of Points

The appropriate choice of points guarantees the correct measurement results with the shortest running time. Recent CMMs can acquire up to large number of points to measure roundness errors. In the literature, two types of methods are used to reduce the number of points; Outer Convex Hull (OCH) and Inner Convex Hull (ICH). In this paper the GN modifier uses OCH, which is, the smallest polygon enclosing the dataset and GX uses ICH. The OCH provides a unique solution against the ICH that is not unique (Nurunnabi et al., 2018) , (Zhao et al., 2018). It is necessary to use appropriate and efficient algorithms that calculate the roundness error of the smallest possible amount of data points. In this article, the number of points is variable and can be $n\in$ [4,100] points. The analysis has been performed with a different number of points, from a small number of points to a high number of points. For each iteration value of n, 1000 circles of n points are generated, with (i) circularity defect c=10% $(0.1mm)$, (ii)measurement noise $v = 10\%$ ($\sigma = 2.5 \times 10^3$ (iii) type of circularity defect is three lobs. According to the results shown in Figure 3.15, the type of modifiers used influences the results obtained. When the diameter is being measured, the moderator type plays an important role. The results for Least Square Size (GG) and Minimal Size (SN) provide similar results for any number of points from 6 to 100. In case of a GN, the greater the number of points, the higher the diameter and operating time. However, Figure 3.15 also shows that an excessive increase in the number

of points is unnecessary when presented with an increase in diameter. In the case where the GX, is the greater number of points, the smaller the diameter and the longer the operating time.

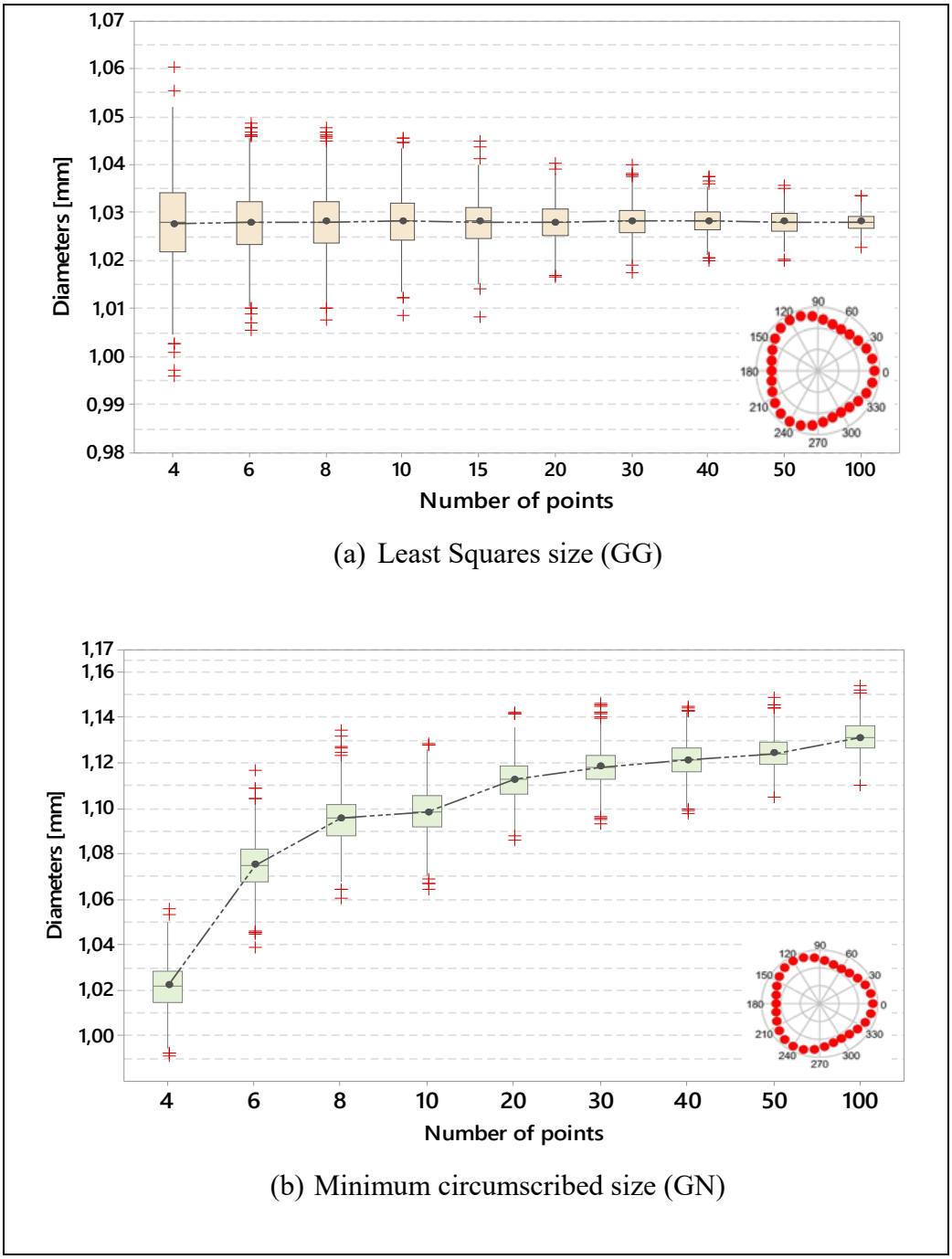

Figure 3. 15 The influence of the defect form on the evaluation of ISO 14405-1 specification methods.

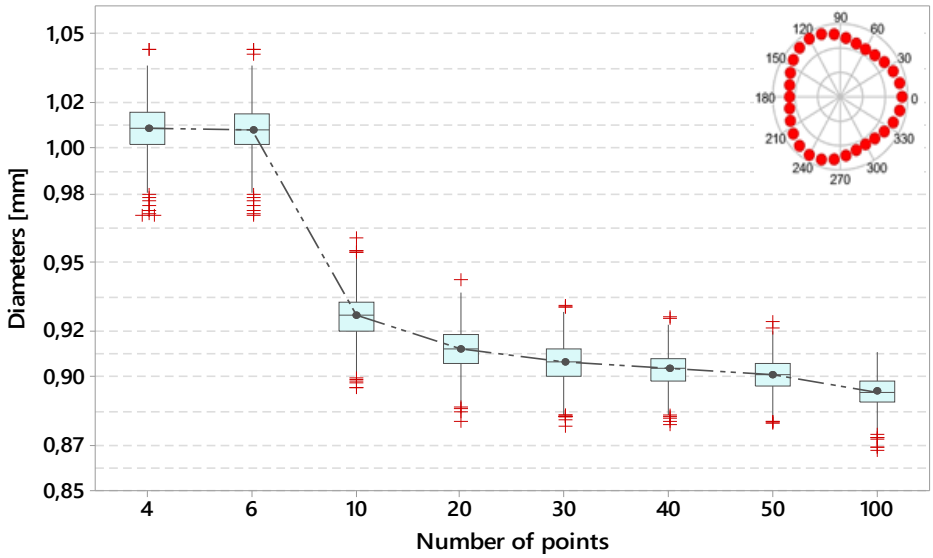

(c) Maximum inscribed Size (GX)

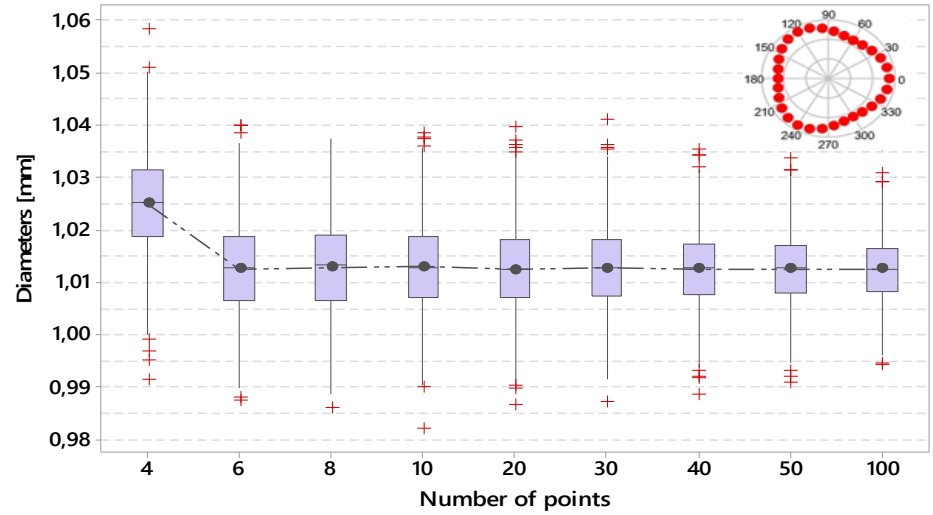

(d) SN Minimum Size

Figure 3.15 (continued)

3.10.2. Influence of measurement noise

To explore the influence of noise on the circle fitting algorithms, 2000 simulated datasets were created in three lob circles of 50 points for every percentage of 2%, 5%, 10%, 15% and 20% ,with the circularity defect is $c = 2\%$, therefore $\sigma = [0.1, 0.25, 0.5, 0.75, 1] \times 10^{-3}$. The

performance measures are computed as in the previous experiments for all cases of percentage noise. An illustration of the influence of noise on specification methods can be found in GN, GX and SN in Figure 3.16. Results are illustrated on the box plot diagrams in Figure 3.17 and Figure 18(a), (b), (c), and (d) for measurement noise

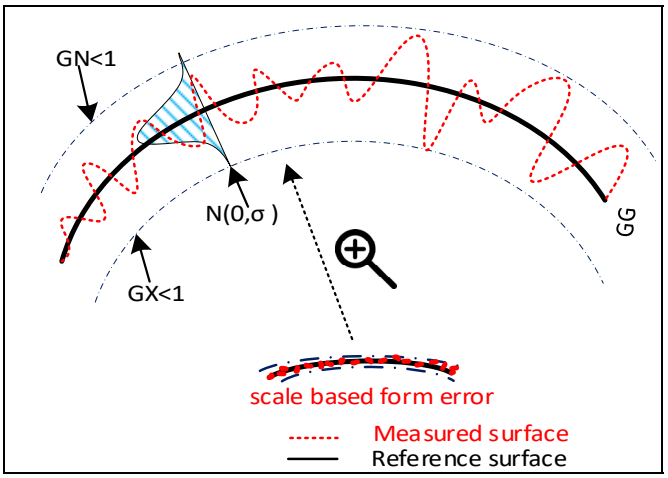

Figure 3. 16 Illustration of the influence of noise on specification methods: GN, GX and SN

Figure 3.16 shows that noise measurement influences all the specification methods. According to the Figures 3.17 and 3.18, the type of fitting element affects the achieved results. The value of the diameter does not depend solely on form deviation models. It also depends on the circle's noise level. The Monte-Carlo simulation realized confirms that the influence of measurement noise is greater on the GN and GX modifiers. This is the expected result in this specific case. In the case of the specification of an outside GN diameter, it is sensitive to high points and relatively insensitive to low points (Figure. 3.18, a). In the case of the specification of an inside diameter (Figure 3.18, b), the GX modifier must be used because it is less sensitive to high points and relatively insensitive to low points. GG (Figure 3.18, c) is relatively insensitive to extreme asperities. Therefore, it provides the most stable center to the OOR value. The SN (Figure 3.18, d) modifier is sensitive to positive and negative asperities. It also provides the optimal solution: it generates the smallest diameter value and the highest OOR value of the four modifiers, thanks to the minimum zone modifier between concentric circles.

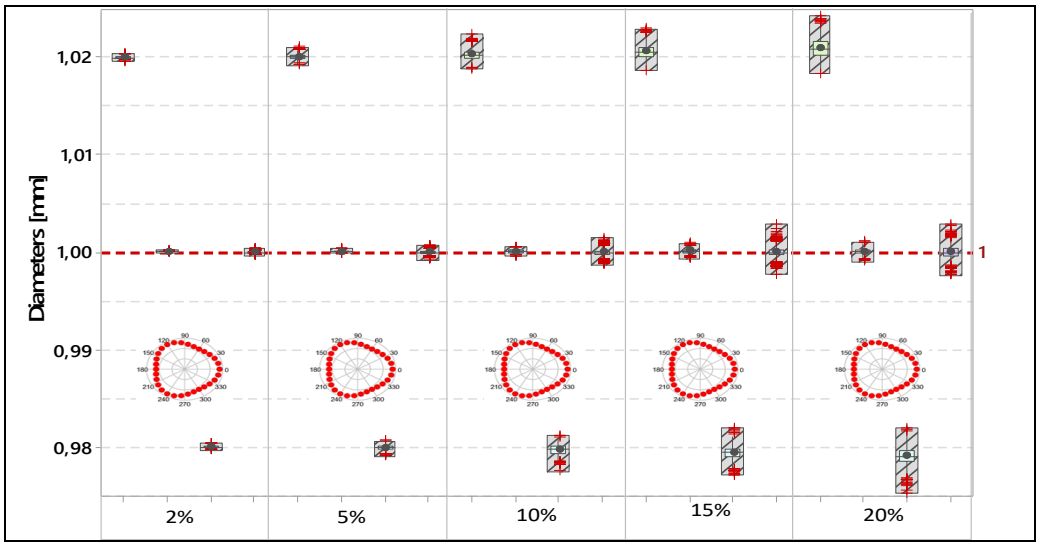

Figure 3. 17 The influence of Noise level on the evaluation
of the 14405-1 specification methods (c=2%, v = [2%, 5%, 10%, 15%, and 20%])

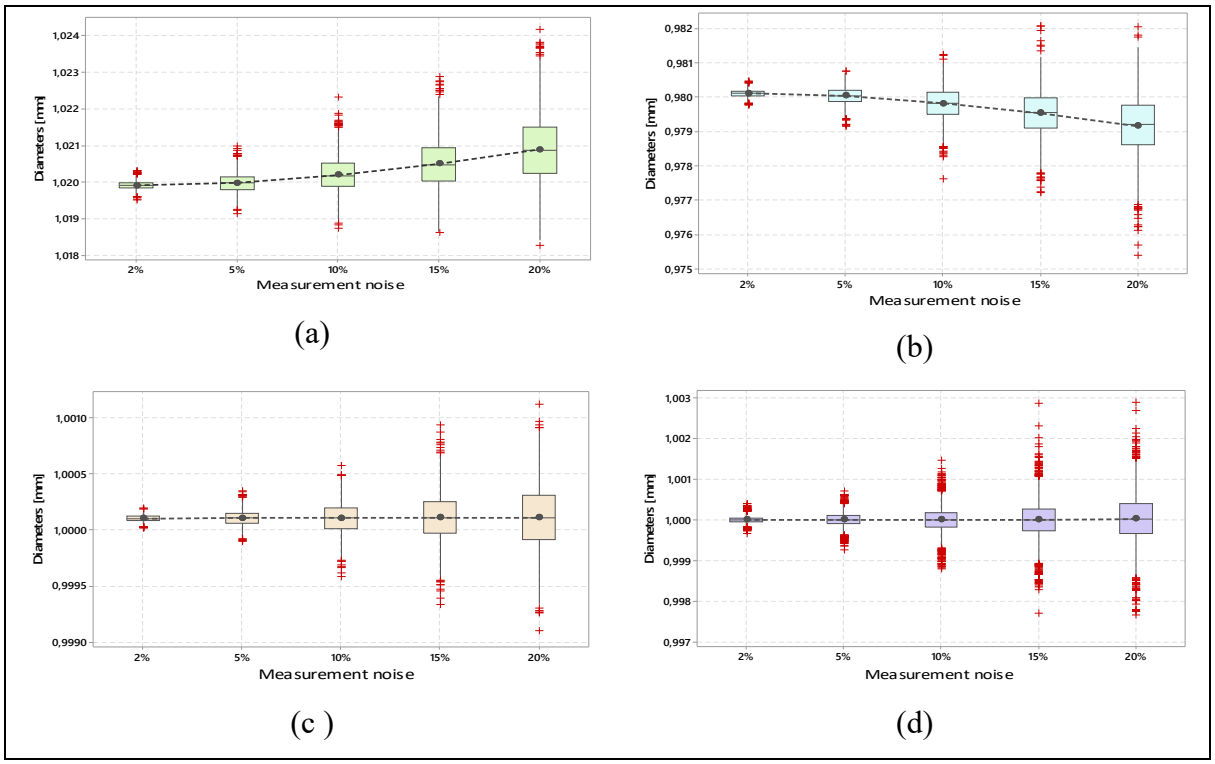

Figure 3. 18 Influence of Noise level on the evaluation of the 14405-1 specification methods (c=2%, v = [2%, 5%, 10%, 15%, and 20%])(a) GN method, (b) GX method, (c) GG method, (d) SN method

3.10.3. Influence of Noise on Form Defect

To see the influence of the presence of from defects in circle fittings, we created 2000-full circles with different form defects (2 lobs, 3 lobs, 4 lobs and asymmetry). The performance measures were computed similarly to previous experiments for all the cases of noise variations with (i) being the number of points fixed at n=50, (ii) circularity defect:c =2%;(iii) the noise level v =10%.

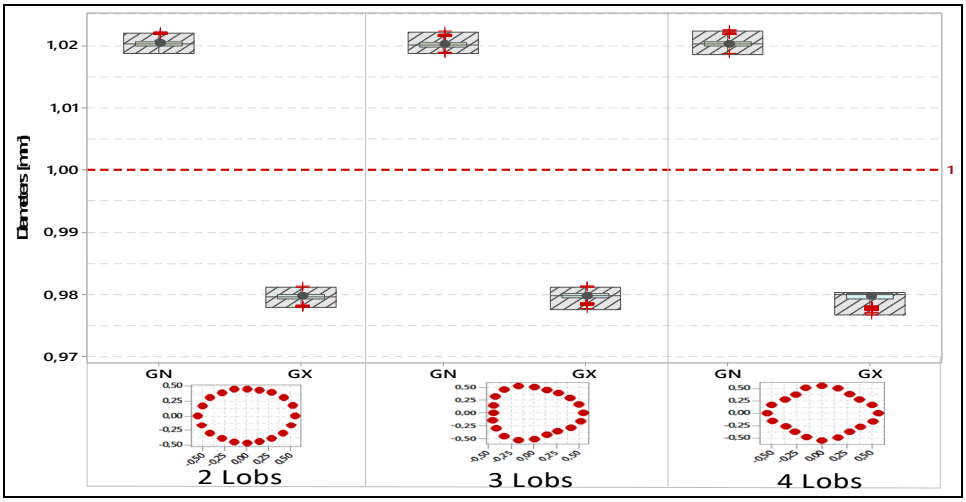

Figure 3. 19 The influence of the form defect on the evaluation of 14405-1 specification methods (GN and GX) with C= 0.02 mm, v =0.1mm.

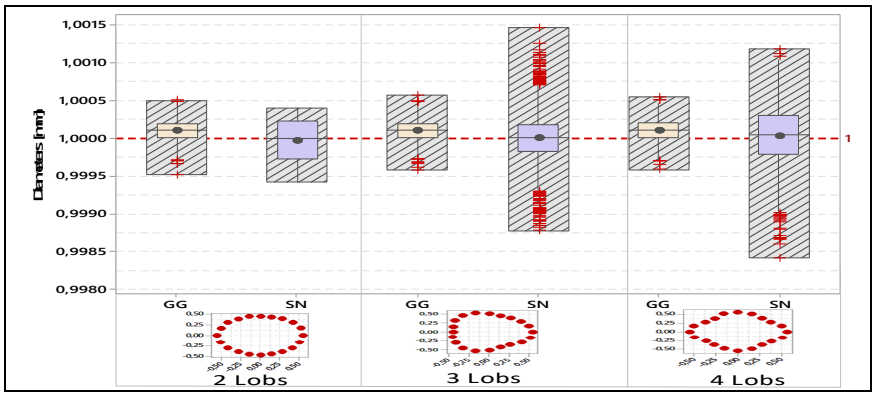

Figure 3. 20 The influence of the form defect on the evaluation of 14405-1 specification methods (GG and SN) with c= 0.02 mm, v =0.1 mm.

According to the results obtained in Figures 3.19 and 3.20, the four types of defect forms generated results in different diameters, which proves the form defect influence on the ISO 14405 modifiers. The Monte Carlo simulation realized denotes that the influence of measurement noise is greater on GN and GX modifiers. Each of the preceding modifiers can have their field of application. The GG modifier is more involved in the metrology field. The GN indicates the size of a feature, the part that contains the maximum amount of material and would have the largest shaft or the smallest hole. It is used for the functional design of assemblies, thus reducing manufacturing and inspection costs. The GX modifier indicates the size of a feature that contains the least amount of material like the smallest shaft or the largest hole. GG is a popular approach for fast quality control for its robustness and computational time. However, each method specification has its own application. However, once a specification is chosen, it important to choice the 'good' approach for the inspection execution.

3.11 Incomplete Data

In a certain case, the scan data can be incomplete for the orientation of the measurement device unit to the surveying objects and the limited access. To address these problems, (Nurunnabi et al., 2018) suggested present that fitting a circle from incomplete data is an important problem. This paper study this problem for fitting circle from incomplete in the presence of noise. We presented simulations of the different cases studies of incomplete data (arc of a circle, semicircle and complete circle). In addition, we studied the influence of parameters (angle and noise measurement) on each type of specification method.

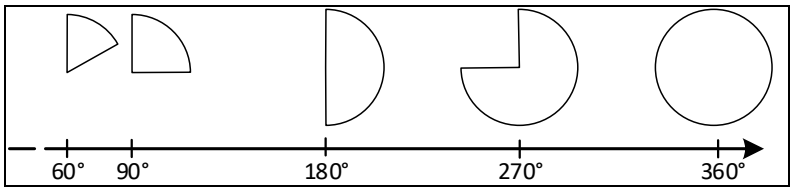

Figure 3. 21 Scale of different angles

To study the angle influence on the specification methods, five case studies were implemented at different angles (60°, 90°, 180°, 270°, 360°) (Figure 3.21) with a number of points where $n = 50$, circularity defect: c=2%;c=0.02 mm, noise measurement :v =5%;v =0.05mm and t=2000 iterations for Monte Carlo's method. According to the results obtained in Figure 3.22, the GN and SN algorithms provided unacceptable results in the case of small angles (60° and 90°). These algorithms generated acceptable results where the angle is greater than 180° (arc of circle). However, the GG algorithm gives the best results out of the four modifiers in the five cases studied. The GX algorithm does not work in the case of a 60° angle. The 90° angle gave unacceptable results and in the other cases, the GX algorithm gave acceptable results. Therefore, the use of the GN, SN, and GX modifier is to be avoided in the case of partial capture (less than 90 deg.) but the use of GG modifier is advised for any different angles (40 deg to 360 deg).

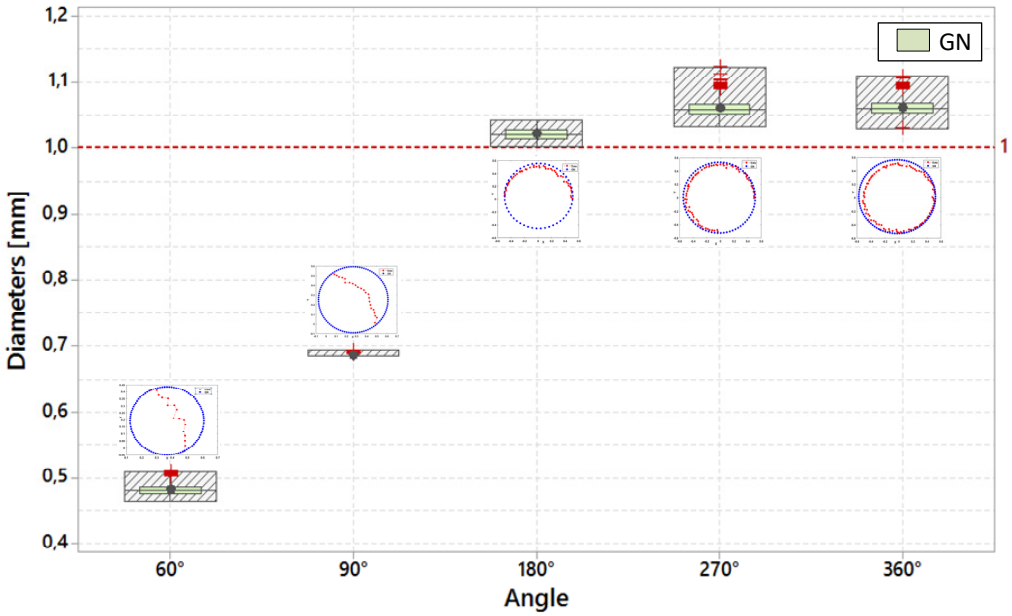

(a) GN algorithm

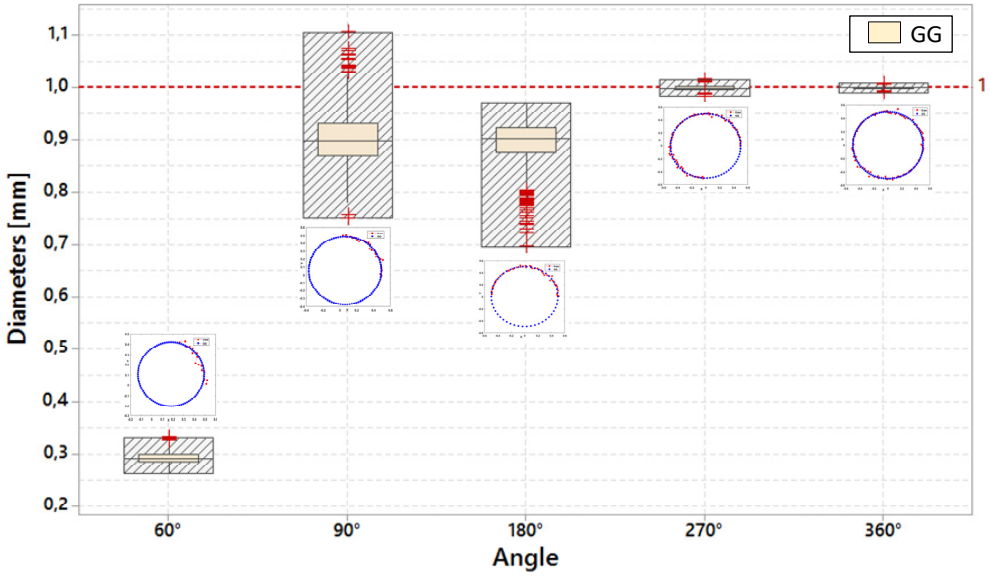

(b) Effect of incomplete data for a GG algorithm

Figure 3. 22 The influence of the angle on the evaluation of 14405-1 specification methods (GN, GX, GG and SN) with c = 0.02 *mm*, v =0.05 *mm*.

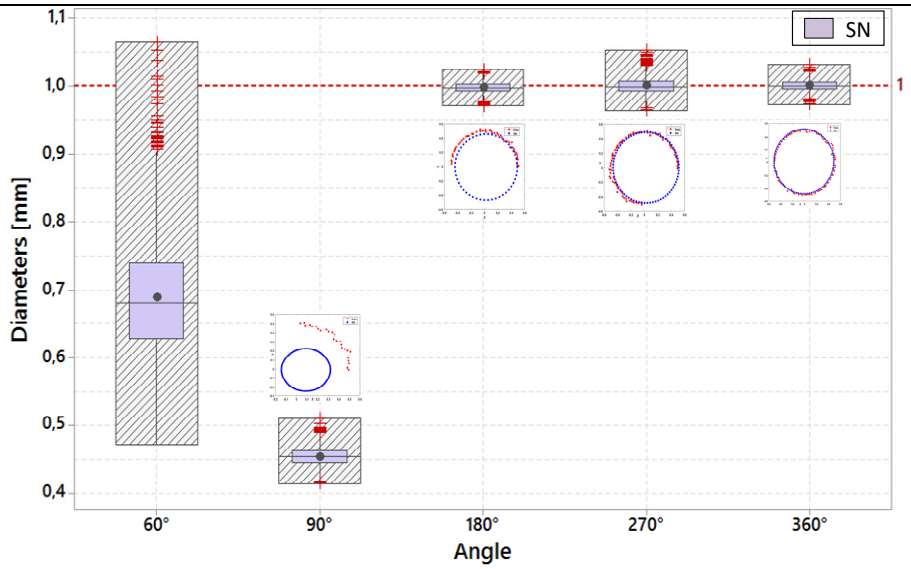

(c) Effect of incomplete data for a SN algorithm

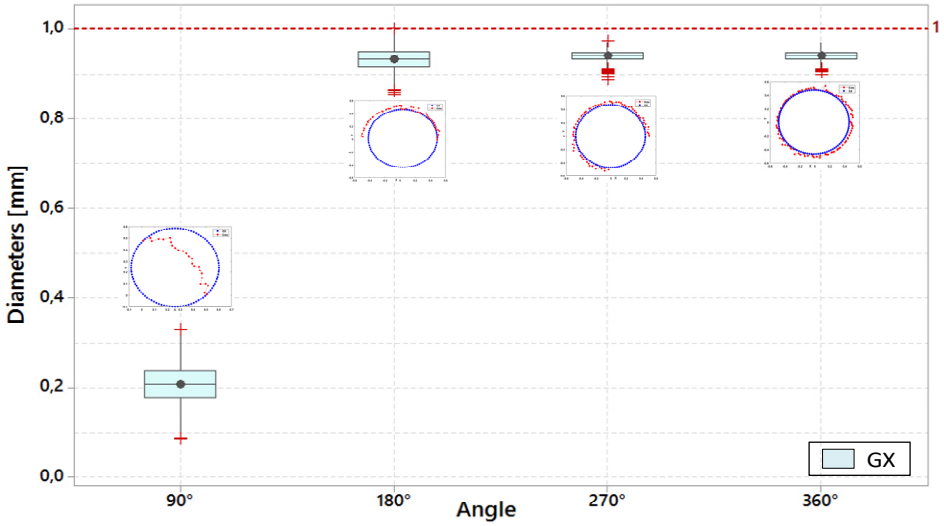

(d) Effect of incomplete data for a GX algorithm

Figure 3.22 (continued)

Several experiments using incomplete artificial data were used to detect the influence of a high percentage of noise with the number of points $n = 50$, Monto-Carlo Simulation: t=2000 and measurement noise v = [1%, 2%, 5%, 10%, 20%].In the case of the specification of a GN diameter, it is sensitive to high points (Figure 3.23, Figure 3.24 a). In the case of the specification of a GX diameter (Figure 3.23, Figure 3.24 b), it is less sensitive to high points

and relatively insensitive to low points. GG (Figure 3.24 c) is relatively insensitive to extreme asperities. The SN modifier is sensitive to positive and negative asperities.

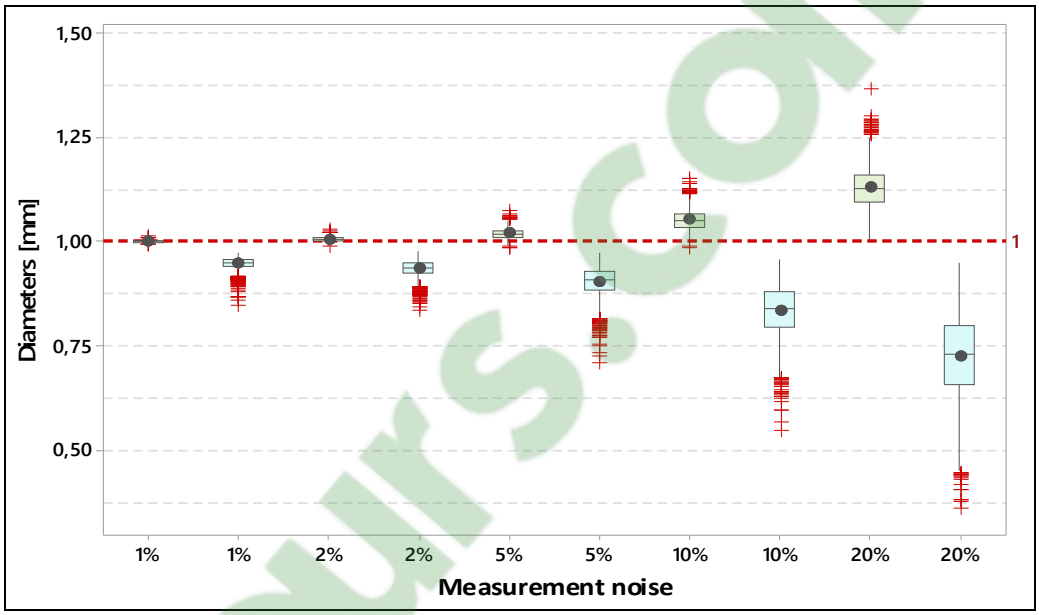

Figure 3. 23 The influence of the angle on the evaluation of 14405-1 specification methods (GN and GX) with v = [0.01, 0.02, 0.05, 0.1, 0.2] *mm*.

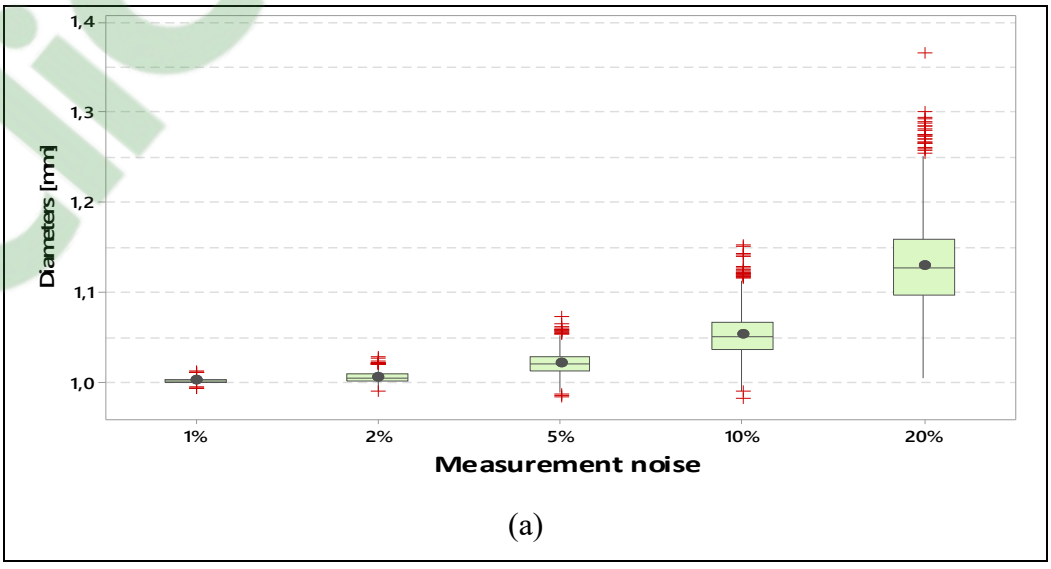

Figure 3. 24 The influence of the Noise level on the evaluation of 14405-1 specification methods (v = [1%,2%, 5%, 10%, 15%, and 20%])(a) GN method, (b) GX method, (c) GG method, (d) SN method

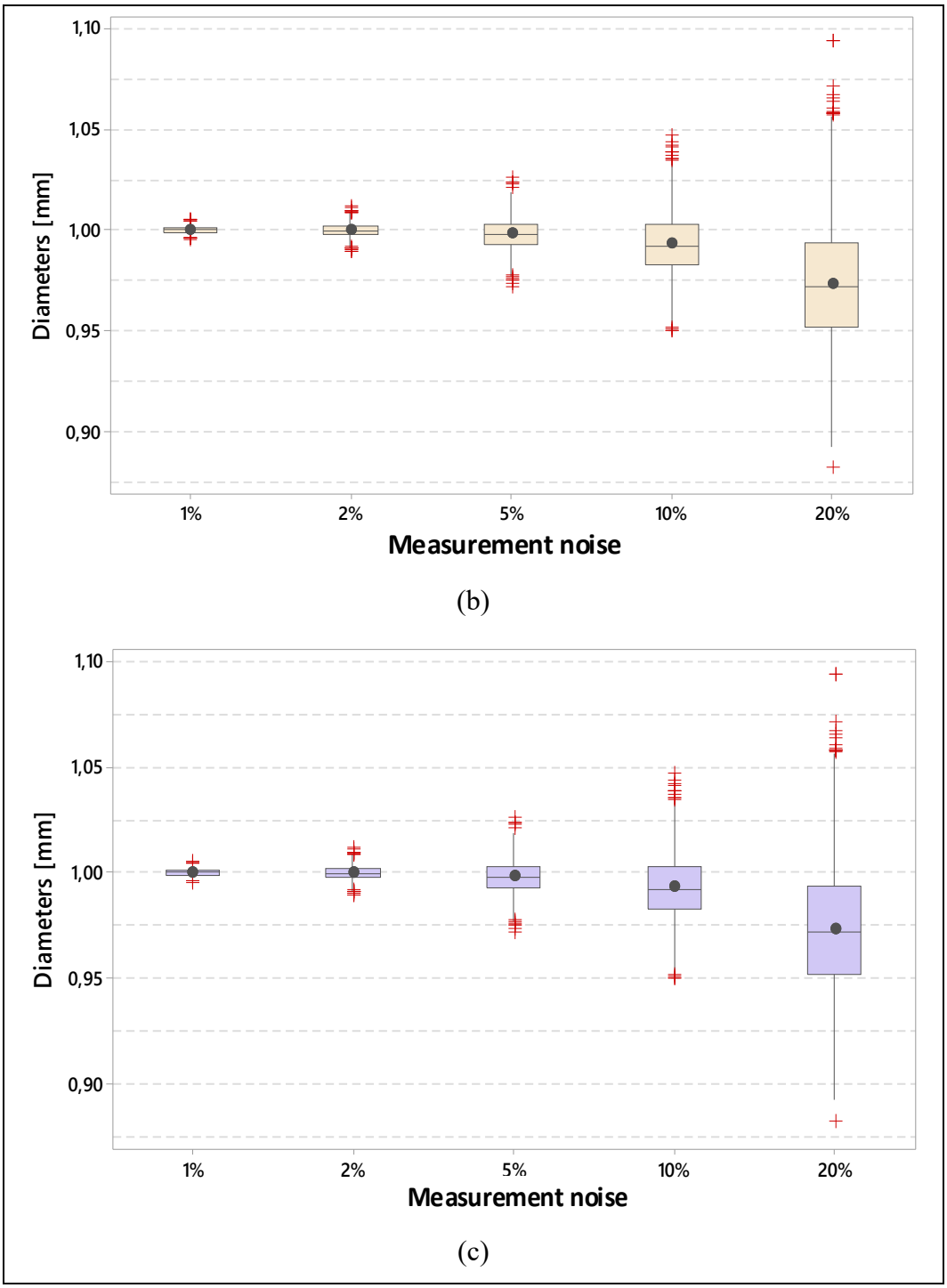

(b)

(c)

Figure 3.24 (continued)

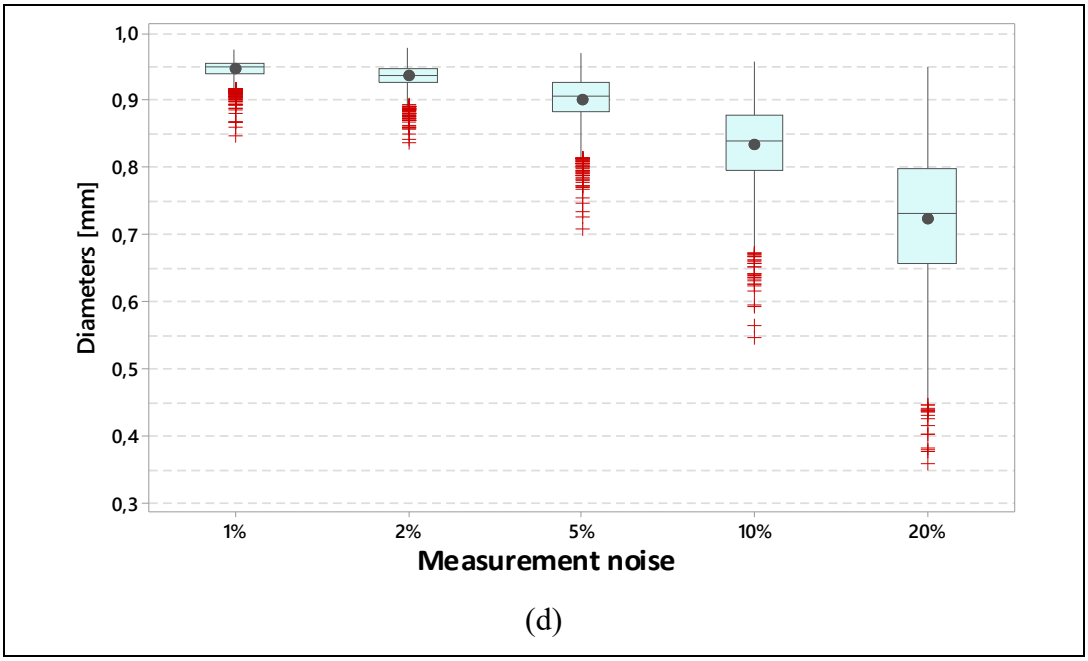

(d)

Figure 3.24 (continued)

3.12 Experimental Datasets

This section presents experiment results done in the LIPPS Laboratory of the École de Technologie Supérieure (ETS) for the fitting circles of four cylinders. We used Polyworks 2018 IR6 to compute roundness errors. For the inspection, we used the CMM Bright Strato (Figure 3.25).

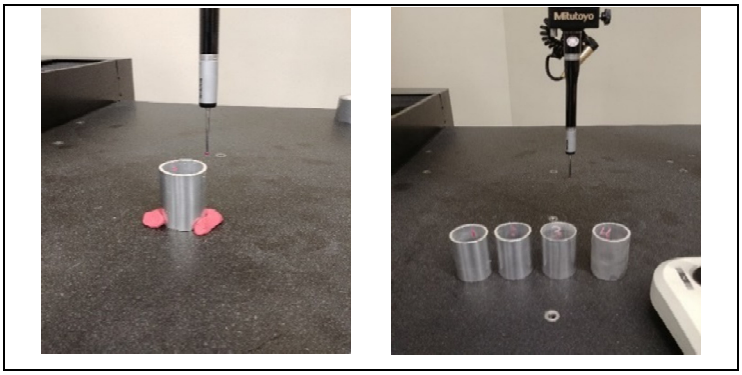

Figure 3. 25 Inspection's operation of circle point clouds

Tableau 3. 2 Feature table of the circles

Name		Nominal $\boldsymbol{d}$ $[\boldsymbol{mm}]$	$\boldsymbol{N}$
Circle 1	$c1$	40,7298	507
Circle 2	$c2$		500
Circle 3	$c3$		547
Circle 4	$c4$		502

Tableau 3. 3 Results of real datasets (Max fit, Min fit best fit and Best Fit Sigma) with d: diameter; OOR: Out-of-roundness

Name		Max $[\boldsymbol{mm}]$	Min $[\boldsymbol{mm}]$	Best Fit$[\boldsymbol{mm}]$
$\boldsymbol{c1}$	d	40.7942	40.7205	40.7529
	OOR	0.0391	0.0391	0.0391
$\boldsymbol{c2}$	d	41.8152	39.3800	40.6154
	OOR	1.2785	1.2785	1.2785
$\boldsymbol{c3}$	d	40.7093	40.4702	40.5817
	OOR	0.1332	0.1332	0.1332
$\boldsymbol{c4}$	d	40.8673	40.0952	40.6120
	OOR	0.5803	0.5803	0.5803

The manufactured Cylinder 1 is without form defects. The defect of the manufactured Cylinder 2 is 3 lobs. For Cylinder 3, we simulated a compression effect on the cylinder. Cylinder 4 has a local fault. Table 2 describes cylinder features such as the nominal diameter, and the number of points measured. The manufactured cylinders are shown in Figure 3.26.

Polyworks 2018 IR6 was used to calculate the roundness evaluation methods. The software contains four methods named Best Fit, Min Fit, Max Fit and Fit Sigma:

- The Best Fit and Fit Sigma methods correspond to GG modifiers
- The Max Fit method corresponds to the GN modifier
- The Min Fit method corresponds to the GX modifier

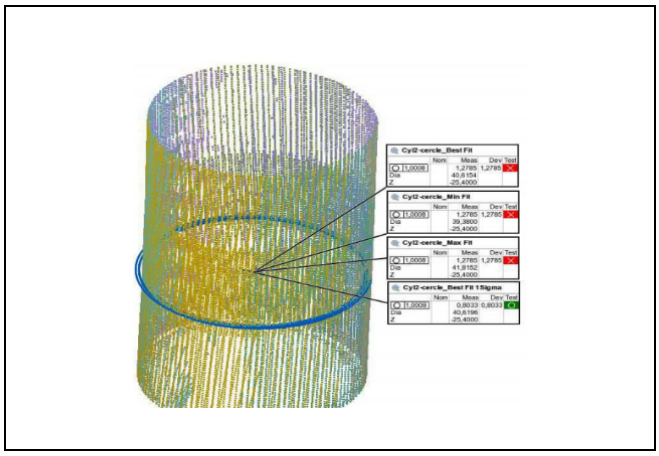

Figure 3. 26 Point clouds of the scan of Cylinder 1

Tableau 3. 4 Results of developed algorithms (GN, GX, GG and SN) With: d DiameterOOR: Out-of-roundness

Circles		GN [$\boldsymbol{mm}$]	GX[$\boldsymbol{mm}$]	GG[$\boldsymbol{mm}$]	SN [$\boldsymbol{mm}$]
$\boldsymbol{c1}$	d	40.7942	40.7205	40.7529	40.7557
	OOR	0.0391	0.0397	0.0397	-0.0391
$\boldsymbol{c2}$	d	41.8152	39.3800	40.6233	40.5350
	OOR	1.3200	1.2924	1.2924	1.3130
$\boldsymbol{c3}$	d	40.7093	40.4702	40.5817	40.5824
	OOR	0.1347	0.1438	0.1438	0.1319
$\boldsymbol{c4}$	d	40.8673	40.0952	40.6131	40.1714
	OOR	0.7462	0.5994	0.5994	-0.7449

According to Tableaux 3.3 and 3.4, the results of the GN and GX modifiers are practically the same in the four circles (Max Fit and Min Fit), but the result of the GG modifier is different to that of Best Fit and Best Fit Sigma.

3.13 Conclusion

The new ISO 14405-1 sets of size specifications provide tools for specifying the geometric requirements necessary for the component to meet the functional requirements of the assembled [mm] product. The addition of these modifiers allows the designer to clarify with more precision and detail than ever which may be one way to solve the measurement problem of the calculated sizes of the circle in the manufacturing industry as soon as possible. The

proposed methodology is anticipated to be an importnat tool for help to industrial inspectors/metrologues to select the appropriate method on the ISO14405 or the algorithm for size and form evaluation. The benchmark and experimental cases studies demonstrate the influence of the algorithm choice, the influence of several parameters and the limits to be respected in certain cases where the data are missing; Some algorithm are not appropriate in some case. the use of the GN, SN, and GX modifier is to be avoided in the case of partial capture (less than 90 deg.) but the use of GG modifier is advised for any different angles (40 deg to 360 deg). Therefore, designers and inspectors must correctly identify the algorithm that corresponds, otherwise an error will occur. Thus, each method specification has its own field applications (functional requirements). Once the method specification is chosen for a particular application has been decided, it becomes to select the good algorithm for the execution of the selected method specification.

3.14 Acknowledgments

The authors would like to thank the Institut Supérieur d'Informatique ET des Techniques de Communication Hammam Sousse (Tunisia), and the École de Technologie Supérieure (ÉTS, Montréal, Canada) for their support.

CHAPITRE 4

REPRODUCIBILITY EXPERIMENTATION AMONG COMPUTER-AIDED INSPECTION SOFTWARE FROM A SINGLE POINT CLOUD

Ibtissem Jbira[a,b,c] , Antoine Tahan[a], Serge Bonsaint[d], Mohamed Ali Mahjoub[c], Borhen Louhichi[e]

[a] École de Technologie Supérieure (ÉTS), 1100 Notre-Dame ouest, Montréal, Québec, H3C 1K3, Canada

[b] Institut Supérieur d'Informatique et des Technologies de Communication, G.P.1 Hammam Sousse-4011, Tunisie

[c] Université de Sousse, École Nationale d'Ingénieurs de Sousse, LATIS- Laboratory of Advanced Technology and Intelligent Systems, Tunisie

[d] Creaform 3D 4700, rue de la Pascaline Lévis (QC), G6W 0L9, Canada

[e] Université de Sousse, Institut Supérieur des Sciences Appliquées et de Technologie de Sousse, LMS, Cité Taffala 4003, Sousse, Tunisie

Article publié en 11 Octobre 2019 dans la revue Journal of Control Science and Engineering

4.1 Abstract

The ISO-GPS and ASME Y14.5 standards have defined dimensional and geometrical tolerance as a way to express the limits of surface part variations with respect to nominal model surfaces. A quality-control process using a measuring device verifies the conformity of the parts to these tolerances. To convert the control measurement points as captured by a device such as a Coordinate Measurement Machine (CMM) or non-contact scan, it is necessary to select the appropriate algorithm (e.g. least square size, maximum inscribed size, etc.) and to include the working hypotheses (e.g. treatment of outliers, noise filtering, missing data, etc.). This means that the operator conducting the analysis must decide on which algorithm to use. Through a literature review of current softwares and algorithms, we found many numerical discrepancies. A benchmark was therefore developed to compare the algorithm performance of three Computer-Aided Inspection (CAI) softwares. From the same point cloud, and on the same

specifications (requirements and tolerances), we tested three CAI options with several dimensional and geometrical features.

Keywords Reproducibility, Computer-Aided Inspection, 3D Metrology, Algorithmic error, Fitting algorithms, Feature extraction.

4.2 Introduction

These days, 3D computer-aided design software provides various options to fit the measured points to a XYZ coordinate system. Most software features a selection of different "fitting algorithms" that adjust the measured points in various methods. Metrologies have the flexibility to fit a part in multiple ways using post-processing software. The performance of a measurement system is an estimate of a combination of various measurement errors (random and systematic) that include hardware (equipment error), software (algorithmic error) and operators. Both the software and operator can still strongly correlate. In this paper, we will focus on algorithmic errors. A novel benchmark model is proposed in this study to compare the fitting algorithms' performance in different CAI software's. According to a Measurement System Analysis (MSA) approach, it is strictly a reproducibility study. The purpose of inspecting is to verify compliance with the design requirements.

To keep track of the process, it is helpful to understand the error levels on the important features. In addition, the inspection report must be useful and easily interpretable to make the necessary corrections if the required tolerances are not respected. Form testing machines allow to measure points to form the profile and estimate circularity errors. Usually, all these machines provided many options for evaluating the circularity errors. Therefore, it is needed to make a decision about the reference form to use for a particular application. This paper aims to analyze algorithmic errors. A quick review of the available literature on this subject finds that the impact of a measurement strategy (amount of data) and software used (including algorithmic, filtering outliers, etc.) is a surprisingly under-explored topic. Recent work in test of fitting

algorithms (maximum inscribed, least square, minimum circumscribed and Chebyshev, etc.) indicates that serious problems can exist in the current commercial software packages.

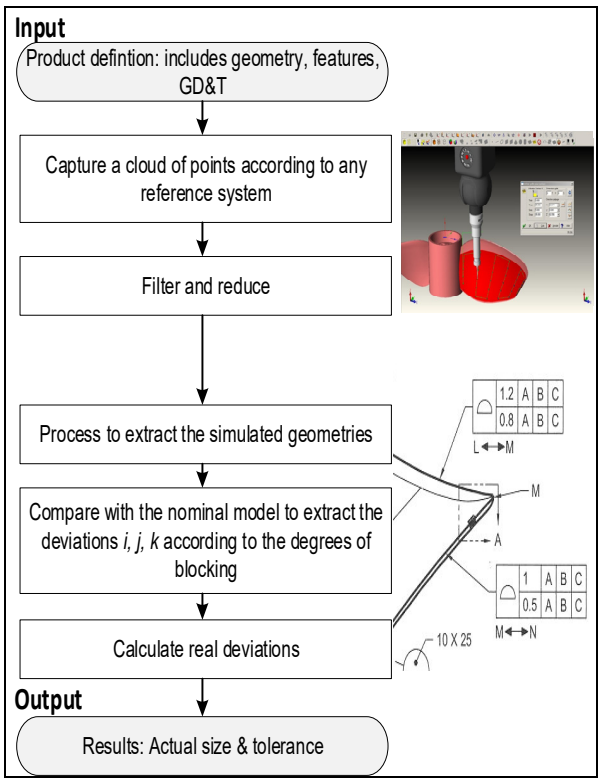

Figure 4. 1 Inspection Process

4.3 Background

Computational metrology includes the implementation of robust algorithms to adjust, and achieve many computations on discrete data collected by measuring machines. The computational coordinate metrology is the most pertinent to validate standards so that conform to tolerance specifications (see Figure 4.1). Now many journals consider computational metrology as a separate topic of interest. Computationally, fitting problem is an optimization problem (defined in Equation 4.1).

$$l_p = argmin\left\{\sum_{i=1}^{n}|d_i|^p\right\}^{\frac{1}{p}} \tag{4.1}$$

Where n is the number of points and d_i is the shortest distance between measurements data and the reference form. If p =2 the fitting problem is the least square fitting, and if $p \to \infty$, l_∞ fitting is the Chebyshev or minimax fitting.

Generally, the fitting problem consists to select an appropriate algorithm to adjust a geometric form (e.g. plane, cylinder, circle, etc.) to data points collected from the inspection of a manufactured part. The perfect form estimation is obtained by a fitting is called a reference feature or substitute feature. The recent publication of ISO 14405-1:2016 determine size as a fundamental geometric descriptor. It also defines a new set of modifiers tools for size (Morse and Srinivasan, 2013); (Jbira et al., 2018a) proposed a methodology to evaluate the algorithmic error of modifiers in the ISO 14405-1 standard. They demonstrated that the noise measurement affects the ISO-14405-1 modifiers.

Various methods have focused on the problem of fitting surfaces applied to many fields. Thus, in the absence of recommendations by the ISO about the method adopted to terminate roundness (Jbira et al., 2018a), the estimation of circularity errors remains a challenge for the improvement of algorithms to calculate the best center.

In this section, we briefly describe some of the algorithms cited in the state of art (Xiuming et al., 2013). particularly in the case of geometric elements of circular cylindrical and spherical forms, In (Liu et al., 2016), a reference circle is calculated from the input data in order to minimize the deviation between actual and reference circles. One of the methods to find this circle is a Voronoi diagram used to determine the Minimum Circumscribed Circle (MCC) or Maximum Inscribed Circle (MIC). To obtain a MCC, the points of the diagram that lie farthest from the center of the diagram are used. The MIC has a center on the Voronoi vertex or on the Voronoi edge. The distance between the circle center and the convex vertex represent the

radius. The Delaunay Triangulation is used to calculate the convex and Voronoi diagram. In (Sui and Zhang, 2012), the roundness error from the input 3D points is evaluated using four methods: Minimum Zone Circle (MZC), Least Squares Circle (LSC), MCC, and MIC. For the MZC method, the roundness error is measured using two concentric circles. For the LSC method, it is estimated inside the profile by minimizing the sum of radial squares between the circle and the profile. Using the center of the LSC, a circumscribed circle and an inscribed circle are obtained. The circularity error (out of roundness) value is the radial separation. The MIC method is used to fit the largest circle inside the profile. In the case of a MCC, a center is calculated by finding the circle that has the smallest radius containing the points of the circle. The circularity error is the difference between the radiuses of the inscribed circle drawn using the found center and the circumscribed circle. (Tran et al., 2015) proposed an algorithm to fit cylinders and to approximate the parameters given by 3D points cloud. The first step is to compute the normal vector of the points. Using curvature information, potential points that could form the cylinder are identified. These points should be updated in a fitting process to check all remaining points that belong to a cylinder. Then, the mean shift clustering method is applied to find the approximated parameters of the valid cylinder. This method is validated using different models featuring various noise and outlier levels. In 2012, (Morse and Srinivasan, 2013, Srinivasan, 2013) proposed a solution to the problems of weighted total least squares fitting of lines, planes, and parallel planes. They demonstrated the need for these algorithms, which is relevant to newer tolerancing standards and instrumentation.

(Saval-Calvo et al., 2015)presented a novel method based on a RANdom SAmple Consensus (RANSAC). This method estimates multiple planes from a point cloud with noise. The proposed method based on two steps: the first step is to divide the data into planar faces and in the second step, the plane models are approximated using multi-constraint RANSAC method. They tested the proposed method with exists methods.

In (Pt et al., 2018) the authors compared different algorithms to facilitate the choice of the adequate execution method for MCC, MIC and MZC in order to calculate roundness errors. In addition, they used a new geometric concept based on reflecting a mapping technique to assess

roundness errors. They proposed a selected benchmark of algorithms in the literature in order to provide the optimal execution method. It was concluded that no single algorithm provides the best solution. Geometric primitive reconstruction (Sui and Zhang, 2012) (Nurunnabi et al., 2018) is an important problem in the field of Computer Aided Design (CAD).

(Goch and Lübke, 2008) proposed a new algorithm to approximate geometry elements using Gauss and Chebyshev criteria, Furthermore, (Chaperon et al., 2001) proposed an algorithm to extract a cylinder from unorganized 3D points. The two main steps of their method were the extraction of the constrained plane in the Gaussian image to define the direction of a possible cylinder and then the cylinder of known directions is extracted from the set of 3D points. They validated their approach by testing the extraction of pipe objects in industrial environments. In the context of pipeline plant detection and reconstruction, the huge number of points makes the problem extremely difficult. Traditional methods of detection cannot be applied directly because of the high complexity. Moreover (Nurunnabi et al., 2018), the authors developed a robust algorithm based on a Principal Component Analysis approach (PCA) to fit cylinders given a set of 3D points. They validated their method using artificial and real point clouds.

Most cylinder approximation methods focus on full data. However, the point cloud data that they obtained through laser scanning was incomplete and contained outliers. (Nurunnabi et al., 2018), described the problem of circle fitting for complete and incomplete datasets with outliers. They proposed a robust approach for circle fitting which had to merge two algorithms: PCA and robust regression. The experimental results confirmed the robustness of the proposed approach with a different percentage of tolerance of clustered outliers. They compared the proposed approach with another exciting method. (Guo and Yang, 2019) proposed a new procedure for circle fitting. They used Taubin's approach to compute the center and radius, and then they identified and removed the outliers by calculating the geometric distances given point cloud to form the adequate circle. Their experiments demonstrated that the iterative procedure could resist against the effect of outliers. More specifically in the case of geometric elements of plane form, (Deschaud and Goulette, 2010) proposed an accurate algorithm to extract planes in noisy point clouds using filtered normal and voxel growing.

The first step is the estimation of the better normal at the data points. The second step consists of computing a score of local planes, and then they apply the growing voxels. Finally, they evaluated the proposed algorithm on different number of points and compared it is with exists algorithms. The presented method has a linear algorithmic complexity and it is able to detect large and small planes in very large data sets. (Long Nguyen et al., 2017) presented a comparative study of the least square plane fitting algorithms with different segmentation methods (e.g. RANSAC, RGPL, Cabo, RDPCA). They validated the study by two real point clouds collected by a Dynascan S250 scan system. The results demonstrated that the RGPL method gives the best results for planar surface extraction in Moving Least Squares (MLS).

(Marriott et al., 2018) presented an unsupervised extraction planar method. They proposed to adjust the data with a piecewise-linear Gaussian mixture regression model whose components were skewed over planes. In (Moroni et al., 2014), the problem of fitting full and half-geometrical primitives (e.g. circular, spherical and cylindrical) is addressed. The authors use the Levenberg Marquardt (LM) method to approximate these geometries. They also proved that using the chaos optimization method improves the initial algorithm estimation. In fact, the chaos–LM algorithm provides efficient results even when the input data points are incomplete and noisy.

4.4 Experimental protocol

This paper is interested in the reproducibility estimation between three computer-aided inspection software's that originate from the same point clouds. According to the industrial guide put out by the Automotive Industry Action Group [AIAG], reproducibility traditionally refers to the variation in average measurements made by different operators using the same gauge and parts.

Typically, the term is defined as the average measurement made by different appraises using the same measuring instrument when measuring identical characteristics on the same part. In our study, we used one part (same drawing, same specifications) with the same measurement point clouds and appraiser but we use three inspections software's. For each software, all

proposed options by each software are tested (e.g. best fit, minimax…). Therefore, variability expresses the algorithmic differences between software's.

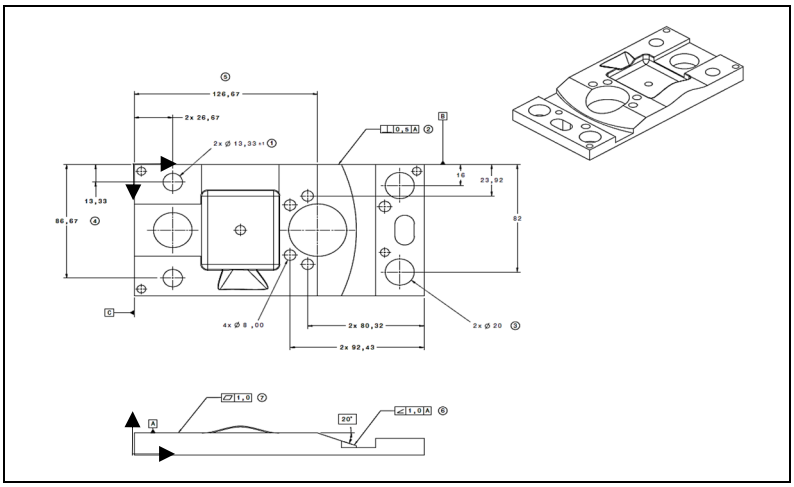

Figure 4. 2 GD&T of the sample part with numbering items

Piece is designed using basic feature geometries (e.g. plans, cylinders). Dimensional and geometrical requirements are presented in Figure 4.2. One part is made out of aluminum and the piece is digitized by a HandySCAN portable 3D scanner (with a resolution of 0.05 mm and an accuracy of up to 0.04 mm). This part is to be used for fitting performance evaluation and inspection algorithms while considering dimensional and geometrical tolerances. In this paper, the standard ASME GD&T Y14.5-2009 was used. In total, five (5) different features with dimensional and geometric tolerances are selected on the test pieces (plan, circle and oblong hole). Only one operator was involved in the study. Three (3) software's are tested with all of their options.

The reproducibility in this study (expressed as a standard uncertainty u_{AV}) represents variations due to the difference between algorithms and how the software deals with outliers and registration fit. Figure 4.3 illustrates the procedure.

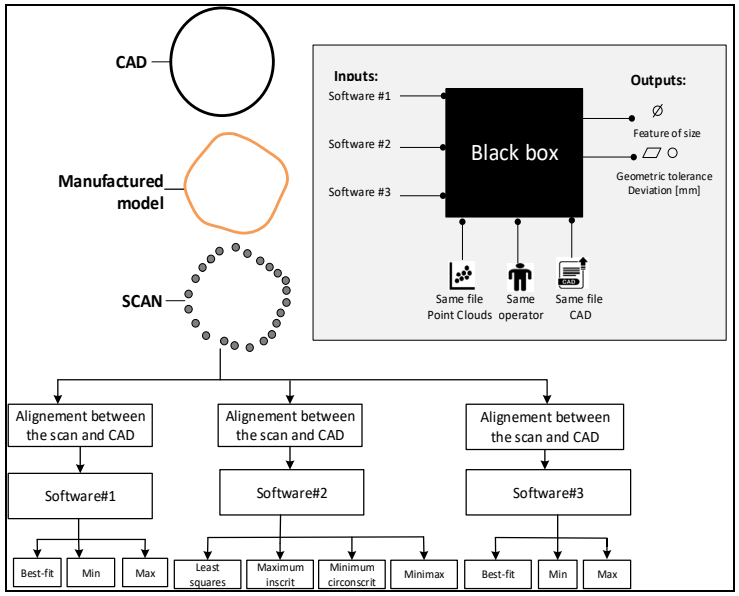

Figure 4. 3 Proposed benchmark

Alignment tools can define a part reference frame if you know the nominal location of point-reducible features on the part (e.g. points, circles, spheres…). Before performing a datum alignment, the operator has to provide a close initial part reference frame. The operator can use any available part alignment tool (e.g. CAD -cloud point alignment with the ICP algorithm (Nurunnabi et al., 2018) or (3-2-1 alignment) to perform this initial part alignment. The geometric Plane - Line - Point (PLP) alignment enables us to align a part to the CAD model using a plane (primary datum), a line (secondary datum), and a point (tertiary datum) to create the nominal coordinate reference system. In this paper, and for each software, the operator has systematically done PLP alignment.

4.5 Methodology analysis

In the case of circle features, the results are the measured diameter, the localization of the center, and the roundness error. In the case of plane features, the result is only the flatness error (Figure 4.4). As mentioned, we tested three software's with all options (Tableau 4.1). The alignment performed is a PLP type alignment using the measured ABC datum using the least squares algorithm.

Tableau 4. 1 Options for three software's

Software	Described options	
#1	Best-fit: An option button that specifies the use of the usual *'Best-Fit'* fit algorithm that performs a least squares approach. Min: An option that specifies the use of the minimum fit algorithm. A primitive Min is the largest primitive that does not encompass any element. Max: An option that specifies the use of the maximum fit algorithm. A Max primitive is the smallest primitive that contains all the elements.	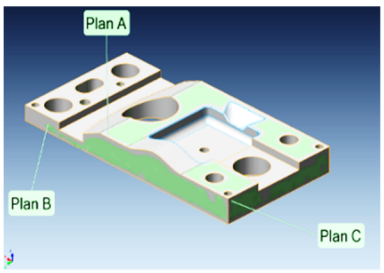
#2	Least square: To create a circle that best fits the probed points. The circle is calculated by minimizing the sum of the squares of the gaps between the circle and each point probed. Maximum inscribed to create the largest circle that fits in the probed points.	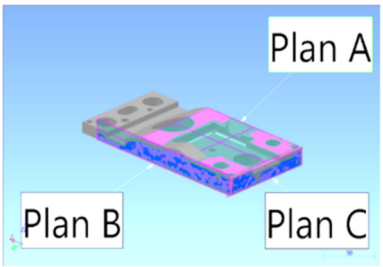

Tableau 4.1. (continued)

Software	Described options	
	Circumscribed Minimum: To create the smallest circle that contains all the probed points. Minimax: To create the circle by averaging between the maximum inscribed circle and the circumscribed minimum, which have the same center (minimizing a circularity error).	
#3	Best-fit: Find geometry using the least squares method from contours or surfaces. Min: Find the maximum circumscribed geometry using the minimum separation method from the contours or surfaces. Used to find the maximum circumscribed. Max: Find the minimum circumscribed geometry using the minimum separation method from the contours or surfaces. Used to find the minimum circumscribed geometry that encounters the furthest point to the positive direction of the normal.	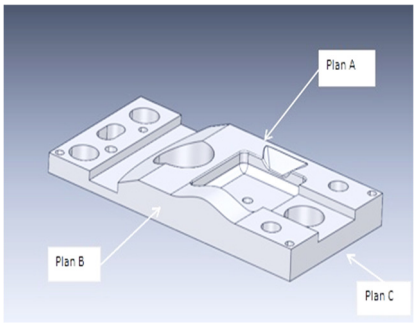

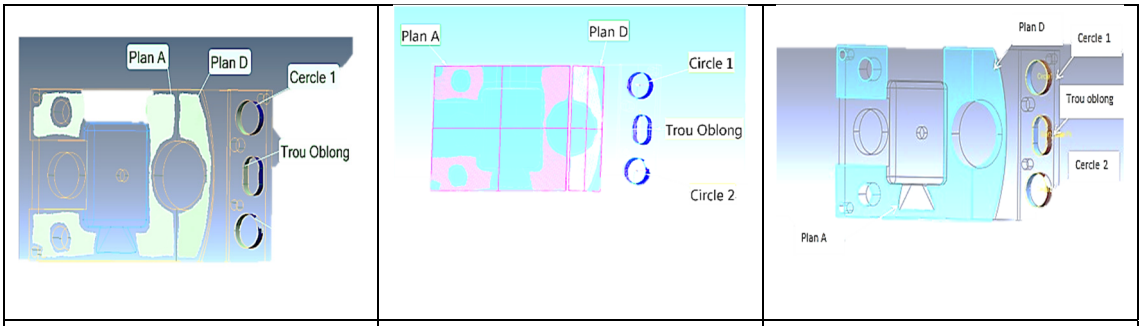

(a) Software #1	(b) Software #2	(c) Software # 3

Figure 4. 4 Elements measured for analysis

4.6 Results

In the measured part, we extracted two circles called circle #1 and circle #2, and an oblong hole for evaluating each option for each one of the three softwares. In addition, we extracted two surface plans called plan A and plan D to calculate the flatness found in each software.

4.6.1 Analysis of circle #1

In the first test, we computed the deviation of the center on the circle in the axis X and axis Y directions (δ_x, δ_y) and we calculated the measured diameter ($\emptyset$), the diameter deviation ($\delta_\emptyset = 20 - \emptyset$) and the roundness error of the circle #1 (Tableau 4.2). Results with the least square option are shown in **bold**, results with the min option are shown with an underscore, results with the max option are shown with a double-underscore and, if applied, results with the minmax option are shown is *italics*. According to Tableau 4.2, CAI software #1 and #3 offer three adjustment algorithms for circle #1(Least square circle (LSC)), Minimum Circumscribed Circle (MCC) and Maximum Inscribed Circle (MIC)).

Four algorithms are available in the CAI software #2 (LSC, MIC, MCC and minimax). The LSC algorithm provides the same value of measured diameters for the three softwares (19,877 mm). It is an expected result, as the LSC is a deterministic algorithm. Software #1 and

#2 with the MCC algorithm provide the same values of measured diameters (20,054 mm), but software #3 gives a bit of a different value (20,059 mm). The range (r) between results is equal to 0,005 mm. Again, the MIC algorithm gives the same values for the software #1 and #2 (19,755 mm), but software #3 gives a little different value (19,745 mm), r=0,01 mm.

Finally, the minimax algorithm is available only by software #2; the value of diameter is 19,903 mm. According to Figure 4.5(a), software #1 and #3 provide the same circularity values for all the methods, and software #2 demonstrates different results for each method used. In the case of size in Figure 4.5(b), the LSC shows the same size for the three softwares despite the fact that the Max and Min algorithms display different results.

Tableau 4. 2 Results for circle #1

	Algorithm	δ_x	δ_y	$\emptyset$	$\delta_\emptyset$	Circularity
#1	**Best-Fit**	0,060	-0,050	**19,877**	**-0,123**	**0,157**
	Min	0,056	-0,043	19,755	-0,245	0,157
	Max	0,058	-0,088	20,054	0,054	0,157
#2	**Least square**	0,058	-0,047	**19,877**	**-0,123**	**0,166**
	Max inscribed	0,055	-0,039	19,755	-0,245	0,168
	Min circumscribed	0,056	-0,085	20,054	0,054	0,184
	Minimax	0,066	-0,054	*19,903*	*-0,097*	*0,157*
#3	**Best-Fit**	0,0629	-0,0354	**19,877**	**-0,123**	**0,047**
	Min	0,0705	-0,0433	19,745	-0,255	0,047
	Max	0,0705	-0,0433	20,059	0,059	0,047

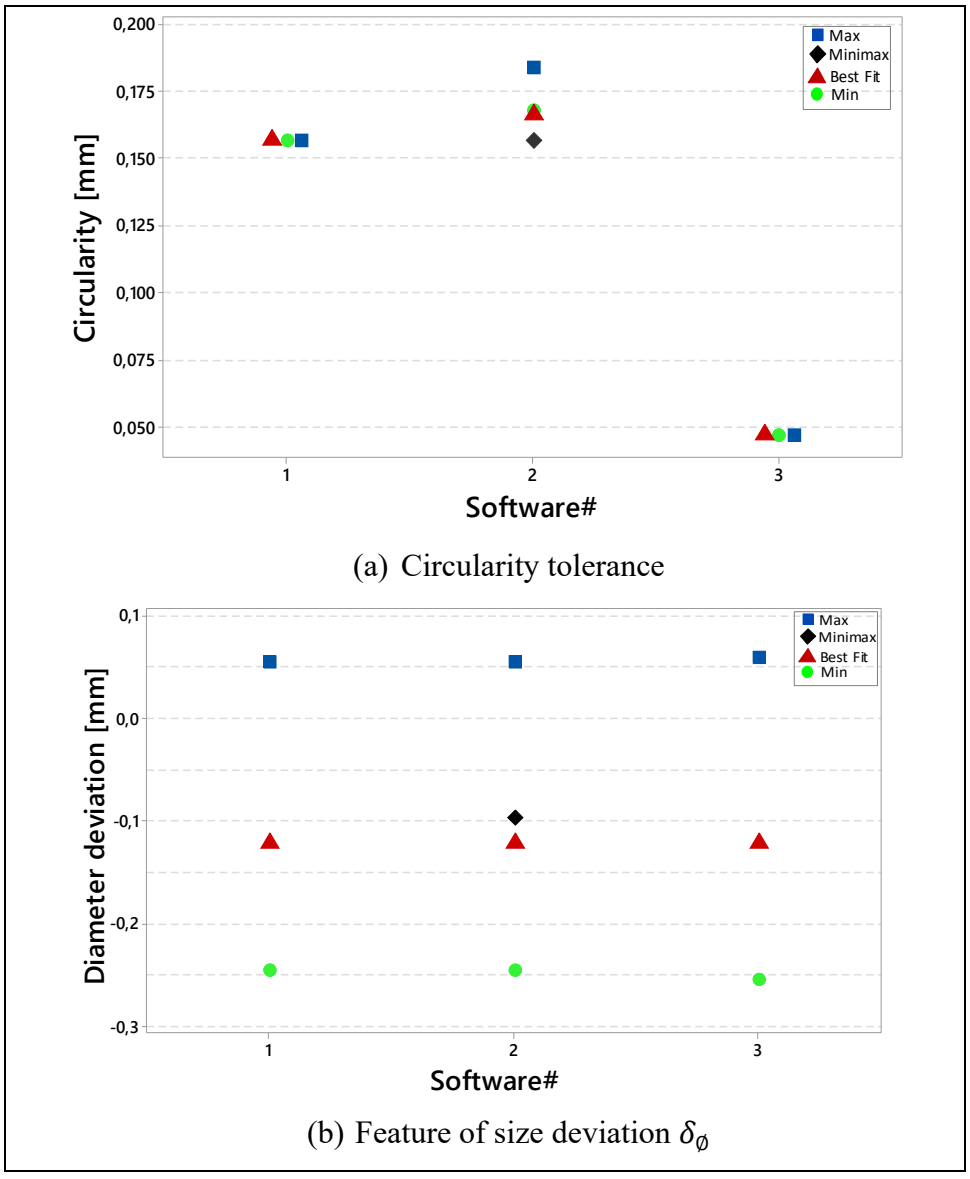

(a) Circularity tolerance

(b) Feature of size deviation $\delta_{\emptyset}$

Figure 4. 5 Results for circle #1

4.6.2 Analysis of circle #2

According to Tableau 4.3, results and conclusions are very similar to Tableau 4.2 (circle #1). The LSC algorithm provides the same value of measured diameters for software #1 and #2 (19,874 mm). In addition, software #1 and #2 with an MCC algorithm provide the same values of measured diameters (20,054 mm), but software #3 shows a bit of a different value

(20,054 mm). The range (r) between results is equal to 0,005mm. Again, the MIC algorithm shows the same values for software #1 and #2 (19,760 mm), but software #3 provides a slightly different value (19,721 mm) with r=0.039mm. Finally, with the minimax algorithm, available only in software #2, the diameter is equal to 19,907 mm. According to Figure 4.6(a), software #1 and #3 provide the same circularity values for all methods (Max, Min, Best Fit and Minimax), and software #2 provides different results for each method. Regarding the size in Figure 4.6(b), the LSC gives the same size for the three software's, despite the Max and Min algorithms displaying different results. According to the circle #1 and circle #2 results, in the case of diameter measurements, there is a small variation. However, in the case of more complex GD&T, there are greater variations (circularity cases).

Tableau 4.3. Results of inspection circle #2 (Ø20 mm)

	Algorithm	δ_x	δ_y	$\emptyset$	$\delta_\emptyset$	Circularity
#1	Best-Fit	0,049	-0,046	**19,874**	**-0,126**	**0,186**
	Min	0,046	-0,053	19,760	-0,240	0,186
	Max	0,046	-0,010	20,091	0,091	0,186
#2	Least square	0,048	-0,043	**19,874**	**-0,126**	**0,205**
	Max inscribed	0,046	-0,049	19,760	-0,240	0,208
	Min circumscribed	0,045	-0,007	20,091	0,091	0,195
	Minimax	0,058	-0,007	*19,907*	*-0,093*	0,185
#3	Best-Fit	0,0635	-0,0312	**19,873**	**-0,126**	**0,034**
	Min	0,0725	0,0049	19,721	-0,279	0,034
	Max	0,0725	0,0049	20,093	0,093	0,034

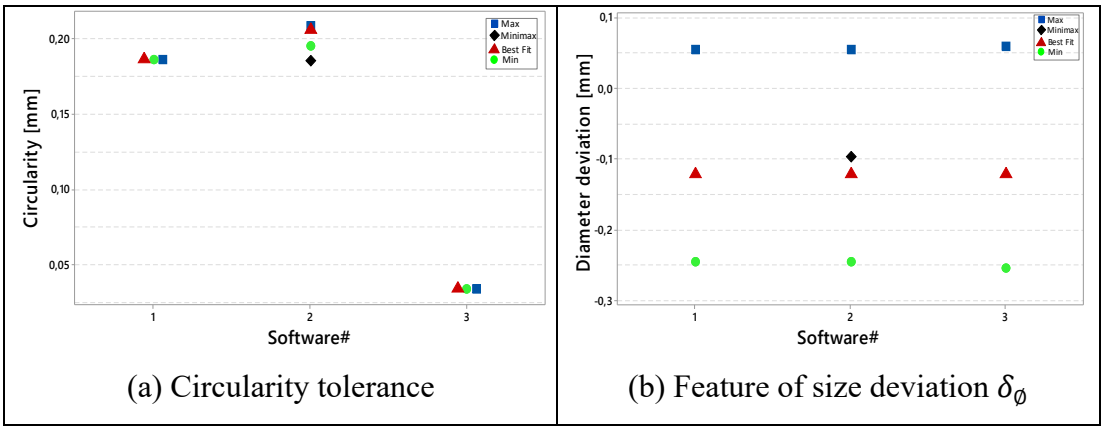

(a) Circularity tolerance (b) Feature of size deviation $\delta_{\emptyset}$

Figure 4. 6 Results of the circle #2 analysis

4.6.3 Analysis of the oblong hole

In the second test, we computed the deviation on the hole location on the axis $X(\delta_x)$ and we calculated the measured length and width (β, γ), the length deviation $(\delta_\beta = 22{,}666 - \beta)$ and the width deviation $(\delta_\gamma = 13{,}333 - \gamma)$ (Tableau 4.4). According to Tableau 4.4, and Figure 4.7 CAI software #1 and #3 offers three adjustment algorithms for oblong holes (LSC, MIC and MCC). Four algorithms are available in CAI software #2 (LSC, MIC, MCC and Minimax). The LSC algorithm displays different values for the measured width on software #1, #2 and #3 (13,139 mm, 13,152 mm and 13,151 mm). This is abnormal, since the LSC is a deterministic algorithm that normally should provide the same value of measured width. Software #1 and #3 with a MCC algorithm displays the same values of measured width (13,320 mm), but software #2 shows a different value (13,316 mm). The range between results is equal to 0,004 mm. Again, the MIC algorithm gives different values of measured width for software #1, #2 and #3 (12,989 mm, 13,048 mm and 13,320 mm). Finally, the minimax algorithm is available only by software #2, where the value of the width is equal to (13,164 mm).

Tableau 4. 4 Results for the inspection of the oblong hole (width =13,333 mm, length=22,666 mm)

Software	Algorithm	δ_x	β	δ_β	γ	δ_γ
	Best-Fit	**-0,143**	22,487	**-0,179**	13,139	**-0,194**
#1	Min	-0,145	22,345	-0,321	12,989	-0,344
	Max	-0,134	22,605	-0,061	13,320	-0,013
	Least square	**-0,143**	22,478	**-0,188**	13,152	**-0,180**
#2	Max inscribed	-0,145	22,306	-0,36	13,048	-0,284
	Min circumscribed	-0,138	22,607	-0,059	13,316	-0,016
	Minimax	*-0,144*	*22,479*	*-0,187*	*13,164*	*-0,168*
	Best-Fit	**-0,132**	22,478	**-0,187**	13,151	**-0,182**
#3	Min	-0,132	22,321	-0,345	12,994	-0,339
	Max	-0,132	22,646	0,020	13,320	-0,013

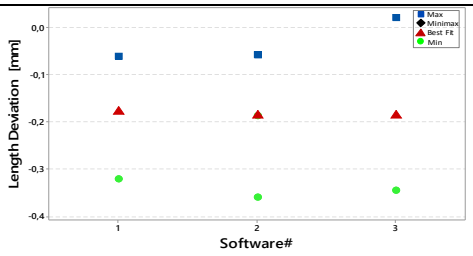

(a) Length deviation

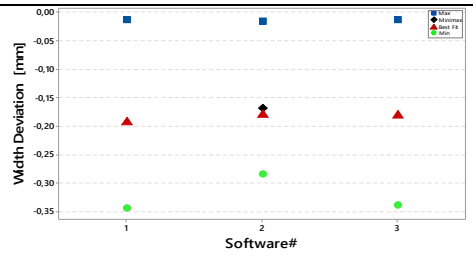

(b) Width deviation

Figure 4. 7 Results for the oblong hole

4.7 Analysis of Plan A

In the third test, we computed the flatness of two plans, Plan A and Plan D (Tableau 4.5). Results with the least square option are shown in bold; results with the min option are shown with an underscore, the max option is displayed using a double-underscore (Figure 4.8).

Tableau 4. 5 Results for the inspection of Plane A

Software	Algorithm	flatness
	Best-Fit	**0,107**
#1	Min	0,107
	Max	0,107
#2	Least square	**0,119**
	Best-Fit	**0,051**
#3	Min	0,051
	Max	0,051

According to Table 4.5, CAI software #1 and #3 offer three adjustment algorithms for Plane A, the Least Square Plane (LSP), Minimum Plane (MP), and Maximum Plane (MIP). The CAI software #2 only offers one algorithm (LSP) to fit plane A. Only the best fit is available. The software #1 gives the same flatness value (0.107 mm) for the three algorithms (LSP, MC and MIP). In the case of software #2, only the best fit is available (0.119 mm).

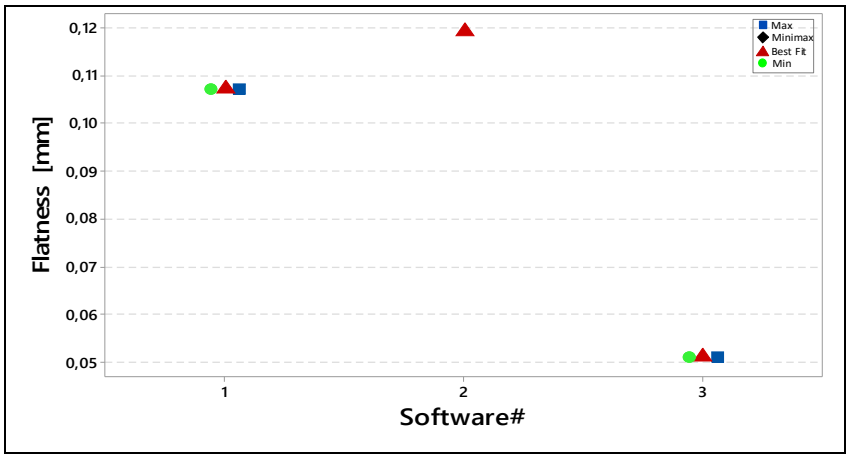

Figure 4. 8 Results of flatness analysis (Plan A)

4.8 Analysis of Plan D

According to Tableau 4.6, the results are similar to Plan A. Software #1 gives the same flatness value (0,070 mm) for the three algorithms (LSP, MC and MIP). In the case of software #2, only the best fit is available (0,0312 mm), but software #3 gives different flatness values for each of the three algorithms (LSP, MC, and MIP) (Figure 4.9).

Tableau 4. 6 Results of inspection of Plane D

Software	Algorithm	Flatness
#1	Best-Fit	**0,070**
	Min	0,070
	Max	0,070
#2	Best-Fit	**0,031**
#3	Min	0,035
	Max	0,035
	Least square	**0,073**

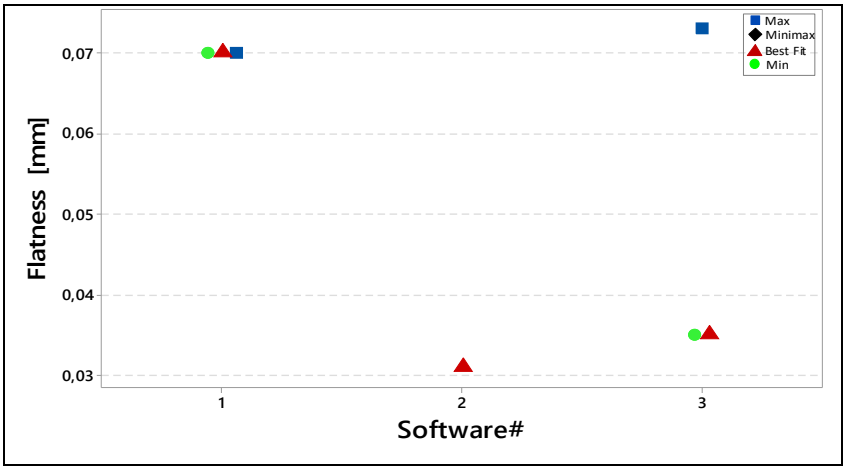

Figure 4. 9 Result of flatness analysis in Plan D

In this paper, an investigation of reproducibility estimation was presented. Similar point clouds, operators, CAD, and many fitting algorithms with different shapes (circle, plan and oblong hole) and features (size, circularity and flatness) were evaluated. The achieved experiences demonstrated that there exists a different variation between the three CAI software's. Using the example of a LS algorithm, the deterministic algorithm and the analytical solution are well-known. The aforementioned results demonstrate that there exists a small (and great) variation between CAI software's, these deviations can be due to filtering and smoothing operations, a reduction in the point density, the treatment of outliers, a calibration of the point cloud to the CAD model, and optimization operations when the tolerances allow for degrees of freedom. All these variation sources have an effect on variations that we call '*algorithmic errors'*.

4.9 Conclusion

The adjustment of measured point cloud is an essential step in measuring machine software. A correct application of adjustment algorithms can be employed to comparative tool not just a control tool. Some fitting algorithms optimize the conformance of geometric tolerances and can be applied in the manufacturing analysis. It is important that the correct algorithm be applied in the specific goal; otherwise, an error will be occurring and the results will not be optimal. An experimental investigation among three-inspection software's to evaluate algorithmic errors was proposed by the same operator, the same CAD, and point cloud. This experience shows that there are indeed variations (large and small) among the three software's. The proposed methodology is set to be an important tool to help industrial designers and inspectors select the appropriate algorithm for size and form evaluation. As such, it is the responsibility of the designer and inspector to carefully select the corresponding algorithm in order to avoid errors. Therefore, each specification method has its own field application (functional requirement). Once the specification method for a special application has been assigned, it becomes important to select the most optimal specifications. The benchmark and experimental case studies demonstrate the influence of the algorithm choice.

4.10 Acknowledgments

The authors would like to thank the *Institut Supérieur d'Informatique et des Techniques de Communication Hammam* (Sousse, Tunisia), and the *École de Technologie Supérieure* (Montréal, Canada) for their support.

CHAPITRE 5

A HYBRID APPROACH FOR DEFORMED CYLINDER FEATURES EXTRACTION BY ROBUST PRINCIPAL COMPONENT ANALYSIS AND ORIENTED BOUNDING BOX USING ISO 14405- 1:2016 SPECIFICATIONS

Ibtissem Jbira[a,b,c] , Antoine Tahan[b], Mohamed Ali Mahjoub[c], Borhen Louhichi[d]

[a]Institut Supérieur d'Informatique et des Technologies de Communication, G.P.1 Hammam Sousse-4011, Tunisie
[b]École de technologie supérieure (ÉTS), 1100 Notre-Dame West Street, Montreal, Quebec, H3C 1K3, Canada
[c]LATIS, ENISo, University of Sousse, Sousse 4023, Tunisia
[d]LMS, ENISo, University of Sousse, Sousse 4023, Tunisia

Article soumis pour publication dans journal Engineering Applications of Artificiel Intelligence en 2019

5.1 Abstract

Cylinders play a fundamental role in representing industrial geometry. The quality control of cylinder objects is an important area of dimensional quality control. Measuring the 'true size' of a cylinder feature can be a complex subject when geometry includes form defects (deformed cylinders), measurement noise, and if the scanned data is incomplete. In industrial settings, it can be impossible to scan the whole object because of limited access. Therefore, robust cylinder fittings in incomplete point cloud data with noise are of great importance. Preciseness, roundness and cylindricity measurements are essential to ensure functional requirement. This paper presents a novel approach using Robust Principal Component Analysis (RPCA) and Oriented Bounding Box (OBB) algorithms. The approach of cylinder fitting is applicable to complete and incomplete point cloud data with form defects and in the presence of noise. The proposed methodology is set to be a new tool to help quality control inspectors to select the appropriate algorithm for size and form evaluation. As such, designers and inspectors must correctly identify the corresponding algorithm, otherwise an error will occur. The standard ISO 14405-1 provides many modifiers adapted for many field applications (functional requirements). Once the method specification for a special application has been fixed, it

becomes important to select the most optimal method specification. The benchmark and experimental case studies demonstrate the influence of the algorithm choice, the influence of several parameters, and the limits to be respected in certain cases where the data are missing. The obtained results demonstrate that measuring precision requirements of the calculated sizes may be one way to resolve the calculated dimension problem of deformed cylinders in the manufacturing industry. The study of the fitting algorithms presented is expected to be an effective aid in making the right selection of algorithms to be used for the purposes of inspection. This paper also discusses ISO 14405-1 modifiers, the consequences of using theses algorithms in conception engineering, and investigates the impact of different measurement parameters.

5.2 Introduction

Cylinder approximation is an essential task in many applications, such as mechanical assemblies, object detection, feature extraction, cell counting, building information modelling, autonomous navigation, forest inventorying, surface reconstruction, and archaeological documentation (Jbira et al., 2017). Many researchers have proposed several algorithms for cylinder reconstruction and extraction based on their types of data and fields of application (e.g., image processing, reverse engineering, quality, computer vision, inspection). Recently laser-scanning techniques can acquire quickly a dense data called Point Cloud Data (PCD). In fact, many authors have considered cylinder fitting a key challenge in the presence of outliers, noise and distortion (Morse and Srinivasan, 2013). Cylindrical parts represent an important task in most industrial products. About 70% of all engineering parts have a circularity form (Pt et al., 2018). Roundness and cylindricity are one of the basic geometrical feature for circular and cylinder parts. It computes how closely a part form is near the ideal circle or cylinder. Since no manufacturing process is perfect, often circularity deviations occur in made parts. The deviations of manufactured parts are due to many reasons such as irregular cutting, temperature change, clamping deformations, etc. Circularity measurement is an important topic for the right functioning of assemblies (Pt et al., 2018). During the assembly phase, out-of-roundness poses major problems and produces a gap between the paired components. In

addition, the measured data points may be incomplete because of the orientation of the measurement device unit and the restricted access of measuring objects. As a result, precise and rapid extraction methods are necessary: ISO14405 2016 and a robust cylinder adjustment in complete and incomplete PCD with form defects and noise is of utmost importance. For a precise quality control, the association operation between an ideal feature (circle, cylinder) with the extracted feature (from measurements) should be accurate. The association algorithm can eventually play a key role in the association operation. However, the ISO and ASME standards do not specify specific algorithm. Different methodologies are available in literature. The role of the association operation is to fit features according to the criteria. The criteria can be classified by statistical and extreme-adjustment. A statistical criterion employs a statistical technique (e.g.: Least Square), which employs all the points to define the associated feature. An extreme-fit criterion (such as minimum zone, maximum inscribed, and minimum circumscribed), utilize extreme points. The new standard ISO-14405 presents a new method specification (algorithm) for fitting geometric objects; the new norm introduced 14 modifiers for fitting criteria. In this paper, we will use four specification methods of ISO-14405. The proposed approach is expected to be an important tool to help industrial designers and inspectors. The proposed benchmarks guarantee the selection of the best appropriate algorithm for roundness computation applications of size and form evaluation. The experimental case studies demonstrate the influence of the algorithm choice, the influence of various parameters and the limits to be respected in certain cases where the data are missing. This paper presents an approach using artificial intelligence-based methods with a robust PCA and OBBs algorithms. The rest of the paper is arranged as follows: a literature review and related methods will be presented in Section 1. The proposed approach is shown in Section 2. Experiments on artificial deformed cylinders are found in Section 3. A brief discussion of the proposed approach is presented in Section 4 and followed by a conclusion in Section 5. Literature review, related principles.

5.3 Literature review

In the quality analysis of cylinder components, circularity error is one of the important parameters in industry. The estimation of this parameter is mainly acquired by using a coordinate measuring machine. Many researchers have proposed different algorithms to calculate reference cylinders that are used to quantify the roundness errors applied in various fields (Moroni et al., 2014). Thus, with limited recommendations by the standards about the suitable algorithm, (Nurunnabi et al., 2018) proposed a new 3D robust cylinder fitting algorithm. They demonstrated a performance on real datasets, in the presence of outliers, and with a different number of points. The developed approach can be used for fitting cylindrical poles. (Pt et al., 2018), presented a comparative study of roundness evaluation algorithms: Minimum Inscribed Circle (MIC), Maximum Circumscribed Circle (MCC), Least Square Circle (LSC) for coordinate measurements. They proposed a benchmark of fitting algorithms in the literature in order to provide the optimal choice of execution. It was concluded that no single algorithm provided the best solution. The estimation of circularity errors remains a challenge in permitting the improvement of algorithms to calculate the best center. Many computational geometrics are used. In laser scanning, cylinder fitting is still an important problem in the presence of noise, outliers, etc. (Zhao et al., 2018) proposed a trained Neural Network Regression (NNR) to compute the calculated sizes. The obtained results satisfied the measuring accuracy requirements. The proposed method can be one way to solve the dimension measurements. (Guo and Yang, 2019) proposed a new procedure for circle fitting. They used Taubin's approach to compute the center and radius, and then they identified and removed the outliers by computing the geometric distances from the data points to the circle. Their experiments demonstrated that an iterative procedure could resist against the effect of outliers. Lastly, (Nurunnabi et al., 2018) proposed a new algorithm for fitting cylinders. They used two algorithms PCA and robust regression. Experimental results demonstrate that the new algorithm is efficient, that the robustness of the new method is demonstrated by comparing the new approach with other existing algorithms (e.g. RANSAC and MSAC), and that the new algorithm performs better than the other existing methods in the presence of outliers. This literature review demonstrates the importance of fitting algorithms. However, based on our

readings, no authors addressed the problem of deviated cylinders with form defects. This problem is very common within industries. Most cylinder approximation methods focus on full data. However, point cloud data acquired from Mobile Laser Scanning are incomplete and feature outliers.

In this paper, we will propose a new approach to evaluate the cylinders with form defects. Our proposed approach incorporates three algorithms: RPCA, OBB, and circle fitting algorithm (ISO 14405-01 specification methods. (Jbira et al., 2018a) proposed a methodology to evaluate the algorithmic errors of the modifiers of the ISO 14405 standard. They demonstrated that the noise measurement affects the ISO 14405 modifiers. This literature review reveals the importance of cylinder fitting problems for industrial designers and inspectors. Therefore, the quality of the deformed cylinders is evaluated by approximation algorithms. The literature provided us with different algorithms for cylinder fittings that are used to quantify roundness errors. Despite the different algorithms proposed, the optimal solution has yet to occur. Therefore, designers need to carefully select the appropriate algorithm. According to the literature, very little research has focused on incomplete data and deformed cylinders.

5.4 Specifications of size tolerances

The publication of the ISO 14405-1:2016 initiated 14 new sets of size specification modifiers. The designers defined the geometry with more details. This paper limits its scope to only 3D geometric features: the “cylinder” (see Figure 5.1). In this particular case, there are only four (4) types of circularity (and diameter) evaluation methods proposed by the ISO 14405- 1:2016: the center of least squares circle (GG); the center of the minimum area (SN); the center of the circumscribed cylinder (GN); the center of the maximum inscribed cylinder (GX). The used ISO 14405-1 modifiers are detailed in the previous works in (Jbira et al., 2018b).

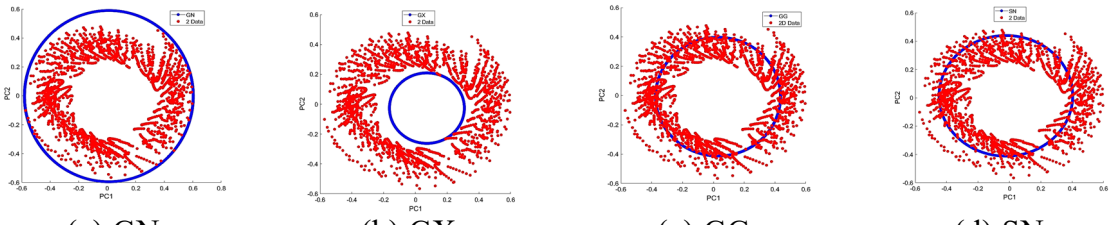

(a) GN (b) GX (c) GG (d) SN

Figure 5. 1 ISO 14405-1: GX, SN, GG & GN methods

5.4.1 GN Algorithm

To calculate the GN, the algorithm is an iterative method : for any three points (x, y) plane $[(x_1, y_1), (x_2, y_2), (x_3, y_3)]$ two options are available: (i) two of the 3 points lie on the circle circumference; (ii) the three points lie on the circle circumference.
The circle with unknown radius R and center (u_x, u_y) must satisfy (5.1), (5.2), and (5.3)

$$(x_1 - u_x)^2 + (y_1 - u_y)^2 = R^2 \quad (5.1)$$

$$(x_2 - u_x)^2 + (y_2 - u_y)^2 = R^2 \quad (5.2)$$

$$(x_3 - u_x)^2 + (y_3 - u_y)^2 = R^2 \quad (5.3)$$

The quadratic terms are eliminated in the unknowns simply by subtracting pairs of those expressions to yield (4) and (5), linear in the unknowns (u_x, u_y).

$$2(x_1 - x_2)\ u_x + 2(y_1 - y_2)\ u_y = x_1^2 - x_2^2 + y_1^2 - y_2^2 \quad (5.4)$$

$$2(x_1 - x_3)\ u_x + 2(y_1 - y_3)\ u_y = x_1^2 - x_3^2 + y_1^2 - x_3^2 \quad (5.5)$$

The linear system of equations should be solved for (u_x, u_y). Then, equation (5.4) is used to obtain R. The Figure 5.2 presents the main steps of the GN algorithm.

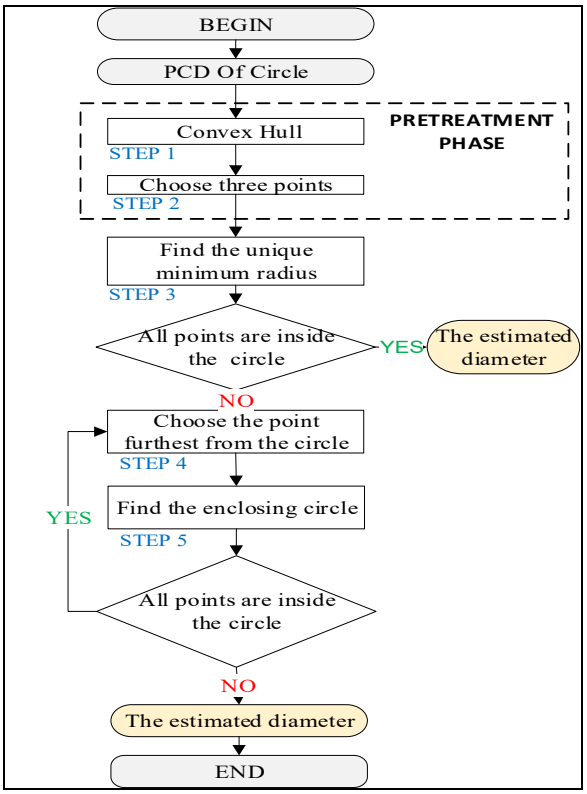

Figure 5. 2 Minimum Circumscribed Circle Algorithm

5.4.2 GX Algorithm

To calculate maximum inscribed circle, Voronoi diagrams are used. The name of Voronoi diagrams is referred to the name of Russian mathematician Georgy Fedoseevich Voronoi. The Voronoi diagrams are basic data structures in computational geometry created in 1908. It divides the space into zones, such that each zone is including the points that are nearer to the data than other. These diagrams can be used to determine the GX; the center of the GX is a Voronoi edge or a Voronoi vertex. The radius is the distance between the circle center and the convex vertex.

Algorithm 5.1. Pseudo-code of the GX algorithm

Pseudo-code of the GX algorithm

Input: n: number of points, $P_i(x_i, y_i)$ with i= [1...n];
Output: the radius r_{GX};

1 Begin
2 Compute the inner hull (IH);

3 Build the Voronoi diagram using the MATLAB predefined function '*voronoi';*

4 Compute Voronoi nodes;

5 Compute the center of GX by maximizing the distance for each node to the closest node;

6 End -Algorithm

5.4.3 GG Algorithm

This method called also regression, it minimizes the Euclidean norm of the deviation vector, and this algorithm is simple in computing. The objective function (F) is defined as

$$F = \sum_{i=1}^{n}(d_i - r_{GG})^2 \qquad (5.\ 6)$$

5.4Where $d_i = \sqrt{(x_i - x_c)^2 + (y_i - y_c)^2}$ is the Euclidean distance between $P_i(x_i, y_i)$ and $c(x_c, y_c)$ and r_{GG} is the circle radius.

5.4.4 SN Algorithm

This method called also Chebychev, it is defined as the two concentric circles where all points are inside them, and here exchange algorithms are employed to compute the GX circle. The optimization criteria are the minimization of deviations range.

Algorithm 5.2 - Pseudo-code of SN algorithm

Pseudo-code of SN algorithm

Input: n: number of points, $P_i(x_i, y_i)$ i= [1… n];
Output: the radius r_{GN};

1 **Begin**
2 Chose the points P_1, P_2 of GN circle (x_{p1}, y_{p1}), (x_{p2}, y_{p2}) by SPF algorithm
3 Chose the points P_3, P_4 on GX circle (x_{p3}, y_{p3}), (x_{p4}, y_{p4}) by SPF algorithm
4 Build the lines L_1 and L_2 connecting P_1, P_2 and P_3, P_4
5 Build the L_3 and L_4 are the two perpendicular lines to L_1 and L_2
6 Compute the center of the GX and GN circles
7 **end- Algorithm**

The GN algorithm is complex (Quadratic complexity), the GX algorithm is of logarithmic complexity, the GG algorithm is linear complexity $O(n)$ and SN algorithm is more complex cubic complexity $O(n^3)$.

5.4.5 Principal Component Analysis (PCA)

A data reduction problem with extra constraints which maximize the variance are used in this paper for fitting cylinders. PCA is applied in statistics and many imaging applications (image processing, image restoration and alignment, rectification, image analysis, image reconstruction and the analysis of brain images, and computer vision). PCA is very sensitive to outliers and necessitates high computation time. This makes PCA inappropriate for high-dimensional point clouds in computer vision and imaging applications. A variety of research has proposed many techniques to address robust PCA problem by decomposition into low rank plus sparse matrices, convex and robust estimators, etc. Therefore, a new algorithm called the Robust Principal Component Analysis (RPCA) is defined to reduce outliers and noise. It has been used in many applications, including 3D. In this paper, the RPCA is used to project 3D point clouds to

get 2D points (see Figure. 5.3); 3D points are projected on the plane passed by the PC2 and PC3 or PC1 and PC2. A circle can be defined by the following parameters: the center, a normal plane, and the radius. In the case of cylinders, the length has to be specified. In general, the cylinder was defined by following parameters: center ($\boldsymbol{C}$), diameter ($\boldsymbol{D}$), length ($\boldsymbol{L}$) and orientation ($\boldsymbol{O}$). The cylinder's center and radius are associated to the circle's center and radius. We approximate firstly a circle using ISO 14405-1:2016 specification's methods and the estimated circle parameters: $\boldsymbol{c}$ and $\boldsymbol{r}$ for cylinder fittings to obtain the parameters cylinder. The following figure shows an example of the RPCA as applied to a cylinder object.

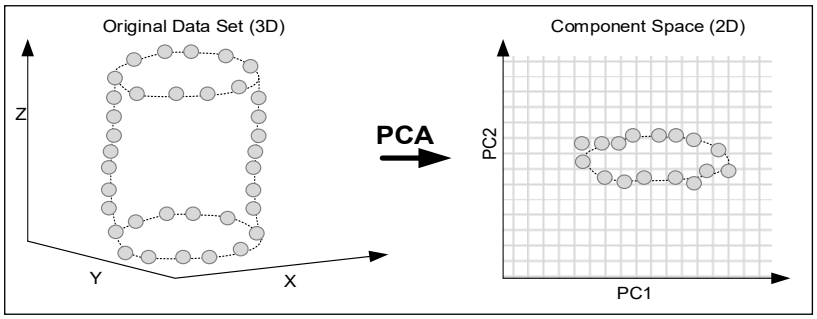

Figure 5. 3 Projection of 3D cylinder on the 2D circle

5.4.6 Oriented Bounding Box

The input for the approach is assumed as 3D PCD forms a 3D cylinder. Therefore, a preprocessing step is necessary to extract cylindrical data. Here, an Oriented Bounding Box (OBB) is used to select the cylinder form. Joseph O'Rourke (1985) who developed a cubic-time algorithm to find the minimum-volume of a three-dimensional point set first introduced the OBB. We assume three-cylinder case studies (see Figure 5.4).

The OBB is used to provide the cylinder case. In general, in industrial settings, we find three types of cylindrical objects:

- Case1: The length L is larger than its radius R.
- Case2: The radius R is larger than its length L.
- Case3: The length L is equal to its radius R.

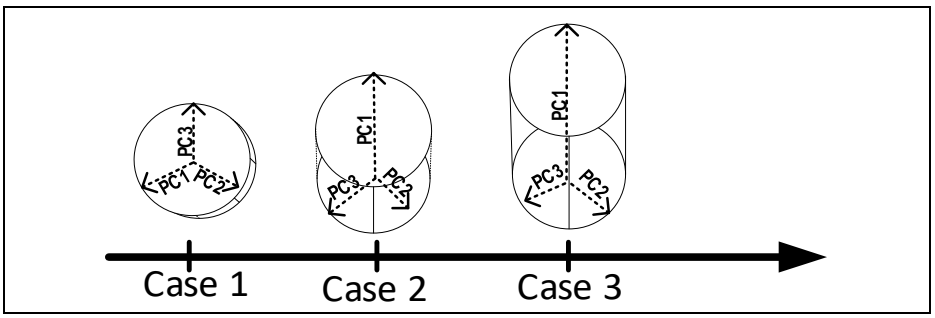

Figure 5. 4 the different cylinders cases in the industry

Case1:$\frac{L}{\emptyset} < 1$; Case 2: $\frac{L}{\emptyset} = 1$; Case 3: $\frac{L}{\emptyset} > 1$

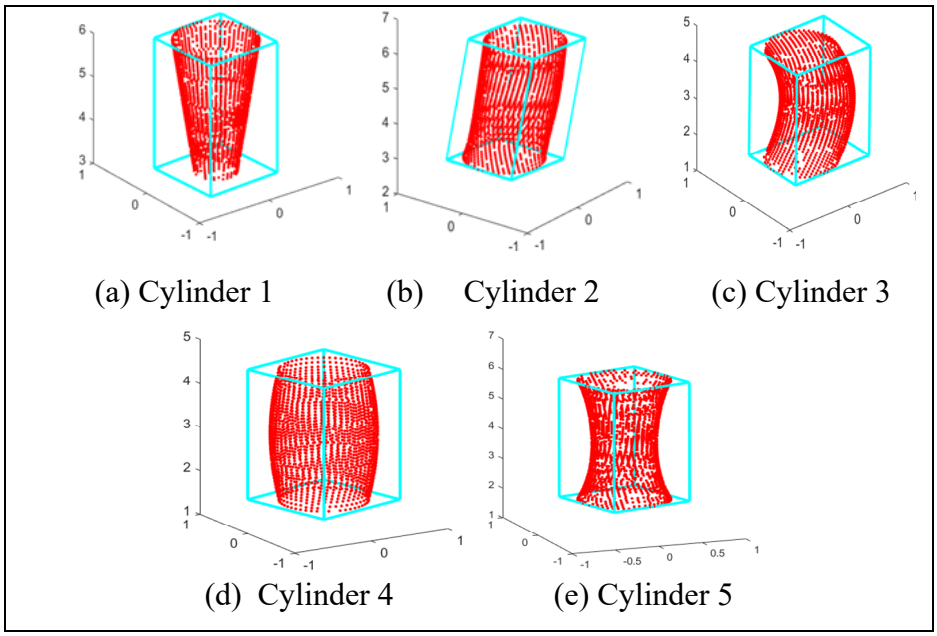

Figure 5. 5 results of the OBB on the created deformed cylinders

5.5 Proposed approach

The proposed algorithm has four steps. The first step is the selection of the cylindrical object using an OBB in order to estimate the cylinder case (Case 1, Case 2 and Case 3). Herein, we assume three-cylinder case studies (see Figure 5.5). In the industrial context, three types of cylinders frequently exist. The second step is to perform RPCA to estimate cylinder orientation. The PCs of the variance-covariance matrix of 3D PCD specify the data variance on the axis. The PC1 or PC3 (depending on cylinder case) indicates the variableness on the cylinder's axis and the PC1 and PC3 or PC2 and PC3, show the variableness vertical to PC1 or PC3 (See Figure 5.6).

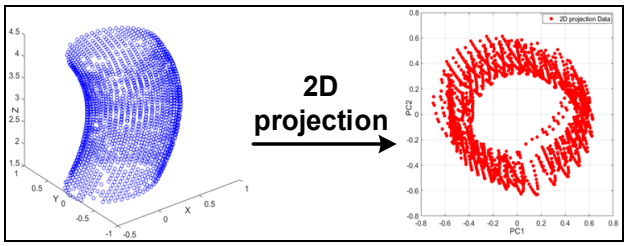

Figure 5. 6 projection of 3D deformed cylinder

Since the classical PCA is very sensitive to outliers, the RPCA is used to reduce the effect of outliers. The reader can refer to (Podosinnikova et al., 2014) for details on RPCA. The next step is a circle adjustment using ISO14405-1:2019 method specifications. The radius and center cylinder parameters are approximate by adjusting a circle to a projected cylinder point. In order to obtain robust PCs therefore increase the performance of the methodology, the Project 3D point cloud gets 2D points: 3D cylinder points are projected onto the spanned plane. For this step, the PCs obtained in the second step are used. Finally, we estimate the cylinder's orientation and length. The Figure 5.7 illustrates the proposed algorithm and the main steps used to estimate the cylinder's parameters.

Algorithm 5.3: Pseudo-code of the proposed algorithm

Pseudo-code of the proposed algorithm

Input: n: Number of points;⌀: Diameter nominal; t: Monte Carlo simulation;v: Measurement noise
Output: The best results(Diameter d, Center C, radius R, Length L, Orientation$O$)

1 **Begin**
2 Create cylinders with form defects;
3 Compute the noise standard deviation σ;
4 Add a Gaussian random number a with mean parameter $N(\mu, \sigma)$:

$x_n = x + a\,cos(theta)$;
$y_n = y + a\,sin(theta)$;
$z_n = z\ \ (j, 1)$

5 Browse all the generated artificial cylinders;
6 Perform OBB;
7 Calculate the Euclidian distance of the three vectors (e_1 , e_2 and e_3);
8 Preform PCA on p_i (x_i, y_i, z_i) and find PCs (eigenvectors v_1 , v_2 and v_3) and eigenvalues γ_1, γ_2, and γ_3;
9 Projects all points onto $v_2$and v_3 baed plane so that projected point's q_i are on circle arc Hence
10 q_i =$(v_2, v_3)^t$ $(p_i$-p$)$
11 Fit circle by using ISO modifications
12 Compute the radius r_{GN} ,of GN method
13 Compute the radius r_{GX} , of GX method
14 Compute the radius r_{GN} , of GG method
15 Compute the radius r_{SN} of GN method
16 Compute cylinder parameters (C, R, L, O):$C = c$, $R = r$,
$L = \max(p_i^t v_2) - \min(p_i^t v_2)$ and $O = v_2$

17 **End-Algorithm**

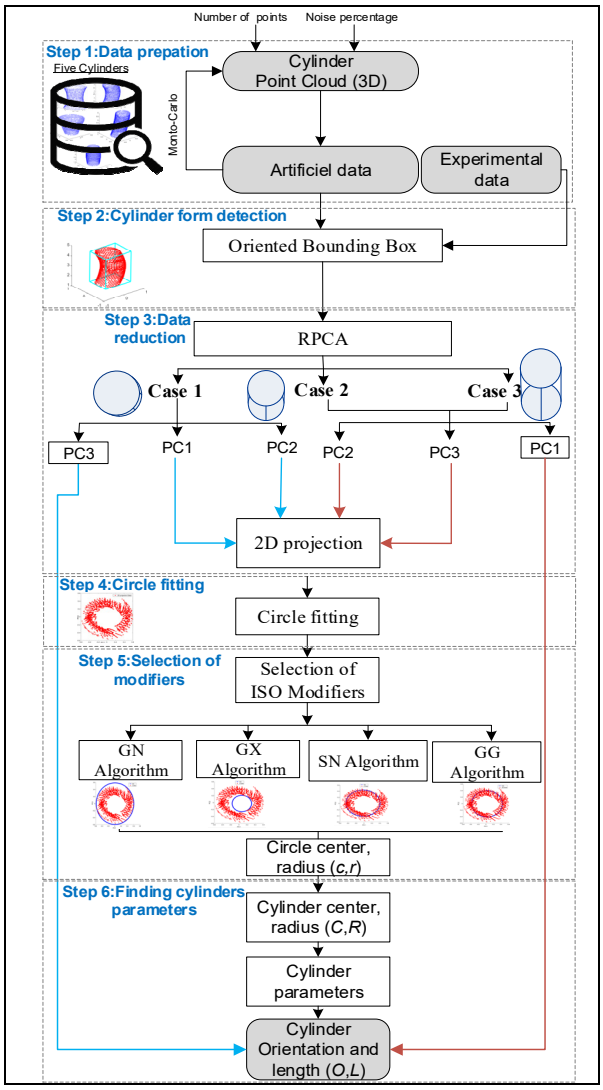

Figure 5. 7 Main steps of cylinder fitting

5.6 Experimental protocol

The number of points for each cylinder is chosen equal n=2000 for synthetic simulated data. The nominal diameter value chosen is equal to one. There are five (5) types with form defects (taper, hourglass, barrel modes, rippled mode). Measurement noise is assumed Gaussian. The amplitude of the standard deviation is chosen in this interval [1%, 2%; 5%, 10%, 15%, 25%] relative to the nominal diameter. The number of simulations for Monte Carlo (2×10^3). Six (6) scan areas are studied ($90°, 180°, 225°, 270°, 300°, 360°$).

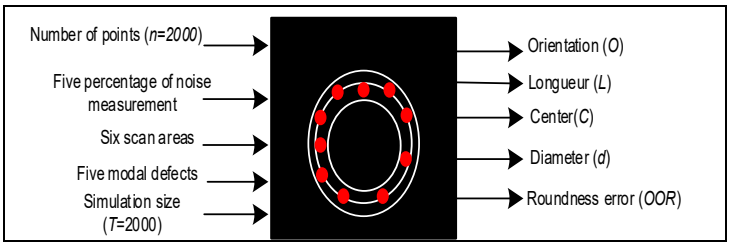

Figure 5. 8 Main steps of cylinder fitting

Some assumptions are made. (1) The reproducibility in this study (u_{AV}) represents the standard deviation due to the algorithmic error (e.g. to feature fitting use least squares fit or minimum zone Chebyshev fit, measurement strategy or in the use of computer programs and how the operator uses all software options. It therefore represents an observed variation. (2) We used a confidence level representing an interval of 95%. If applicable, outliers and missing data were included in the calculations. Statistical treatment is done on a Minitab® v.18 software. (3)Four specifications of size tolerances, as defined in ISO 14405-1, are presented (GN, GX, GG, and SN). (4) The manufacturing defects were stimulated by modal decomposition; this method is used to create artificial cylinders with form defects (deformed cylinders), the application of translations due to modal vectors are used to obtain deformed cylinders (Homri et al. 2014). A utilization of a realistic simulation provides design and manufacturing optimization (Figure 5.8). (5) All measurements are done in controlled environment (metrology laboratory or facilities). Therefore, the uncertainty induced by environmental conditions can be considerate as negligible in this study compared to amplitude defects.

Five cylinders with form defects are manufactured (material: aluminum) with different geometrical defects in order to envisage interesting and particular measurement scenario. The manufactured Cylinder 1 is without intended form defects. The defect of the manufactured Cylinder 2 is 3 lobs form. For Cylinder 3, we simulated a compression effect on the cylinder. Cylinder 4 has a local fault. Tableau 5.3 describes cylinder features such as the nominal diameter, and the number of points measured.

For virtual cases, the manufacturing defects were stimulated by modal decomposition; this method is used to create artificial cylinders with form defects (deformed cylinders), the application of translations due to modal vectors are used to obtain deformed cylinders (Figure 5.9)

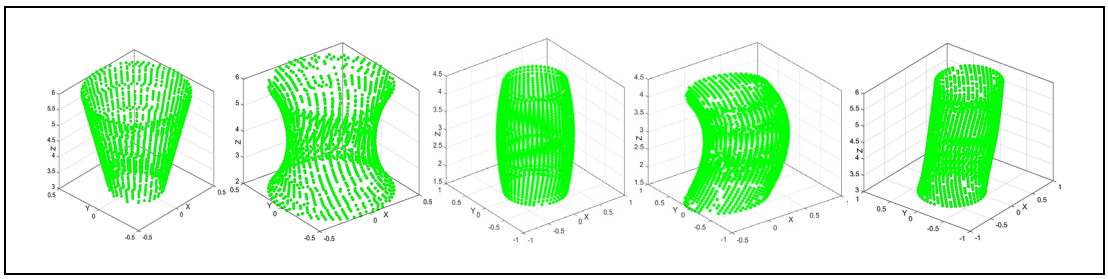

Figure 5. 9 Synthetic data with form error simulations on cylinder surfaces, n =2000

To analyze the sensitivity of the algorithm to measurement noise in the dataset, 2×10^3 simulations are generated. We used simulated defects similar to deviations in real manufacturing to reflect the deviations on actual parts so that the manufacturing defects be as close to reality as possible. A random noise following a normal distribution is generated among the points with a mean of zero and StD in all (x and y) directions (Figure. 5.10).

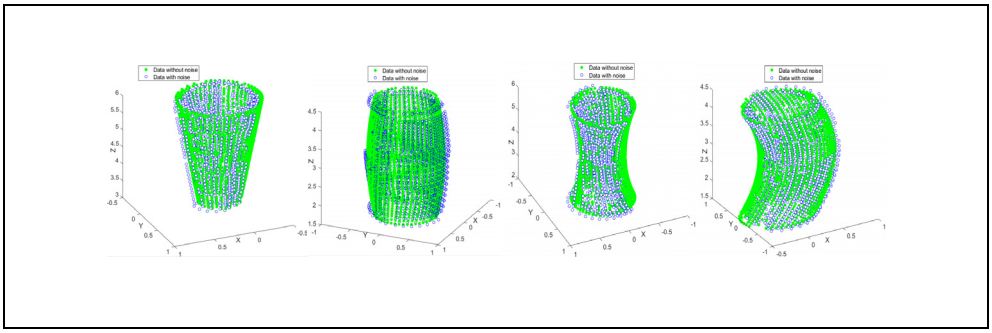

Figure 5. 10 Example of synthetic data with noise (v=0.1 mm and n =2000)

5.7 Artificial Datasets

The benefit of using simulated data is that the original parameters are well known. In this paper, an artificial dataset was created to simulate data to form defects, with a diameter D= 1 (mm) radius and a 6 mm axis. A Monte-Carlo simulation was used to generate 2000 cylinders to obtain statistically representative results. This paper introduces a new approach of cylinder fitting applicable to complete and incomplete 3D PCD with noise to compare the sensitivity of different parameters: (i) the measurement noise; (ii) different deformed cylinders; (iii) different number of points; (iv) missing data.

5.7.1 Cylinder fitting for missing data

In a certain case, the scanned data can be incomplete because of the measurement device orientation and limited access. (Nurunnabi et al 2018) suggested that fitting a circle from incomplete data still is an important problem (Figure 5.11).

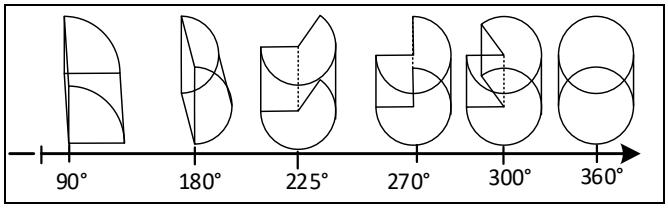

Figure 5. 11 Scale of different angles

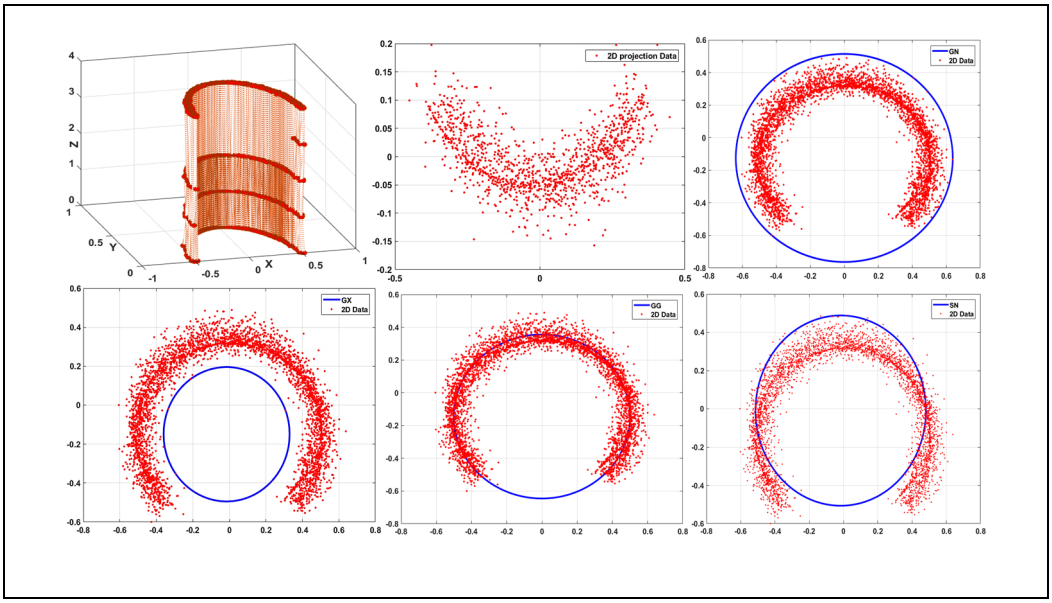

Figure 5. 12 Results of fitting incomplete data n=750×5, v=20%, and T=2000.

We have tested the new approach with different scan areas on the four algorithms of ISO14405-01 (GN, GX, GG and SN) (See Figure 5.12). To visualize the results of these algorithms, we drew the CDF of each algorithm with six scan zones: zone 1: 90°, zone 2: 180°. zone 3: 225°, zone 4: 270°, zone 5: 300°, zone 6: 360°. According to the results obtained, the algorithm with the best fit (GG) provides the best result and is able to approximate the cylinder for any scan zones beginning at ≥ 90°. The optimization algorithms (GN, SN and GX) are very sensitive to the different scan areas; the SN is unable to approximate the cylinder in the case of zone 1: 90° (bug in the code). GN gives unacceptable results in the case of zone 1 (90°). Therefore, designers and inspectors will be able to identify the suitable algorithm, otherwise unacceptable results or algorithmic errors will occur. The experimental case studies (see Figure 5.13) prove the influence of the algorithm choice.

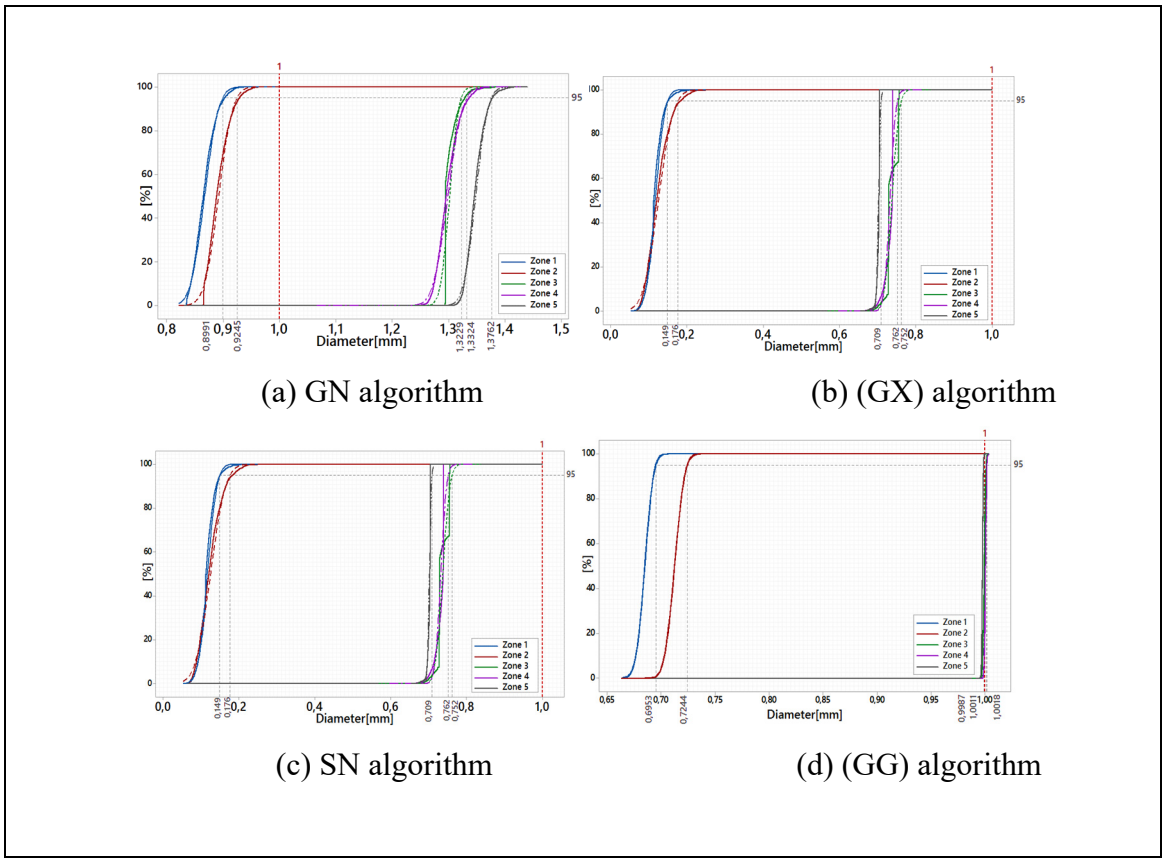

Figure 5. 13 Empirical cumulative for diameters; the influence of incomplete data on the evaluation of ISO 14405-1 specification methods: (a) GG method, (b) GN method, (a) GX method, (d) SN method.

5.7.2 Influence of noise measurement

To explore the influence of noise on cylinder fitting algorithms, 2000 simulated datasets were created for every percentage of 2%, 5%, 10%, 15% and 20% ($\sigma = [5; 12.5; 25; 37.5; 50] \times 10^{-3}$). The performance measurements are computed as box plot digammas for measurement noise. An illustration of the influence of noise on specification methods can be found in GN, GX, GG and SN in Figure 5.14. Results are illustrated on the box plot digammas in Figure 5.14 (a), (b), (c), and (d) for measurement noise.

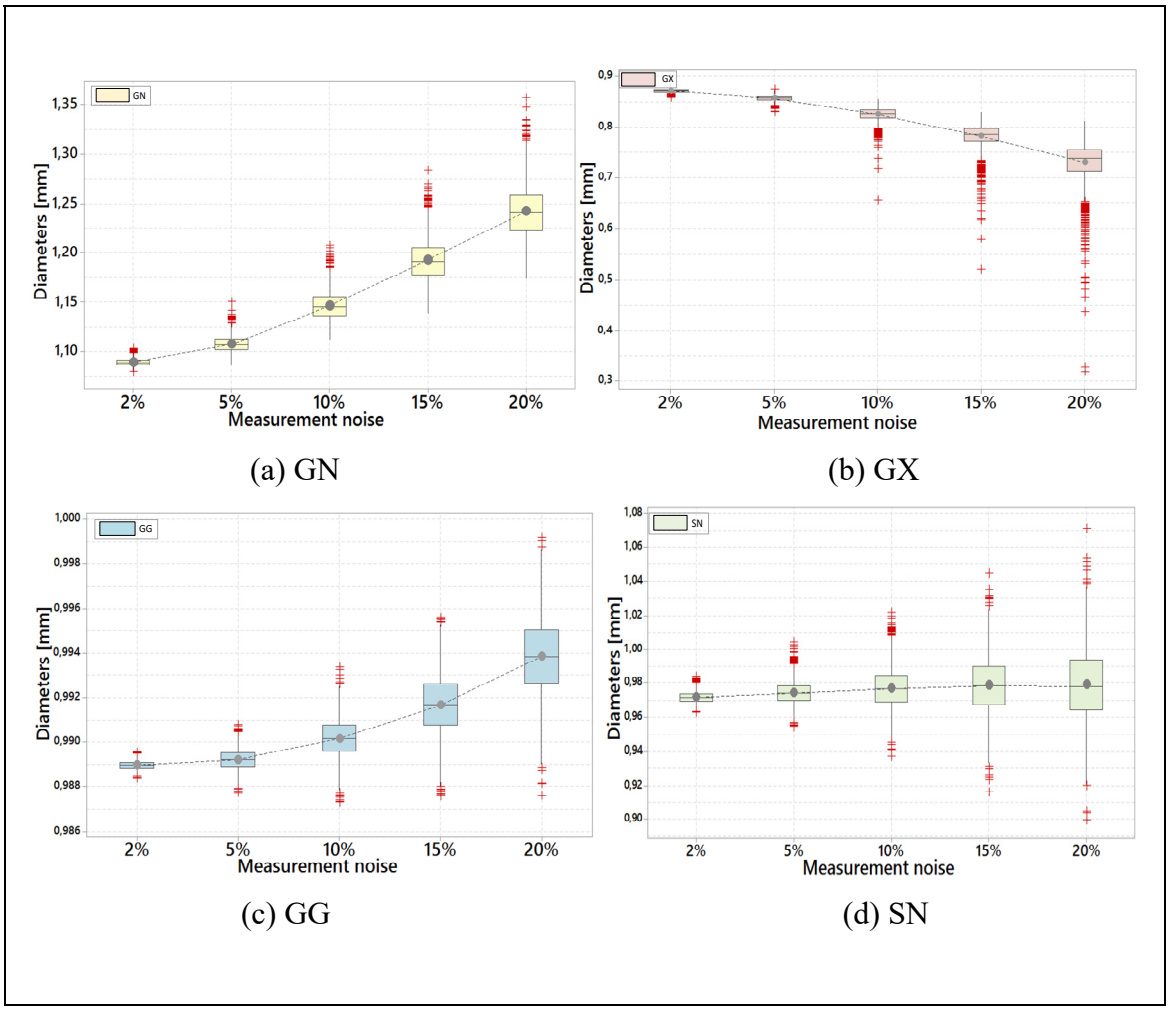

Figure 5. 14 The influence of noise level on the evaluation of 14405-1 specification methods (v = [1%,2%, 5%, 10%, 15%, and 20%])(a) GN method, (b) GX method, (c) GG method, (d) SN method (Cylinder 4)

Figure 5.14 demonstrates that noise measurement influences all the specification algorithms. The value of the diameter depends on the cylinder's noise level. The Monte-Carlo simulation confirms that the GN and GX modifiers have the greater influence on measurement noise. In the case of the specification of an outside GN diameter, it depends on high points (Figure. 5.14, a). In the other case of an inside diameter GX modifier (Figure 5.14, b), it depends on low points. The GG modifier is insensitive to extreme roughness (Figure 5.14, c). Finally, the SN modifier (Figure 5.14, d) depends on positive and negative roughness.

5.7.3 Influence of Deformed cylinders

To see the influence of the presence of from defects in cylinder fittings, we created 2000 fully deformed cylinders. The performance measurements were computed similarly to previous experiments for all the cases of noise variations with (i) being the number of points fixed at n=2000, (ii) the noise level v =20%.

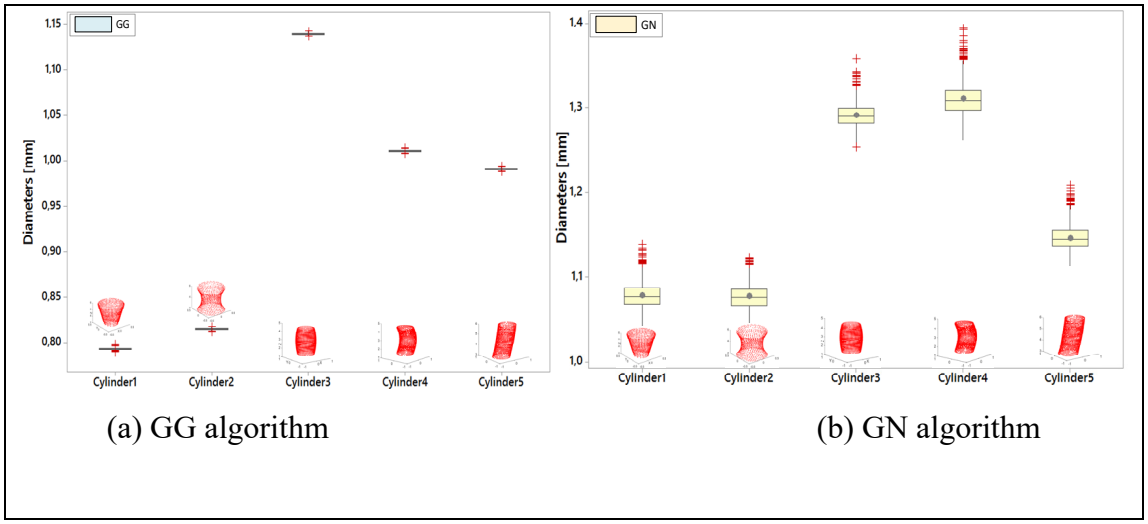

(a) GG algorithm (b) GN algorithm

Figure 5. 15 the influence of defect forms on the evaluation of ISO 14405-1 specification methods: (a) GG method, (b) GN method, (c) GX method, (d) Sn method

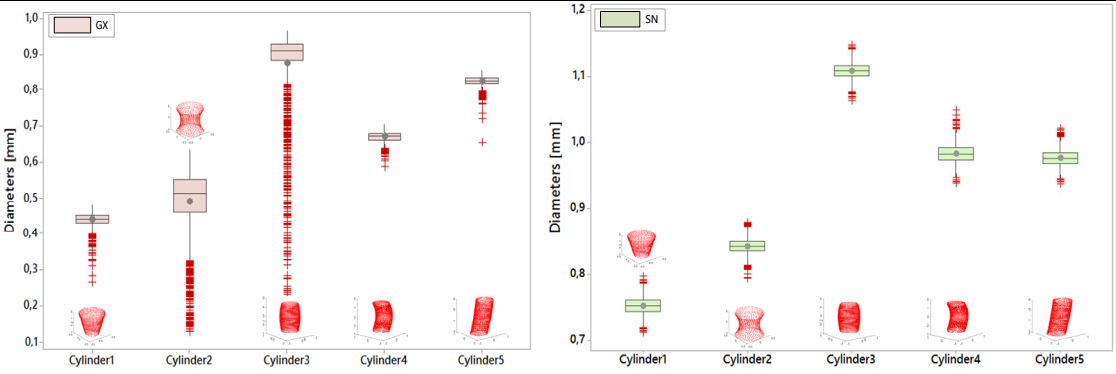

(c) GX algorithm (d) SN algorithm

Figure 5.15 (continued)

According to the results obtained in Figure 5.15, the four types of defect forms generated results in different diameters. This proves that form defects have an influence on the ISO-14405 fitting algorithms.

5.8 Experimental datasets

Polyworks 2018 IR6 was used to calculate the roundness evaluation methods. The software contains four methods named Best Fit, Min Fit, Max Fit and Fit Sigma. (*i*) The Best Fit and Fit Sigma methods correspond to GG modifiers. (*ii*) The Max Fit method corresponds to the GN modifier. (*iii*) The Min Fit method corresponds to the GX modifier.

Tableau 5. 1 Feature table of the cylinder

Name		Nominal $\boldsymbol{D}$ $[\boldsymbol{mm}]$	$\boldsymbol{N}$
Cylinder 1	$C1$	40,7298	34033
Cylinder 2	$C2$		33445
Cylinder 3	$C3$		35704
Cylinder 4	$C4$		34243

The manufactured Cylinder 1 is without form defects. The defect of the manufactured Cylinder 2 is 3 lobs. For Cylinder 3, we simulated a compression effect on the cylinder. Cylinder 4 has a local fault. Table 5.2 describes cylinder features such as the nominal diameter, and the number of points measured. The manufactured cylinders are shown in Figure 5.16.

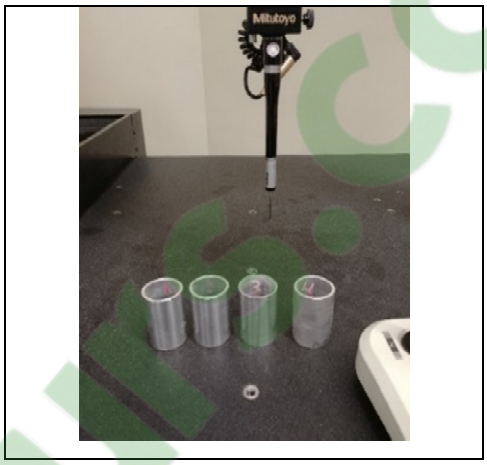

Figure 5. 16 the four cylinders made
at his laboratory LIPPS ETS

Tableau 5. 2 Results of real datasets
(Max fit, Min fit, best fit and Best Fit Sigma)
with d: diameter; OOR: Out-of-roundness

Name		Max $[\boldsymbol{mm}]$	Min $[\boldsymbol{mm}]$	Best Fit$[\boldsymbol{mm}]$
$\boldsymbol{C1}$	d	40.7942	40.7205	40.7529
	OOR	0.0391	0.0391	0.0391
$\boldsymbol{C2}$	d	41.8152	39.3800	40.6154
	OOR	1.2785	1.2785	1.2785
$\boldsymbol{C3}$	d	40.7093	40.4702	40.5817
	OOR	0.1332	0.1332	0.1332

Tableau 5.2 (continued)

Name		Max $[mm]$	Min $[mm]$	Best Fit$[mm]$
$C4$	d	40.8673	40.0952	40.6120
	OOR	0.5803	0.5803	0.5803

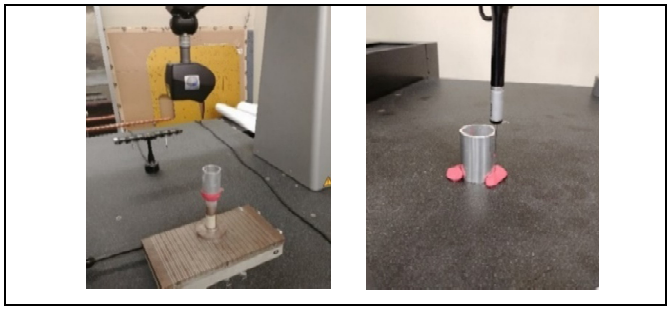

Figure 5. 17 Measurement and evaluation process of the four cylinders

A comparative analysis between the model (proposed approach) and the experimental results using poly-works 2018 IR6 (Figure 5.17), this test consists of a statistical adequacy test on both models. Also we compute the deviation diameter as range ($\delta_{\emptyset}$) between results is equal ($\delta_{\emptyset} = d_{\text{Measured}} - d_{\text{Model}}$), the Tableau 5.3 presents the results of the comparative test.

Tableau 5. 3 Comparing the results of a model with experimental measurements

Cylinder	Algorithm	d_{Measured}	d_{Model}	$\delta_{\emptyset}$
C1	GN	40.7942	40.7755	0,0187
	GX	40.7205	40,5035	0,217
	GG	40.7529	40.6761	0,0768
	SN		40,2941	
C2	GN	41.8152	42,0365	-0,2213
	GX	39.3800	38,9946	0,3854
	GN	40.6154	40.2425	0,3729
	SN		40.6468	
C3	GN	40.7093	40,8973	-0,188

Tableau 5. 4 (continued)

Cylinder	Algorithm	$d_{Measured}$	d_{Model}	$\delta_{\emptyset}$
C3	GX	40.4702	39,9498	0,5204
	GG	40.5817	40.3775	0,2042
	SN		39.7817	
C4	GN	40.8673	40,7682	0,0991
	GX	40.0952	39,3892	0,706
	GG	40.6120	40.6137	-0,0017
	SN		40.2660	

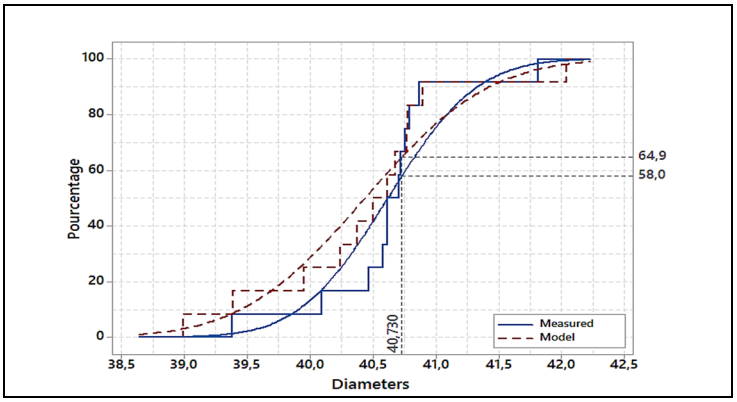

Figure 5. 18 Empirical cumulative of proposed approach and measured results

To validate the proposed approach, linear regression between the diameters' values of the proposed approach and the values of the diameters of experimental results is made according to Figure 5.18, the linear regression is made by MINITAB 18; according to the linear regression results. The percentage of total dependent variable variation $R^2 = 92.35\%$, the value of R^2 nearer to 1%. Therefore, R^2: describes a better fitted.

5.9 Conclusion

This paper presented a novel approach to cylinder fitting algorithms applicable to missing PCD with form defects in the presence of noise using artificial intelligence based methods: Robust Principal Component Analysis (RPCA) and Oriented Bounding Box (OBB) using ISO 14405-1 specifications. The obtained results demonstrated that the measurement precision

requirements of calculated dimension’s that can be an efficient way for the industry to resolve the cylinder dimension measurement problems by implementing ISO 14405-1 in industry. The study of the ISO specifications (modifiers) presented is expected to be effective in choosing the right algorithm to be used for the purposes of inspections. This paper also discussed artificial datasets, ISO 14405-1 specifications, the consequences of using theses standardized size modifiers in engineering design, and investigated the influence of different parameters. This proposed methodology will hopefully be an important tool for industrial designers and inspectors looking to select the appropriate modifier or algorithm for size and form evaluation. The benchmark and artificial case studies demonstrated the influence of algorithm choice, the influence of several parameters, and the limits to be respected in certain cases where the data was missing. Some algorithms are not appropriate in certain cases. As such, designers and inspectors must correctly identify algorithms that correspond, otherwise errors will occur. Thus, each method specification has its own field application (functional requirement). Once the specification method for a particular application was selected, it important to choose the most optimal algorithm for of the selected specification method.

5.10 Acknowledgments

The authors would like to thank the Institut Supérieur d'Informatique et des Techniques de Communication Hammam Sousse (Tunisia), and the École de Technologie Supérieure (ÉTS, Montréal, Canada) for their support.

CONCLUSION

Cette thèse s'intéresse à la modélisation, la simulation et l'inspection des défauts de forme des composants mécaniques. Plusieurs approches ont été développées et investiguées afin de répondre aux quatre questions fondamentales que nous avons posées au début de nos travaux. 1) Comment peut-on modéliser des surfaces ayant des défauts de forme ? 2) Comment les défauts de forme influent l'identification des requis dimensionnels et géométriques ? 3) Comment peut-on simuler le comportement à l'assemblage des composants rigides ayant un défaut de forme ? 4) Comment vérifier des requis dimensionnels et géométriques des surfaces avec de défauts de forme ? Au démarrage de nos travaux, nous avons accepté la conjoncture que les approches développées contribueront au développement des méthodes de modélisation d'assemblage réaliste.

Nous avons présenté dans le Chapitre 1 une revue succincte de la littérature scientifique et de l'état de l'art dans le domaine. Nous y avons aussi présenté la méthodologie proposée pour tenter d'y répondre aux questions de recherche et la structure de la thèse. Plus spécifiquement, la revue de littérature a abordé les phases typiques de la gestion de défauts de forme : (*i*) modélisation des défauts de forme (*ii*) simulation de défauts de forme dans l'assemblage, et (*iii*) l'estimation de défauts de forme à partir d'un nuage de points mesurés.

La première partie est décomposée en deux groupes. Le premier décrit les différents modèles de tolérancement, les avantages et les inconvénients chaque modèle. Le deuxième décrit les algorithmes de paramétrages des surfaces avec défaut de forme, les travaux réalisés au cours des années, la description mathématique et les domaines d'utilisation de chaque algorithme. La deuxième partie discute les travaux réalisés dans le domaine de simulation de défauts de forme dans l'assemblage. Toutes les recherches effectuées montrent que les défauts de forme ont une influence sur l'assemblage final. La non-prise en compte de défauts de forme risque de conduire à calculer des spécifications qui engendrent des assemblages non conformes. La dernière partie de revue de littérature s'intéresse à étudier l'estimation de défauts de forme à

partir d'un nuage de points mesurés. Dans cette partie nous avons étudié comment les stratégies de mesure des systèmes influents sur différents algorithmes.

Dans le Chapitre 2, la première étape de gestion de défauts de forme a été abordée. Elle vise à modéliser les défauts de formes pour divers éléments géométriques primitifs (ex. cylindre, plan, etc.) en considérant une rigidité infinie, et d'employer ces modèles dans les simulations cinématiques des assemblages. Nous avons développé une méthode de modélisation d'assemblage réaliste. À cette étape, nous avons développé des algorithmes qui permettent de générer automatiquement des assemblages réalistes tout en respectant les contraintes d'assemblage. Cette modélisation réaliste joue un outil qui permet une analyse de tolérances de forme en prenant compte l'évolution des contacts entre les composants. Les impacts des défauts de forme sur le mouvement lors de l'assemblage réaliste ont été quantifiés. Nous sommes convaincus que cette approche fournit un résultat d'assemblage plus proche de l'assemblage réel. Cette partie de notre recherche a fait l'objet d'une publication dans une revue avec comité de lecture ainsi qu'un exposé dans une conférence.

Comme corollaire à cette première étape, une étude sur l'influence de défauts de forme sur l'identification des requis dimensionnels et géométriques a été présentée dans le Chapitre 3. Nous avons étudié spécifiquement l'influence de défauts de forme (amplitude et allure) des éléments circulaires et cylindriques sur l'identification des géométriques simulées à partir d'un nuage de points de mesure. Plus précisément, nous avons examiné l'usage des nouveaux modificateurs de spécifications des tolérances de taille, telle que définie dans ISO 14405-1 :2016, et nous avons étudié comment les stratégies de mesure des systèmes et les algorithmes employés influent l'évaluation de ces nouvelles spécifications. Cette étude a fait l'objet d'une deuxième publication dans un journal avec comité de lecture, ainsi qu'un article dans une conférence internationale.

Dans le Chapitre 4, nous avons réalisé une étude expérimentale pour investiguer la reproductibilité des logiciels d'inspection assistée par ordinateur dans le cas de l'évaluation des défauts dimensionnels et les défauts de forme. Cette étude a été soumise pour une

publication dans un journal avec comité de lecture. Les résultats préliminaires ont fait l'objet d'une affiche dans un colloque et d'une conférence internationale.

Finalement, un nouvel algorithme a été proposé dans le Chapitre 5 pour l'estimation de la taille et de l'erreur de forme des éléments cylindriques affectés par un défaut de fabrication, en présence d'un bruit de mesure et en considérant que le nuage de point ne couvre que partiellement l'élément. L'approche est basée sur un alignement qui utilise l'analyse en composantes principales et la boite englobante orientée. Cette nouvelle approche a été validée par des simulations numériques et sur des études de cas fabriquées et mesurées dans le laboratoire LIPPS. Comme mentionné, cette étude est limitée sur une forme cylindrique, mais elle a démontré sa robustesse. Cette étude fait l'objet de deux publications acceptées et prévues dans deux conférences internationales en 2019.

Lors de la rédaction de cette *Conclusion*, nous constatons que seulement une partie de la tâche a été réalisée et qu'il demeure encore plusieurs travaux à approfondir ou à explorer et à développer. Bien sûr, les contraintes temporelles et les impératives académiques nous obligent de mettre un terme à notre étude et à produire un rapport. *Mais, une recherche scientifique sera-t-elle un jour terminée ?*

RECOMMANDATIONS

La principale motivation de cette thèse était de contribuer au développement d'outils de simulation, de gestion, d'application et d'inspection pour assister les concepteurs dans leurs exercices de synthèse de tolérances ou encore pour assister l'ingénierie des méthodes lors de la création des gammes de fabrication et d'inspection.

Dans le cadre de cette thèse, on a proposé le développement des algorithmes pour modéliser un nuage de points avec de défauts de forme, pour divers éléments géométriques primitifs (ex. cylindre, plan, etc.) en considérant une rigidité infinie, et dans le but de simuler l'effet de défauts de forme dans l'assemblage. Nous avons développé des méthodes de modélisation d'assemblage réaliste. Nous avons également étudié comment les stratégies de mesure des systèmes (captation partielle ou complète) ainsi que le choix algorithmique influent l'évaluation des spécifications.

Comme constaté par le lecteur, plusieurs questions demeurent largement ouvertes. Nous nous permettons de proposer quelques recommandations et quelques idées, dictées par notre expérience, et que nous sommes convaincus qu'elles méritent de futurs travaux de recherche.

- Dans l'article 1 publié dans ADES (2017), une nouvelle approche pour intégrer les tolérances dans les modèles de CAO a été proposée. Les tolérances de position, d'orientation et de forme sont prises en compte. Les composants à tolérances géométriques sont modélisés dans le modèle CAD à l'aide de deux algorithmes. Par contre, le travail est limité au cas des éléments géométriques primitives : surfaces planes et cylindriques. Il sera judicieux d'étendre l'approche vers le cas général : surface libre (*Free Form*).

  Aussi, l'analyse de tolérance permet de détecter la conformité ou non d'une exigence fonctionnelle. Une amélioration du modèle peut être obtenue en estimant la valeur optimale de la spécification ce qui nécessite l'utilisation d'un algorithme d'optimisation. De plus, afin de définir les paramètres de modélisation des défauts de forme, l'utilisation de la DMU permet d'éviter les incertitudes de mesure et la nécessité de

mesurer un grand nombre de pièces réalisées. La précision des résultats numériques dépend donc du choix des valeurs des hyper paramètres. Une étude comparative entre les résultats numériques et expérimentaux permettre de valider le choix des paramètres.

- Dans l'article 2 publié dans IJSA (2019), nous avons étudié l'influence de défauts de forme (amplitude et allure) sur l'identification des géométriques simulées sur les formes géométriques du type cercle ou cylindre. Dans des futurs travaux, il sera judicieux d'étudier d'autre type de surface, telles que surface plane, sphère…), et le cas général : une surface de forme libre. Une analyse plus fine des autres paramètres tels que les valeurs aberrantes reste aussi un sujet intéressant à explorer.

- Toujours dans l'article 2, l'algorithme GX qui se base sur le calcul de maximum cylindre inscrit est incapable de fonctionner dans le cas de données manquantes ou partielles (exemple arc d'un cercle). Nous recommandons de développer un algorithme qui permet d'approximer le modèle nominal des formes géométriques simples (cercle, plan) et des formes géométriques complexes.

- Finalement, l'algorithme Langeberg-Marquet (LM) nécessite une *bonne sélection* de l'hyper paramètre λ. Ce dernier représente un paramètre d'amortissement initial et influent la convergence de l'algorithme GX ou GN. Par conséquent, le meilleur facteur sera celui qui minimiser le temps de calcul (nombre d'itération) tout en garantissant une bonne précision. On propose ici d'appliquer un algorithme d'optimisation globale (par exemple, algorithme génétique, algorithme de Gauss-Newton, algorithme du simplexe, etc.) qui permettra d'optimiser le choix de cet hyper paramètre. λ.

ANNEXE I

ARTICLE MOSIM 2016

Article présenté dans la conférence MOSIM 2016

11th International Conference onModeling, Optimization and Simulation - MOSIM'16
August 22-24
Montréal, Québec, Canada
"Innovation in Technology for performant Systems"

CAD TOLERANCING INTEGRATION: MECHANICAL SYSTEM WITH POSITION, ORIENTATION AND FORM DEFECTS

I. JBIRA[a,b], M. TLIJA[a], B. LOUHICHI[a], A. TAHAN[b]

[a]ISSAT Sousse, Cité Taffala (Ibn Khaldoun), 4003 Sousse, Tunisie

[b]École de Technologie Supérieure, 1100, rue Notre-Dame Ouest,Montréal, Québec, H3C 1K3, Canada

ABSTRACT: *Manufacturing processes are incapable of producing mechanical components with exact sizes and shapes. Thus, designers use Geometric dimensioning and Tolerancing (GD&T) to specify allowable limits for geometry variations based on ISO standards. However, the realistic modeling of mechanical assemblies still to be an important challenge in Computer-Aided Tolerancing (CAT) research.*
In our previous works (Tlija, 2013) (Louhichi, 2015), an approach to consider the dimensional, positional and orientation tolerances in CAD model was developed. In this paper, the above approach is improved to tack into account the form defects in CAD model. To model the component with form defects, the toleranced face is modelled by gird vertices. According to the form tolerance value a White Gaussian Noise (WGN) of gird vertices is computed. The realistic face is obtained by an interpolation based on the tessellation using Thin Plate Surface (TPS) modeling. The realistic assembly configurations were performed by updating the mating constraints. In fact, in realistic modeling, a new method to redefine constraints, while respecting an Objective Function of the Assembly (OFA), is established. In the case of a planar joint, a sub-algorithm based on Oriented Bounding Box (OBB) and the matrix transformation is developed. Relative part displacements are simulated with or without guaranteeing contact. Tolerance impacts on the realistic assembly motion are quantified. The realistic cylindrical joint is performed using an optimisation method.
This paper proposes a new approach to integrating the tolerances in CAD models by determining configurations with positional, orientation and form defects.

KEYWORDS: *CAD, Form tolerances, mating constrains, realistic assembly.*

1 INTRODUCTION

The geometric deviations affect the assemblability and functional compliance of products, since small part variations accumulate through large-scale assemblies and lead to malfunction. The Digital Muck up (DMU) requires the tolerance consideration in CAD model.In our previous researches (Tlija, 2013) (Louhichi, 2015) a new approach to integrate the tolerances in CAD models by determining configurations with CAD part defects used in a mechanical system is established. The realistic parts are computed according to the dimensional, positional and orientation tolerances. However, the non-consideration of form defects generates non-compliant assemblies of compliant parts especially in the case of small clearance (Adragna, 2010) and form defects have impacts on the functional specifications of a mechanism (Grandjean, 2012). Thus, form deviations should be considered in assembly simulations. In this paper a new method allows for tolerance analysis is proposed while considering the following requirements:dimensional, positional, orientation and form tolerances, assembly process planning, contact types and assembly motion.This paper is organized as follows. First, a review of literature is presented. Then, the realistic component modeling approach is proposed: The algorithms used to model components with position and orientation defects, as well as components with form defects are detailed. Subsequently, the realistic assemblies modelling approach is proposed: the redefinition of the mating constraints is introduced and followed by the tolerance analysis that enables to verify and validate the mechanical system assemblability: The algorithms used to simulate relative part displacements with or without guaranteeing contact are detailed. Tolerance impacts on the realistic assembly motion are quantified. After that a sub algorithm to simulate the cylindrical joint between parts with defects is proposed using an optimized cylinder algorithm: the minimum cylinder inside a realistic hole and the maximum cylinder outside a realistic pin. The conclusions and perspectives for this work are presented at the end.

2 STATE OF THE ART

Zou and Morse (2003) propose the GapSpace model to capture the Fitting Conditions (FC) existing in 2D mechanical assemblies. The model uses gaps to describe the possible mating or clearance condition between features inside assemblies.The value of each gap is the shortest distance between the two related features. A GapSpace sine law is computed to describe the characteristic inside each constraining simplex. Using an assembly graph, an algorithm is developed to search the FC inside the assembly. Each FC is represented by a

ANNEXE II

ARTICLE IDETC/CIE 2018

Article publié dans proceedings d'ASME 2018

Proceedings of the ASME 2018 International Design Engineering
Technical Conferences and Computers and Information in Engineering Conference
IDETC/CIE 2018
August 26-29, 2018, Quebec City, Quebec, Canada

DETC2018-85669

EVALUATION OF THE ALGORITHMIC ERROR OF NEW SPECIFICATION TOOLS FOR AN ISO 14405-1:2016 SIZE

Ibtissem Jbira
École de Technologie Supérieure
1100, Rue Notre-Dame Ouest, Montréal, Québec H3C 1K3, Canada
Institut Supérieur d'Informatique et des Technologies de Communication de Hammam Sousse, Tunisie
Email: ibtissem.jbira.1@ens.etsmtl.ca

Antoine Tahan
École de Technologie Supérieure
Montréal, Québec, Canada
1100, Rue Notre-Dame Ouest, Montréal, Québec H3C 1K3, Canada
Email: Antoine.Tahan@etsmtl.ca

Mohamed Ali Mahjoub
École nationale d'ingénieurs de Sousse
Pôle technologique de Sousse, Route de Ceinture
Sahloul, 4054, Tunisie

Borhen Louhichi
Institut supérieur des sciences appliquées et de technologie
Rue Tahar Ben Achour, Sousse 4003, Tunisie
LMS, ENISo, Université de Sousse, Sousse 4023, Tunisie

ABSTRACT

Due to machine tool imprecisions during manufacturing, the actual product cannot be the same as the nominal model. The product's geometric variations influence the geometrical requirements of functionality and assembly [6, 8]; this remains a problem of industrial performance and plays a major role in the quality and cost of products; hence the need for a reliable strategy to evaluate errors in the final inspection of part quality. Among all the geometric characteristics, the circular characteristic is very common on most parts. Therefore, the measurement and evaluation of circularity with a high degree of accuracy is of utmost importance. Size, form and orientation are the basic descriptors of the geometric quality of the objects. The recent publication of ISO 14405-1: 2016 defines the size as the fundamental geometric descriptor; it described a new set of specification tools for the size of part characteristics that directly apply to the ideal geometry of the component [13]. These tools present new challenges for an inspector using a coordinate metrology system. The study of the influence of form defects on the identification of dimensional and geometrical requirements seems necessary. This paper studies four modifiers ISO 14405-1:2016 (Minimum circumscribed size (GN), Maximum recorded size (GX), least squares size Minimum (GG) and Minimum area (MZ)) will be studied. This paper presents simple and effective algorithms for evaluating the circularity error of a large number of points using four specification modifiers of ISO 14405-1:2016, and a study on the influence of measurement system strategies on different algorithms for the evaluation of these new specifications. An analysis software was developed to compare the sensitivity of different parameters (number of points, noise amplitude and circularity defect) on ISO 14405-1:2016 modifiers.

INTRODUCTION

A common problem in the quality control of circular parts is the measure of their roundness [12]. This is one of the basic geometric shapes expected from circular features that are very common on most engineered parts[1. 2]. In manufacturing environments, it is impossible to produce ideal circular parts. Deviations are a natural result of production. These deviations must be determined and are due to imperfect rotation, cutting work pieces, improper lubrication, faulty machine parts, machine tool inaccuracies, chuck jaw misalignments, distortion of various elements of the machine tool, etc. [4]. The resulting geometric errors can greatly affect the functionality and accuracy of assemblies. Therefore is required a reliable strategy to accurately assess errors during the final inspection of part quality [3].

A designer assigns the appropriate geometric requirements for each element of a product so that the elements work properly when they are assembled. These geometrical specifications are indicated in the form of dimensions and tolerances in a "*drawing*" part by symbols described in international standards. [5] presents the basic ideas of parametric and geometrical tolerancing systems, with a focus on metrology. However, tighter tolerances require manufacturing machines and equipment specific measures, which involve high production costs to meet

ANNEXE III

ARTICLE GMAI 2019

Article publié dans proceedings de IEEE 2019

2019 23rd International Conference Information Visualisation (IV)

A comparative study of extraction cylinder features in industrial point clouds

Ibtissem Jbira[123], Aicha Ben Makhlouf[23], Borhen Louhichi[4], Antoine Tahan[1], Mohamed Ali Mahjoub[2], Dominique Deneux[5]
[1]École de technologie supérieure (ÉTS), 1100 Notre-Dame, Montréal, Québec H3C 1K3, Canada
[2]LATIS, ENISo, University of Sousse, 4023 Sousse, Tunisia
[3]ISITCom, University of Sousse, 4023 Sousse, Tunisia
[4]LMS, ENISo, University of Sousse, 4023 Sousse, Tunisia
[5]CNRS, UMR 8201-LAMIH, Univ. Polytechnique Hauts-de-France, F-59313 Valenciennes, France

Borhen.louhichi@etsmtl.ca; Antoine.Tahan@etsmtl.ca; mohamedali.mahjoub@eniso.u-sousse.tn; Dominique.Deneux@uphf.fr

***Abstract*—With the technological advancement in the field of Computer Aided Design such as the rapid development of scanning technologies, the reconstruction of complete and incomplete cylinders given noisy point clouds with form defects becomes an important issue. In fact, cylindrical surfaces are found in domestic to industrial contexts. In this paper, a comparative study of cylinder fitting algorithms manufactured in the LIPPS laboratory is proposed. The aim of the proposed approach is to determine the diameter of cylindrical feature for minimizing roundness error from experimental data-points. The roundness error is evaluated using two internationally defined methods: Minimum Circumscribed Cylinder (MCC) and Maximum Inscribed Cylinder (MIC). All algorithms give similar results in the case where the scanned cylinder is complete and without form defects, but in the case of missing data some algorithms give unacceptable results. The two reference cylinders have been independently analyzed, respecting six criteria (calculation complexity, damping parameter, initial guess, time, circularity error and complexity cylinder). The results of algorithms are also compared to help manufacturers and inspectors facilitate and improve the application of these methods and to select the appropriate algorithm for size and form evaluation.**

Keywords—Computer Aided Design, Form defects, Roundness error, Minimum Circumscribed Cylinder, Maximum Inscribed Cylinder, Feature extraction, Cylinder fitting

I. Introduction

Cylinder adjustment [1] is an essential task in many applications, such as object detection, feature extraction, cell counting, building information modeling, autonomous navigation, forest inventorying, surface reconstruction and archaeological documentation. Many researchers have proposed several algorithms for cylinder reconstruction and extraction based on their types of data and fields of application (e.g., image processing, reverse engineering, Quality, computer vision, inspection). Recently laser scanning techniques approved that can acquire a dense data called Point Cloud Data (PCD). In fact, many authors (cf., [2]) have considered cylinder fitting a key challenge in the presence of outliers, noise and distortion. Cylindrical parts represent an important task in most of industrial products, particularly in industry. About 70% of all the engineering parts have circularity form. Roundness is one of the basic geometrical forms for circular parts. It computes how closely a part form is near the ideal cylinder. Since no manufacturing process is ever ideal, frequently the deviations of the circularity occur in the machined parts. The deviations of the manufactured parts are due to many reasons such as irregular cutting, temperature change, clamping deformations, etc. Irregularity causes many problems during assembly and inspection. Therefore, the circularity measurement has become an important topic for the right functioning of assemblies, making circularity a necessary parameter of quality control in manufacturing industries. During the assembly phase, the out-of-roundness poses major problems and produces a gap between the paired components. Thus, an accurate roundness error is important for the operation of assemblies. The roundness is therefore a necessary quality control parameter in the industry. In addition to the difficulties encountered during rounding operations (rapid assembly operations are more and more in demand), the measured data points may be incomplete because of the orientation of the measurement device unit and restricted access while measuring objects. The roundness measurement time can thus increase. So, a rapid inspection operation is necessary to reduce inspection costs and minimize the product expense. As a result, precise and rapid extraction methods are required [3].

The proposed study is anticipated to be an important tool for help to industrial designers and inspectors, it facilitates and ameliorates the application of fitting algorithms. The proposed benchmarks lead the selection of the best

2375-0138/19/$31.00 ©2019 IEEE
DOI 10.1109/IV.2019.00079

ANNEXE III

ARTICLE GMAI 2019

Étude comparative des algorithmes développés (issu de la publication de GMAI 2019)

Chaque algorithme développé (d'estimation de taille) a sa propre condition d'application. Il est donc impossible de distinguer le meilleur algorithme d'un seul critère. Dans notre étude proposée, les algorithmes développés sont comparés en utilisant différents critères indépendamment. Ensuite, une comparaison globale basée sur différents critères a été présentée ainsi une description conceptuelle de chaque algorithme d'estimation de taille. Nous référons le lecteur au (Jbira et al., 2019).
Le but de cette contribution est de guider les inspecteurs dans leur recherche de la meilleure solution (algorithme). Nous présentons quelques résultats (Complexité, Temps de réponse, et hyper paramètre.) de cette étude:

- ***Complexité et temps de calcul***

Étant donné que les utilisateurs ont besoin dans différents cas de simuler des données avec un grand nombre de points. Par suite la complexité du calcul d'estimation de taille des données avec de défauts de forme joue un rôle critique. Dans le cas de l'algorithme LM, la matrice d'inertie et les vecteurs propres sont calculés pour chaque itération de l'étape d'optimisation. Avec l'augmentation du nombre de points, le temps utilisé pour calculer le vecteur propre augmente également. Par conséquent, le temps utilisé pour calculer la taille augmente. Le temps d'exécution est variable d'un algorithme à un autre. Même si le temps est important pour une méthode spécifique, le résultat obtenu pourrait être meilleur. Cela dépend principalement des performances des ordinateurs utilisés pour l'exécution, mais également du nombre de points utilisés.

Le tableau ci-dessous montre la complexité algorithmique et la durée d'exécution de chaque algorithme:

Numéro	Algorithme	Complexité	Temps de réponse (en secondes)
1	GN- Enveloppe convexe	$O(n^2)$	1.056
2	GN-Optimisation	$O(n^3)$	3.002
3	GX-LMA	$O(n^2)$	7.651
4	GX-Diagramme de Voronoï	$O(n\ log\ (n))$	2.337
5	GN-LMA	$O(n^2)$	7.599

L'algorithme 4 (diagramme de Voronoï) est de complexité logarithmique. L'algorithme 1 (Enveloppe convexe), L'algorithme 3 (LMA) et L'algorithme 5 (LMA) ont une complexité quadratique. L'algorithme 2 est plus complexe (complexité cubique).

- ***Hyperparamètre***

Le paramètre λ de Levenberg Marquardt a pour rôle de basculer entre la méthode de Gauss-Newton et la méthode de descente de gradient. Il donne de la vitesse et génère une erreur minimale si un meilleur choix de λ est fixé.

LISTE DE RÉFÉRENCES BIBLIOGRAPHIQUES

Abdessalem Hassani, N. A., Abdelmajid Benamara, Serge Samper 2010. Méthodologie D'analyse Et D'optimisation Des Tolérances Dans Un Contexte De Conception Intégrée. *Hal*.

Adragna, P.-A., Samper, S. & Favreliere, H. How Form Errors Impact On 2D Precision Assembly With Clearance?, 2010 Berlin, Heidelberg. Springer Berlin Heidelberg, 50-59.

Ahmed, N., Natarajan, T. & RAO, K. R. 1974. Discrete Cosine Transfom. *Ieee Trans. Comput.,* 23**,** 90-93.

Anselmetti, B. 2007. Calcul Tridimensionnel De La Résultante Des Chaînes De Cotes En Cotation Iso. *Mécanique & Industries***,** 173-185.

Anselmetti, B. 2010. Part Optimization And Tolerances Synthesis. *The International Journal Of Advanced Manufacturing Technology,* 48**,** 1221-1237.

Asme-Y14-5m. 1994. ASME Dimensioning And Tolerancing.

Ballu, A., Gomes, R., Mimoso, P., Cristovao, C. & Correia, N. 2017. Comparison Of Mode Decomposition Methods Tested On Simulated Surfaces. *Advances On Mechanics, Design Engineering And Manufacturing : Proceedings Of The International Joint Conference On Mechanics, Design Engineering & Advanced Manufacturing (Jcm 2016), 14-16 September, 2016, Catania, Italy.* Cham: Springer International Publishing.

Beaucaire, P., Gayton, N., Duc, E. & Dantan, J. Y. 2013. Statistical Tolerance Analysis Of A Mechanism With Gaps Based On System Reliability Methods. *Procedia Cirp,* 10**,** 2-8.

Bourdet, P. 1987. *Contribution A La Mesure Tridimensionnelle: Modèle D'identification Géométrique Des Surfaces, Métrologie Fonctionnelle Des Pièces Mécaniques, Correction Géométrique Des Machines A Mesurer Tridimensionnelles.* Université De Nancy (France).

Ceglarek, H. A. 2002. Mode-Based Decomposition Of Part Form Error By Discrete-Cosine-Transform With Implementation To Assembly And Stamping System With Compliant Parts. *Cirp Annals - Manufacturing Technology,* 51**,** 21-26.

Chang, H. & Lin, T. W. 1993. Evaluation Of Circularity Tolerance Using Monte Carlo Simulation For Coordinate Measuring Machine. *International Journal Of Production Research,* 31**,** 2079-2086.

Chaperon, T., Fran, O. 2001. Extracting Cylinders In Full 3d Data Using A Random Sampling Method And The Gaussian Image. *Proceedings Of The Vision Modeling And Visualization Conference 2001.* Aka Gmbh.

Chase, K. W. & Parkinson, A. R. 1991. A Survey Of Research In The Application Of Tolerance Analysis To The Design Of Mechanical Assemblies. *Research In Engineering Design,* 3**,** 23-37.

Chien, A. Y. 1982. Approximate Harmonic Models For Roundness Profiles With Equivalent Energy Mean Square Values. *Wear,* 77**,** 247-252.

Clément, A., Rivière, A. & Temmerman, M. 1994. *Cotation Tridimensionnelle Des Systèmes Mécaniques: Théorie Et Pratique*, Pyc.

Dantan, J.-Y., Mathieu, L., Ballu, A. & Martin, P. 2005. Tolerance Synthesis: Quantifier Notion And Virtual Boundary. *Computer-Aided Design,* 37**,** 231-240.

Deschaud, J.-E. & Goulette, F. https://Hal-Mines-Paristech.Archives-Ouvertes.Fr/Hal-01097361/Document. A Fast And Accurate Plane Detection Algorithm For Large Noisy Point Clouds Using Filtered Normals And Voxel Growing. 3dpvt, 2010-05-17 2010 Paris, France.

Favreliere, H. 2009. *Tolérancement Modal: De La Métrologie Vers Les Spécifications.* Université De Savoie.

Fleming, A. 1988. Geometric Relationships Between Toleranced Features. *Artificial Intelligence,* 37**,** 403-412.

Gaurav , A. 2007. Tolerance-Maps Applied To A Point-Line Cluster Of Features. *Journal Of Mechanical Design,* 129**,** 782–792.

Germain, F. 2007. *Tolérancement Statistique Tridimensionnel, Intégration En Cfao.* Université De Savoie.

Goch, G. & Lübke, K. 2008. Tschebyscheff Approximation For The Calculation Of Maximum Inscribed/Minimum Circumscribed Geometry Elements And Form Deviations. *Cirp Annals,* 57**,** 517-520.

Grandjean, J., Ledoux, Y. & Samper, S. 2013. On The Role Of Form Defects In Assemblies Subject To Local Deformations And Mechanical Loads. *The International Journal Of Advanced Manufacturing Technology,* 65**,** 1769-1778.

Guo, J. & Yang, J. 2019. An Iterative Procedure For Robust Circle Fitting. *Communications In Statistics - Simulation And Computation,* 48**,** 1872-1879.

Henke, R. P., Summerhays, K. D., Baldwin, J. M., Cassou, R. M. & Brown, C. W. 1999. Methods For Evaluation Of Systematic Geometric Deviations In Machined Parts And Their Relationships To Process Variables. *Precision Engineering,* 23**,** 273-292.

Huang, W. & Ceglarek, D. 2002. Mode-Based Decomposition Of Part Form Error By Discrete-Cosine-Transform With Implementation To Assembly And Stamping System With Compliant Parts. *Cirp Annals,* 51**,** 21-26.

Jbira, I., Makhlouf, A. B., Louhich, B., Tahan, A., Mahjoub, M. A. & Deneux, D. A Comparative Study Of Extraction Cylinder Features In Industrial Point Clouds. 2019 23rd International Conference Information Visualisation (Iv), 2-5 July 2019 2019. 431-441.

Jbira, I., Tahan, A., Mahjoub, M. A. & Louhichi, B. 2018a. Evaluation Of The Algorithmic Error Of New Specification Tools For An Iso 14405-1:2016. *Proceedings Of The Asme International Design Engineering Technical Conferences And Computers And Information In Engineering Conference, 2018, Vol 1a*.

Jbira, I., Tahan, A., Mahjoub, M. A. & Louhichi, B. 2018b. Evaluation Of The Algorithmic Error Of New Specification Tools For An Iso 14405-1:2016 Size. V01at02a006.

Jbira, I., Tlija, M., Louhichi, B. & Tahan, A. 2017. CAD/Tolerancing Integration: Mechanical Assembly With Form Defects. *Advances In Engineering Software,* 114**,** 312-324.

Jian, A. D., Ameta, G., Davidson, J. K. & Shah, J. J. Tolerance Analysis And Allocation Using Tolerance-Maps For A Power Saw Assembly. 2007 Dordrecht. Springer Netherlands, 267-276.

Jin, S., Ding, S., Li, Z., Yang, F. & MA, X. 2018. Point-Based Solution Using Jacobian-Torsor Theory Into Partial Parallel Chains For Revolving Components Assembly. *Journal Of Manufacturing Systems,* 46**,** 46-58.

Kanada, T. 1995. Evaluation Of Spherical Form Errors—Computation Of Sphericity By Means Of Minimum Zone Method And Some Examinations With Using Simulated Data. *Precision Engineering,* 17**,** 281-289.

Kass, M., Witkin, A. & Terzopoulos, D. 1988. Snakes: Active Contour Models. *International Journal Of Computer Vision,* 1**,** 321-331.

Kataya, B. 2002. *Modélisation Des Tolérances Géométriques Des Mécanismes Pour Leur Intégration En Conception Assistée Par Ordinateur.* Université De Savoie.

Kethara Pasupathy, T. M., Morse, E. P. & Wilhelm, R. G. 2003. A Survey Of Mathematical Methods For The Construction Of Geometric Tolerance Zones. *Journal Of Computing And Information Science In Engineering,* 3**,** 64-75.

Lê, H.-N., Ledoux, Y. & Ballu, A. 2014. Experimental And Theoretical Investigations Of Mechanical Joints With Form Defects. *Journal Of Computing And Information Science In Engineering,* 14**,** 041004-041004-10.

Lecompte, J., Legoff, O. & Hascoet, J.-Y. 2010. Technological Form Defects Identification Using Discrete Cosine Transform Method. *The International Journal Of Advanced Manufacturing Technology,* 51**,** 1033-1044.

Liu, F., Xu, G., Liang, L., Zhang, Q. & Liu, D. 2016. Minimum Circumscribed Circle And Maximum Inscribed Circle Of Roundness Deviation Evaluation With Intersecting Chord Method. *Ieee Transactions On Instrumentation And Measurement,* 65**,** 2787-2796.

Long Nguyen, H., Belton, D. & Helmholz, P. 2017. Comparative Study Of Automatic Plane Fitting Registration For Mls Sparse Point Clouds With Different Plane Segmentation Methods. *Isprs Ann. Photogramm. Remote Sens. Spatial Inf. Sci.,* Iv-2/W4**,** 115-122.

Louhichi, B., Tlija, M., Benamara, A. & Tahan, A. 2015. An Algorithm For CAD Tolerancing Integration: Generation Of Assembly Configurations According To Dimensional And Geometrical Tolerances. *Computer-Aided Design,* 62**,** 259-274.

Marriott, R. T., Pashevich, A. & Horaud, R. 2018. Plane-Extraction From Depth-Data Using A Gaussian Mixture Regression Model. *Pattern Recognition Letters,* 110**,** 44-50.

Mehdi, T., Borhen, L. & Benamara, A. Mates Updating Of Rigid And Fully Constrained Assembly With Defects. *In:* Haddar, M., Romdhane, L., Louati, J. & Ben Amara, A., Eds. Design And Modeling Of Mechanical Systems, 2013// 2013 Berlin, Heidelberg. Springer Berlin Heidelberg, 655-662.

Morière, S., Mailhé, J., Linares, J.-M. & Sprauel, J.-M. 2010. *Assembly Method Comparison Including Form Defect*.

Moroni, G., Syam, W. P. & Petrò, S. 2014. Performance Improvement For Optimization Of The Non-Linear Geometric Fitting Problem In Manufacturing Metrology. *Measurement Science And Technology,* 25**,** 085008.

Morse, E. P. & Srinivasan, V. 2013. Size Tolerancing Revisited: A Basic Notion And Its Evolution In Standards. *Proceedings Of The Institution Of Mechanical Engineers, Part B: Journal Of Engineering Manufacture,* 227**,** 662-671.

Novotni, M. & Klein, R. 2004. Shape Retrieval Using 3d Zernike Descriptors. *Computer-Aided Design,* 36**,** 1047-1062.

Nurunnabi, A., Sadahiro, Y. & Laefer, D. F. 2018. Robust Statistical Approaches For Circle Fitting In Laser Scanning Three-Dimensional Point Cloud Data. *Pattern Recognition,* 81**,** 417-431.

Nurunnabi, A., Sadahiro, Y., Lindenbergh, R. & Belton, D. 2019. Robust Cylinder Fitting In Laser Scanning Point Cloud Data. *Measurement $V 138***,** 632-651.

Pearson, K. 1901. On Lines And Planes Of Closest Fit To Systems Of Points In Space. *The London, Edinburgh, And Dublin Philosophical Magazine And Journal Of Science,* 2**,** 559-572.

Petit, J. P. 2004. Specification Geometrique Des Produits : Methode D'analyse De Tolerances. Application En Conception Assistee Par Ordinateur. *Thése*.

Petrík, M. 2009. Roundness: Determining The Reference Circle For Mcci And Mici System. *Measurement*.

Pierce, R. S. & Rosen, D. 2007. A Method For Integrating Form Errors Into Geometric Tolerance Analysis. *Journal Of Mechanical Design,* 130**,** 011002-011002-11.

Pino, L. 2000a. *Kinematic Modeling And Analysis Of Geometric Tolerances For Mechanism Assembly.* Université De Nantes.

Pino, L. 2000b. *Modélisation Et Analyse Cinématique Des Tolérances Géométriques Pour L'assemblage De Systèmes Mécaniques.* Ecole Centrale De Nantes.

Pitard, G., Legoïc, G., Mansouri, A., Favrelière, H., Desage, S.-F., Samper, S. & Pillet, M. 2017. Discrete Modal Decomposition: A New Approach For The Reflectance Modeling And Rendering Of Real Surfaces. *Machine Vision And Applications,* 28**,** 607-621.

Podosinnikova, A., Setzer, S. & Hein, M. Robust Pca: Optimization Of The Robust Reconstruction Error Over The Stiefel Manifold. 2014 Cham. Springer International Publishing, 121-131.

Portman, V. & Weill, R. 1996. Modelling Spatial Dimensional Chains For Cad/Cam Applications. *Computer-Aided Tolerancing.* Springer.

Pt, R., P, S., Sudhakaran, N., Anirudh, V., Lawrence K, D. & Mathew, J. 2018. Comparative Study Of Roundness Evaluation Algorithms For Coordinate Measurement And Form Data. *Precision Engineering,* 51**,** 458-467.

Raja, J. & Radhakrishnan, V. 1977. Analysis And Synthesis Of Surface Profiles Using Fourier Series. *International Journal Of Machine Tool Design And Research,* 17**,** 245-251.

Requicha, A. A. G. 1984. Representation Of Tolerances In Solid Modeling: Issues And Alternative Approaches. *In:* Pickett, M. S. & Boyse, J. W. (Eds.) *Solid Modeling By Computers: From Theory To Applications.* Boston, Ma: Springer Us.

Requicha, A. A. G. 1993. Mathematical Meaning And Computational Representation Of Tolerance Specifications. *Forum On Dimensional Tolerancing And Metrology, Asme,* 27**,** 61–68.

Rivest, L. 1994. Modélisation Et Analyse Tridimensionnelles Des Tolérances Dimensionnelles Et Géométrique. . *Thèse De L'université De Montréal, Ecole Polytechnique*.

Rivest, L., Fortin, C. & Morel, C. 1994. Tolerancing A Solid Model With A Kinematic Formulation. *Computer-Aided Design,* 26**,** 465-476.

Robinson, D. M. 1998. Geometric Tolerancing For Assembly With Maximum Material Parts. *In:* Elmaraghy, H. A. (Ed.) *Geometric Design Tolerancing: Theories, Standards And Applications.* Boston, Ma: Springer Us.

Salomons, O., Haalboom, F., Poerink, H. J., Van Slooten, F., Van Houten, F. & Kals, H. 1996. A Computer Aided Tolerancing Tool Ii: Tolerance Analysis. *Computers In Industry,* 31**,** 175-186.

Samper, S. 2007. *Tolérancement Et Analyse Des Structures Au Service Des Systèmes Souples Et Du Défaut De Forme.* Université De Savoie.

Samper, S., Adragna, P.-A., Favreliere, H. & Pillet, M. 2009. Modeling Of 2d And 3d Assemblies Taking Into Account Form Errors Of Plane Surfaces. *Journal Of Computing And Information Science In Engineering,* 9**,** 041005-041005-12.

Saval-Calvo, M., Azorin-Lopez, J., Fuster-Guillo, A. & Garcia-Rodriguez, J. 2015. Three-Dimensional Planar Model Estimation Using Multi-Constraint Knowledge Based On K-Means And Ransac. *Applied Soft Computing,* 34**,** 572-586.

Schleich, B., Anwer, N., Mathieu, L. & Wartzack, S. 2014. Skin Model Shapes: A New Paradigm Shift For Geometric Variations Modelling In Mechanical Engineering. *Computer-Aided Design,* 50**,** 1-15.

Schleich, B. & Wartzack, S. 2015. Approaches For The Assembly Simulation Of Skin Model Shapes. *Computer-Aided Design,* 65**,** 18-33.

Schleich, B. & Wartzack, S. 2016. A Quantitative Comparison Of Tolerance Analysis Approaches For Rigid Mechanical Assemblies. *Procedia Cirp,* 43**,** 172-177.

Shen, Z. 2003. Tolerance Analysis With Eds/Visvsa. *Journal Of Computing And Information Science In Engineering,* 3**,** 95-99.

Shen, Z., Ameta, G., Shah, J. J. & Davidson, J. K. 2005. A Comparative Study Of Tolerance Analysis Methods. *Journal Of Computing And Information Science In Engineering,* 5**,** 247-256.

Sicam, V. A. D. P., Coppens, J., Van Den Berg, T. J. T. P. & Van Der Heijde, R. G. L. 2004. Corneal Surface Reconstruction Algorithm That Uses Zernike Polynomial Representation. *Journal Of The Optical Society Of America A,* 21**,** 1300-1306.

Srinivasan, V. 2013. Reflections On The Role Of Science In The Evolution Of Dimensioning And Tolerancing Standards. *Proceedings Of The Institution Of Mechanical Engineers, Part B: Journal Of Engineering Manufacture,* 227**,** 3-11.

Srinivasan, V. & Jayaraman, R. Issues In Conditional Tolerances For Cad Systems. Proceedings. 1985 Ieee International Conference On Robotics And Automation, 25-28 March 1985 1985. 373-375.

Sui, W. & Zhang, D. 2012. Four Methods For Roundness Evaluation. *Physics Procedia,* 24**,** 2159-2164.

Summerhays, K. D., Henke, R. P., Baldwin, J. M., Cassou, R. M. & Brown, C. W. 2002. Optimizing Discrete Point Sample Patterns And Measurement Data Analysis On Internal Cylindrical Surfaces With Systematic Form Deviations. *Precision Engineering,* 26**,** 105-121.

Tlija, M. 2014. *Contribution A La Prise En Compte Des Tolérances Dimensionnelles Et Géométriques Dans Les Modeleurs Cao.* Ecole Nationale D'ingénieurs De Monastir.

Tlija, M., Korbi, A., Louhichi, B. & Benamara, A. 2019. A Novel Model For The Tolerancing Of Nonrigid Part Assemblies In Computer Aided Design. *Journal Of Computing And Information Science In Engineering,* 19**,** 041008-041008-10.

Tran, T.-T., Cao, V.-T. & Laurendeau, D. 2015. Extraction Of Cylinders And Estimation Of Their Parameters From Point Clouds. *Comput. Graph.,* 46**,** 345-357.

Turner, J. U. 1993. A Feasibility Space Approach For Automated Tolerancing. *Journal Of Engineering For Industry,* 115**,** 341-346.

Wang, M., Cheraghi, S. H. & Masud, A. S. M. 1999. Circularity Error Evaluation: Theory And Algorithm. *Precision Engineering,* 23**,** 164-176.

Wang, S. F. & Lai, S. H. 2008. Reconstructing 3d Shape, Albedo And Illumination From A Single Face Image. *Computer Graphics Forum,* 27**,** 1729-1736.

Wirtz, A. 1993. Vectorial Ta Basic Element For Quality Control. *3 Rd Cirp Seminar On Computer-Aided Tolerancinolerancing*, 115–227.

Xiuming, L., Jingcai, Z. & Hongqi, L. 2013. Determination Of The Minimum Zone Circle Based On The Minimum Circumscribed Circle. *Measurement Science And Technology,* 25, 017002.

Yan, X. & Ballu, A. 2017. Generation Of Consistent Skin Model Shape Based On Fea Method. *The International Journal Of Advanced Manufacturing Technology,* 92, 789-802.

Yan, X. & Ballu, A. 2018. Tolerance Analysis Using Skin Model Shapes And Linear Complementarity Conditions. *Journal Of Manufacturing Systems,* 48, 140-156.

Zhao, H.-K., Osher, S., Merriman, B. & Kang, M. 2000. Implicit And Nonparametric Shape Reconstruction From Unorganized Data Using A Variational Level Set Method. *Computer Vision And Image Understanding,* 80, 295-314.

Zhao, Z., Xi, J., Zhao, X., Zhang, G. & Shang, M. 2018. Evaluation Of The Calculated Sizes Based On The Neural Network Regression. *Mathematical Problems In Engineering,* 2018, 11.

Zou, Z. & Morse, E. P. 2004. A Gap-Based Approach To Capture Fitting Conditions For Mechanical Assembly. *Computer-Aided Design,* 36, 691-700.